Stem Cells International

# Mechanobiology of Musculoskeletal Stem and Progenitor Cells

Lead Guest Editor: Qiang Zhou
Guest Editors: Guangdong Zhou, Yang Song, Jian Chen, and Bo Gao

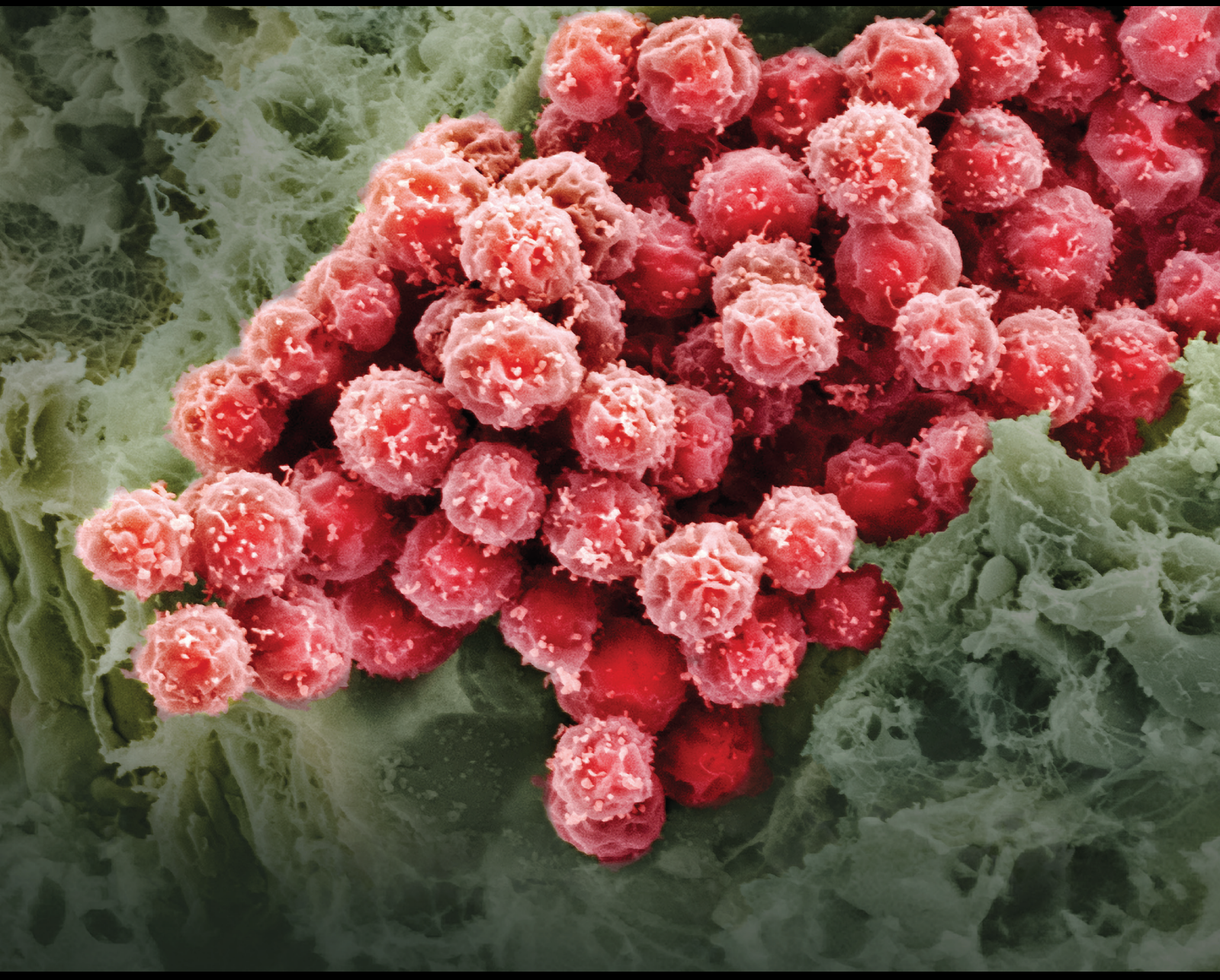

# Mechanobiology of Musculoskeletal Stem and Progenitor Cells

Stem Cells International

# Mechanobiology of Musculoskeletal Stem and Progenitor Cells

Lead Guest Editor: Qiang Zhou
Guest Editors: Guangdong Zhou, Yang Song, Jian Chen, and Bo Gao

# Contents

Hindawi
Stem Cells International
Volume 2022, Article ID 9896444, 12 pages
https://doi.org/10.1155/2022/9896444

*Research Article*

# BMSC-Derived Exosomes Alleviate Intervertebral Disc Degeneration by Modulating AKT/mTOR-Mediated Autophagy of Nucleus Pulposus Cells

**Quan Xiao,[1,2] Zhe Zhao,[3] Yun Teng,[4] Lungang Wu,[2] Jinlong Wang,[2] Hongjun Xu,[5] Sumei Chen,[2] and Quan Zhou[2]**

[1]*Trauma Center, The Affiliated Lianshui County People's Hospital of Kangda College of Nanjing Medical University, Huai'an, Jiangsu Province 223400, China*
[2]*Department of Orthopaedics, The Affiliated Huai'an Hospital of Xuzhou Medical University, Huai'an, Jiangsu Province 223002, China*
[3]*Department of Orthopaedics, Xuyi People's Hospital, Kangda College of Nanjing Medical University, Huai'an, Jiangsu Province 211700, China*
[4]*Department of Orthopaedic Surgery, The First Affiliated Hospital of Soochow University, Suzhou, Jiangsu, China*
[5]*Department of Orthopaedics, The Affiliated Lianshui County People's Hospital of Kangda College of Nanjing Medical University, Huai'an, Jiangsu Province 223400, China*

Correspondence should be addressed to Quan Zhou; wuque1@126.com

Received 10 March 2022; Revised 28 April 2022; Accepted 6 June 2022; Published 9 July 2022

Academic Editor: Qiang Zhou



The pathogenesis of intervertebral disc degeneration (IDD) is still unclear. It has been shown that the pathological process of IDD is most closely related to inflammation of nucleus pulposus cells (NPCs), in which inflammatory factors play an important role. Exosomes are the main paracrine mediators and are microvesicles with biological functions similar to those of the cells from which they are derived. Studies have shown that bone mesenchymal stem cells (BMSCs) can inhibit apoptosis of NPCs by sending exosomes as anti-inflammatory and antioxidant, which has been proved to be effective on IDD. However, the specific mechanism of inhibiting apoptosis of NPCs is still unclear. In our study, BMSC-derived exosomes (BMSC-Exo) were isolated from the BMSC culture medium, and their antiapoptotic effects were evaluated in cells and rat models to explore the possible mechanisms. We observed that BMSC-Exo promotes autophagy in NPCs and inhibits the release of inflammatory factors such as IL-1$\beta$ and TNF-$\alpha$ in LPS-treated NPCs and inhibits apoptosis in NPCs. Further studies showed that BMSC-Exo inhibited the Akt-mTOR pathway. Intramuscular injection of BMSC-Exo alleviates disc degeneration in rat IDD models. In conclusion, our results suggest that BMSC-Exo can reduce NPC apoptosis and alleviate IDD by promoting autophagy by inhibiting the Akt-mTOR pathway. Our study confers a promising therapeutic strategy for IDD.

## 1. Introduction

There are many causes of low back pain, but intervertebral disc degeneration (IDD) is the main cause and has become one of the most common diseases that seriously affect human health [1]. Currently, the main treatments for IDD include conservative treatment and surgical treatments such as removal of nucleus pulposus, which are aimed at treating symptoms, but there is no effective radical cure for IDD [2], which is largely due to the fact that its current pathogenesis is still poorly defined and known effective therapeutic targets are fewer. Therefore, it is of great significance to further explore the regulatory mechanism of IDD and find effective interventions for its prevention. Autophagy, as a hot topic in the field of biology, is believed to be involved in the occurrence and development of various degenerative diseases. It is currently believed that autophagy plays an essential role in the repair, degeneration, and death of intervertebral disc

cells [3–5]. Related studies have found that autophagy plays a role like a two-edged sword during degeneration. On the one hand, normal bodies have a basal level of autophagy, which is of great significance for the renewal and repair of cells themselves [6–8]. On the other hand, excessive autophagy may lead to cell death, and the control of excessive autophagy in nucleus pulposus cells (NPCs) can reduce cell apoptosis and thus delay the progression of IDD [9]. Therefore, it is extremely meaningful to determine how to regulate disc autophagy and exert its benefits to limit its disadvantages.

Regenerative medicine with stem cell transplantation as the main therapy has gradually emerged in recent decades. Bone mesenchymal stem cells (BMSCs) can make direct contact with the NPCs and promote their proliferation through paracrine [10]. It was found that BMSCs could inhibit NPC apoptosis and relieve IDD by delivering exosomes as an anti-inflammatory and antioxidant agent [11]. However, the specific mechanism of bone mesenchymal stem cell-derived exosomes (BMSC-Exo) in inhibiting NPC apoptosis is still unclear. It has been found that the knockdown of the nuclear factor kappa-B (NF-$\kappa$B) promotes cellular autophagy through the AKT/mTOR pathway and that the autophagy caused by NF-$\kappa$B inhibition plays a protective role in the NPCs degeneration induced by lipopolysaccharide (LPS) [12]. Our previous study also found that BMSC-Exo inhibited NPC apoptosis by inhibiting the NF-$\kappa$B signaling pathway [13]. We, therefore, hypothesized that BMSC-Exo is likely to promote autophagy of NPCs through the AKT/mTOR pathway to reduce cellular inflammation and subsequently inhibit NPCs' apoptosis. This study intends to explore the possibility of BMSC-Exo regulating NPC autophagy to inhibit apoptosis and its specific mechanism, so as to provide new ideas for the treatment of IDD.

## 2. Material and Methods

*2.1. Chemicals and Reagents.* The chemicals and reagents are as follows: IMDM cell medium, F12 cell medium (Gibco); osteogenic/adipogenic/chondrogenic induced differentiation medium (Suzhou Syagen); II-type collagenase, LPS, 3-MA, IGF-1Triton, and X-100 Tween (Sigma); Rabbit type II collagen primary antibody, rabbit Cleaved Caspase-3 primary antibody, rabbit Bax primary antibody, rabbit LC3 primary antibody, rabbit Beclin-1 primary antibody, rabbit $\beta$-actin primary antibody, rabbit p-Akt primary antibody, rabbit Akt primary antibody, rabbit p-mTOR primary antibody, rabbit mTOR primary antibody, HRP-labeled goat anti-rabbit secondary antibody, rabbit CD45 primary antibody, rabbit CD34 primary antibody, rabbit CD29 primary antibody, rabbit CD90 primary antibody, rabbit CD63 primary antibody, rabbit CD9 primary antibody, Rabbit GAPDH primary antibody, and rabbit TSG101 primary antibody (Abcam); TBS buffer, PBS buffer (Biosharp); Exosome Isolation Kit (Life technologies); primary antibody dilutions, secondary antibody dilutions, Trizol Lysate, ECL kit, PKH67 Staining Kit, BCA Protein Quantitative Kit, Annexin V-APC/PI Apoptosis Detection Kit, DAPI staining solution, RIPA Lysate (Medium), and PMSF (Beyotime, Jiangsu); 5 All-In-One RT MasterMix, SYBR Green Supermix (Abm), PAGE Gel Rapid Preparation Kit (12.5%) (Shanghai Epizyme); TNF-$\alpha$ ELISA Detection Kit, IL-1$\beta$ ELISA Detection Kit, and Shanghai Enzyme Link.

*2.2. Experimental Animals.* Eight SD male SPF rats (aged 6-8 weeks) weighing $200 \pm 20$ g, were purchased from Zhaoyan (Suzhou) New Drug Research Center Co., Ltd., License No. SCXK (Suzhou) 2018-0016, Qualification Certificate No. 202008469. The protocol was approved by the animal committee of the First Affiliated Hospital of Soochow University (approval number 353/2020). The experimental rats were adaptively fed in a mode of light and day alternation (light time: 07:00-18:00), with a temperature of about 25°C, the humidity of about 50%, and good ventilation, as well as free diet and drinking water.

*2.3. Cell Isolation and Culture.* BMSCs were isolated from 6-8-week-old SD male rats and cultured as the following description. Briefly, the bone marrow was separated from the femurs and tibias of rats by flushing with a serum-free culture medium (IMDM; Gibco, USA). The cells were lysed in the red blood cell lysate and cultured in IMDM (containing 10% FBS) at 37°C, humidity 95%-100% with 5% $CO_2$. First change of medium was performed after 24-48 h, at the frequency of once every 2-3 d later. The cells were passaged and divided when they grew to about 80%-90% filling in the incubator. BMSCs used in this study were P4 generation cells.

The nucleus pulposus tissue was fragmented and digested for 180 min in the type II collagenase; the tissue residue was filtered by 100 $\mu$m filter and centrifuged at 4°C for 5 min, with a radius of 1000 r/min; and the supernatant was removed. F12 medium was blown and mixed uniformly, repeated 3 times, inoculated according to $1 \times 10^6$ cells per incubator for static culture, and passaged at the right time. All the NPCs used in this experiment were P3-generation cells. The cells were identified by toluidine blue staining and type II collagen immunocytochemical staining.

*2.4. Evaluation of the Mutipotency of BMSCs.* P4-generation BMSCs were inoculated with 6-orifice plates at $2 \times 10^4$/well density, which was divided into adipogenic induction, osteogenic induction, and chondrogenic induction, respectively. BMSCs were cultured in the following medium types: (1) adipogenic differentiation medium containing high-glucose DMEM, 10% FBS, 0.1 mmol/L 3-isobutyl-1-methylxanthine, 10 $\mu$g/ml insulin, 10 nM dexamethasone, 50 $\mu$g/ml indomethacin, 100 U/ml streptomycin, and 100 U/ml penicillin; (2) osteogenic differentiation medium containing high-glucose DMEM, 10% FBS, 50 $\mu$g/ml ascorbic acid, 10 mM $\beta$-glycerophosphate, 10 nM dexamethasone, 100 U/ml streptomycin, and 100 U/ml penicillin; and (3) chondrogenic differentiation medium containing high-glucose DMEM, 50 $\mu$g/ml ascorbic acid, 100 nM dexamethasone, 1 mM sodium pyruvate, 40 $\mu$g/ml proline, 100 U/ml streptomycin, 100 U/ml penicillin, 10 ng/ml TGF$\beta$3, ITS+premix (final concentrations, 6.25 $\mu$g/ml bovine insulin, 6.25 $\mu$g/ml transferrin, 6.25 $\mu$g/ml selenous acid, 5.33 $\mu$g/ml linoleic

acid, and 1.25 mg/ml bovine serum albumin). The induction medium was changed every 3 days. At day 14, cells were fixed and stained with Oil Red O for adipocytes, Alizarin Red for osteocytes, and Alcian Blue for chondrocytes.

*2.5. Characterization of BMSCs by Flow Cytometry.* Flow cytometry was utilized to determine the stemness features of BMSCs by analysis of specific cell surface markers. After being trypsinized, the cells were resuspended in 0.5 ml phosphate-buffered saline (PBS) and incubated for 30-40 min at 4°C with fluorescently labeled antibody (blank control tube without antibody) and resuspended in 0.3 ml PBS and then analyzed.

*2.6. Extraction and Identification of BMSC-Exo.* When P4-generation BMSCs were grown up to 80%, serum-free IMDM was cultured for 48 h, and after collecting the supernatant, the exocrine was extracted by ultra-high-speed centrifugation. Briefly, culture supernatant was collected and centrifuged at 300 × g for 10 min at 4°C and retain the supernatant, continue 2000 × g centrifugation at the same temperature for 20 min and retain the supernatant, continue 10000 × g centrifugation at the same temperature for 30 min and retain the supernatant, and continue 100000 × g centrifugation at the same temperature for 70 min; the precipitation obtained is exosomes, diluted with 1 × PBS, and stored in a refrigerator at -80°C. BMSC-Exo morphology was observed by a transmission electron microscope. A small amount of exosome samples were taken in three portions for dilution, and 1, 3, and 7 times volumes of 1 × PBS were added, respectively. Then, drop 20 $\mu$l of each diluted sample onto the surface of copper mesh covered with carbon film, let it stand for 60-90 s, use filter paper to absorb the excess samples, and let it stand for drying. Then, 10 $\mu$l of uranium acetate was added to each sample for staining under dark conditions. After 1 min, the residual dye was absorbed by filter paper and dried at room temperature. The staining was observed under TEM and photographed. The distribution of exosome particle diameter data was detected by a nanoparticle tracking analyzer. Exosomes obtained after centrifugation were diluted with 1 × PBS (1 : 500). The pipetting gun absorbed 200 $\mu$l, the instrument was used for corresponding predetection, and the concentration was adjusted to the appropriate range. The exosomes diluted to an appropriate concentration were detected by the computer, and the data distribution diagram of exosome particle diameter was obtained. BMSCs and exosome surface marker proteins were detected and identified by Western blot.

*2.7. Exosome Labeling and Cellular Uptake.* After taking the mother solution of the PKH67 staining kit at room temperature, the exosomes containing 100 $\mu$g protein were added and incubated for 15 min at room temperature. 10 ml 1 × PBS was added before adding half of the reagent from the exosome extraction kit, mixing and resting it at 4°C for 1 h, then centrifuged at 10,000 × g for 30 min, and the precipitation was resuspended with 200 $\mu$l 1 × PBS; then, PKH67-labeled exosomes were obtained. They were incubated with adherent NPCs for 48 h, fixed in paraformaldehyde (4%), and washed three times with PBST (1 × PBS + 0.1% Triton X-100) for 10 min each. 3 ml of 1% BSA was added to incubate for 30 min and washed with PBST (1 × PBS + 0.1% Tween) 3 times, 10 min each time. 3 mL DAPI staining solution at 0.5 $\mu$g/ml was added and incubated for 10 min, washed 3 more times with PBST (1 × PBS + 0.1% Tween) or 10 min each, then photographed and observed under a fluorescence inverted microscope.

*2.8. Detection of NPC Viability by CCK-8.* The digested NPCs were inoculated in 96-orifice plate $2 \times 10^4$ cells/orifice. 24 hours later, the cells were cultured in the medium containing different concentrations of LPS (0, 100, 200, 500, and 1000 $\mu$g/ml) for 24 hours, with six replicates for each concentration. Each orifice was incubated with 10 $\mu$l CCK-8 reagent for 60 min. The *A* value of each orifice was measured by a microplate reader at a wavelength of 450 nm, showing the vitality of NPCs. The cell survival rate is calculated as follows: cell viability = $[(\mathrm{As} - \mathrm{Ab})/(\mathrm{Ac} - \mathrm{Ab})] \times 100\%$, where As is a value of experimental orifices (culture medium containing nucleus pulposus cells, CCK-8, and LPS); Ac is LPS concentration = a value of cell orificeat 0 $\mu$g/ml; Ab is a value of blank orifice (medium without nucleus pulposus cells, LPS, and CCK-8); andAb = 0.002in this experiment. The appropriate concentration of LPS was selected according to the results to induce apoptosis of NPCs.

*2.9. Effect of Exosomes on Apoptosis and Autophagy in NPCs*

*2.9.1. Establishment of NPC Inflammation Model.* The specific groups are as follows: control group: normal cultured NPCs; model group: normally cultured NPCs were incubated with 2 ml of F12 complete medium containing 500 $\mu$g/ml LPS for 48 h to establish the inflammatory model of NPCs; exosome treatment group: normally cultured NPCs were incubated with 2 ml of F12 complete medium containing LPS of 500 $\mu$g/ml as well as BMSC-Exo 20 $\mu$g for 48 h; autophagy inhibitory group: normally cultured NPCs were incubated with 2 ml of F12 complete medium containing LPS of 500 $\mu$g/ml and 10 mM of autophagy inhibitor 3-methyladenine (3-MA) as well as BMSC-Exo 20 $\mu$g for 48 h.

*2.9.2. Reverse Transcription-PCR.* The cells were collected, and RNA was extracted to detect the concentration of extracted RNA. RNA was reverse transcribed to generate cDNA and amplified using this as a template. Set the extended parameter to 95°C, 40s, 95°C, 10s, 60°C, and 35 s, for a total of 30 cycles. The result data were analyzed using 7300 System SDS Software and the relative expression levels of type II collagen (COL2A1), Beclin-1, and IL-1$\beta$ in nucleus pulposus cells for each group using reference GAPDH as a control, i.e., $2^{-\triangle\triangle Ct}$ value. $2^{-\triangle\triangle Ct} = (CT_{\text{Target genes of experimental group}} - CT_{\text{GAPDH of experimental group}}) - (CT_{\text{target genes of Control group}} - CT_{\text{GAPDH of Control group}})$. The expression levels of type II collagen, Beclin-1, and IL-1$\beta$ were detected with GAPDH as the internal reference. The primer sequence is shown in Table 1.

*2.9.3. Western Blot Analysis.* The protein of nucleus pulposus cells in each group was extracted and quantified by the

Table 1: Oligonucleotide primers used for RT-qPCR.

| Genes | Forward primer | Reverse primer | Annealing (°C) |
|---|---|---|---|
| GAPDH | CTTCTCTTGTGACAAAGTGGA | TTAGCGGGATCTCGCTC | 60 |
| COL2A1 | CCTGAAACTCTGCCACCCAG | GTTCTTCCGAGGCACAGTCG | 60 |
| Beclin-1 | GTTCTCTCAGTTGCCTTTC | AGCTGTAACCTGTCGCCGAGTCCC | 60 |
| IL-1$\beta$ | CCGGAGTCTGACTGGAAAGCC | GCATACAGGAAGTCGGCCTCC | 60 |

BCA method. Following the electrophoresis separation with 30 $\mu$g protein samples, membrane transfer, membrane cutting, and sealing, as well as incubation with primary antibody and secondary antibody, were carried out and then exposed and photographed. Using actin as the internal reference, the gray value of each band was calculated to obtain the relative expression of each histone.

*2.9.4. Enzyme-Linked Immunosorbent Assay (ELISA).* The supernatants of each group were collected; centrifuged at room temperature, 500 × g, 5 min; and gently absorbed with a pipette gun, and the contents of IL-1$\beta$ and TNF-$\alpha$ were measured according to the instructions of IL-1$\beta$ and TNF-$\alpha$ ELISA kits.

*2.10. BMSC-Exo Promotes Autophagy by Inhibiting the Akt-mTOR Pathway.* NPCs were divided into the following groups: degeneration group: normally cultured NPCs were incubated with 2 ml of F12 complete medium containing 500 $\mu$g/ml LPS for 48 h; exosome group: normally cultured NPCs were incubated with 2 ml of F12 complete medium containing LPS of 500 $\mu$g/ml as well as BMSC-Exo 20 $\mu$g for 48 h; pathway activation group: normally cultured NPCs were incubated with F12 complete medium at 20 ng/ml containing LPS of 500 $\mu$ g/ml and Akt-mTOR pathway insulin-like growth factor-1 (IGF-1) as well as BMSC-Exo 20 $\mu$g for 48 h. Western blot detects Akt-mTOR pathway protein expression in NPCs.

*2.11. Establishment of Animal Model*

*2.11.1. Animals Were Divided into Three Groups. Control group*: the animal model of IDD in rats was established by needle puncture of the annulus fibrosus. The specific method was as follows: healthy SPF male SD rats were anesthetized by intraperitoneal injection of 1% pentobarbital sodium solution at 0.4 mL/kg; they were placed in a prone position to disinfect the skeletons and tails. The No. 21 injection needle was used to puncture the intervertebral space vertically through the dorsal center for about 5 mm; the needle was rotated 360 degrees and stayed for 30 s. After disinfection, the rats were free to move and then, the animal model of intervertebral disc degeneration was established. A little saline was then injected into the site of the disc space.

*Exosome treatment group (exosome)*: exosomes were injected for 30 $\mu$g into the exposed disc space in the rat IDD model.

*Pathway activation group (IGF-1)*: IGF-1 60 ng as well as 30 $\mu$g of exosomes was injected into the site of the exposed disc space in the rat IDD model.

*2.11.2. Histological Examination.* Rats were sacrificed after 8 weeks; Co9/10 disc tissue was taken and fixed with 10% neutral formaldehyde, paraffin-embedded after decalcification with 10% EDTA for 4 weeks, then sectioned, followed by HE staining and immunohistochemical staining for type II collagen; and then, nucleus pulposus tissue damage was observed under a microscope. The acquired images were collected on an image analysis system and analyzed with Image-Pro Plus 6.0 software.

*2.11.3. Inspection.* An MRI examination was performed 4 weeks and 8 weeks after injection to assess the degree of disc degeneration. 1.5 T MRI (GE HDx, Milwaukee, WI, USA) was used to obtain sagittal T2-weighted images, on which the three groups of model animals were classified from grades I to V according to the modified Thompson score (I means normal; II means slightly decreased signal, but the high signal area decreased significantly; III means moderately decreased signal; and IV means significantly decreased signal intensity).

*2.12. Statistical Analysis.* The measurement data were expressed by mean ± standard deviation ($\bar{x} \pm S$), the comparison among multiple groups was analyzed by ANOVA analysis, a $t$-test was used for the comparison between two groups, and SPSS 20.0 software was used for statistical analysis of experimental data, and $P < 0.05$ was considered statistically significant.

## 3. Result

*3.1. The Identification of Rat BMSCs, NPCs, and BMSC-Exo.* The BMSCs grew evenly in a long spindle-like morphology (Figure 1(a)) under light microscopy (×100). Oil Red O staining (Figure 1(b)), Alizarin Red staining (Figure 1(c)), and Alcian Blue staining (Figure 1(d)) showed that the BMSCs could differentiate into adipocytes, osteoblasts, or chondrocytes. Flow cytometry was used to detect the specific expression of CD90 and CD29 on the membrane surface of BMSCs, while the expression of CD34 and CD45 was not detected (Figure 1(e)). Primary NPCs were cultured for 14 d and the morphology changed to a long spindle containing secretory granules (Figure 1(f)). Toluidine blue-stained nuclei were blue and showed a slightly lighter extracellular matrix, indicating that cells can secrete glycosaminoglycans (Figure 1(g)). Type II collagen immunocytochemical staining showed that the cytoplasm was stained in brown-yellow, indicating type II collagen expression within the cytoplasm (Figure 1(h)). The BMSC-Exo was characterized via TEM, NTA, and Western blot. TEM data showed that exosomes

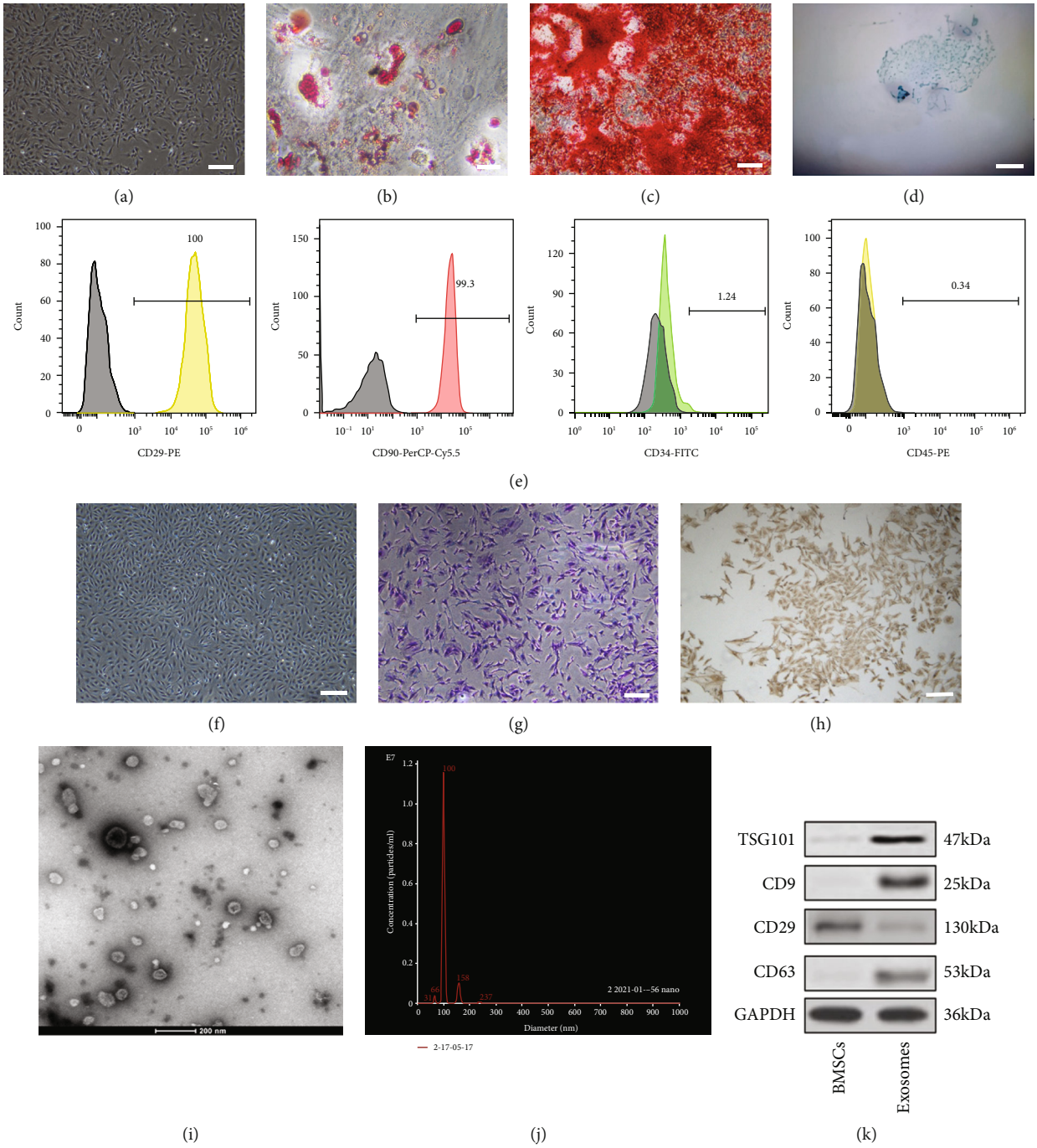


Figure 1: Continued.

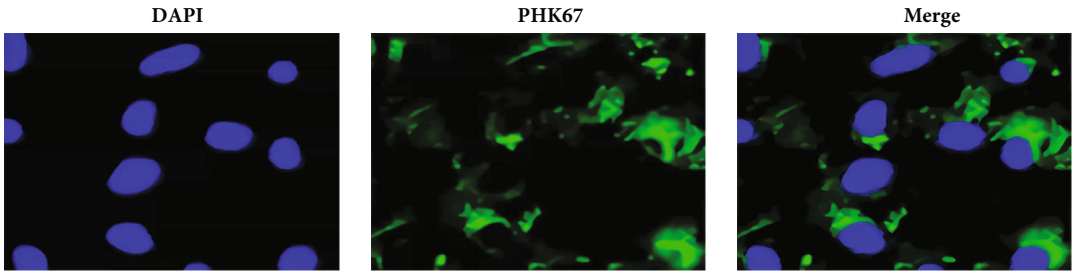


(l)

Figure 1: Morphology and characterization of BMSCs, NPCs, and BMSC-Exos: (a) P0-generation BMSC morphology (scale bar: 200 $\mu$m); (b) Oil Red O staining (scale bar: 100 $\mu$m); (c) Alizarin Red staining (scale bar: 100 $\mu$m); (d) Alcian Blue staining (scale bar: 50 $\mu$m), $n = 3$; (e) flow cytometric analysis of BMSC surface markers (CD29, CD90, CD34, and CD45); (f) NPC morphology (scale bar: 200 $\mu$m); (g) toluidine blue staining of NPCs (scale bar: 100 $\mu$m); (h) type II collagen immunochemical staining of NPCs (scale bar: 100 $\mu$m); (i) transmission electron microscopy (TEM) image of BMSC-Exo (scale bar: 200 nm); (j) NanoSight tracking analysis (NTA) for the diameters of BMSC-Exo; (k) Western blot analysis of CD9, CD63, and TSG101, $n = 3$; (l) analysis of cellular exosome uptake by NPCs. $n = 3$. Scale bar: 25 $\mu$m.

had a cup-shaped structure with a diameter of about 100 nm (×50,000) (Figure 1(i)). NTA demonstrated that the diameter of exosomes was mostly 100 nm (Figure 1(j)). Western blot results showed that the maker proteins of the exosome membrane, CD9, CD63, and TSG101, were expressed in exosomes and CD29 in BMSCs (Figure 1(k)). The exosomes stained by PKH67 staining showed green fluorescence, and the nucleus in NPCs stained by DAPI staining showed blue fluorescence, through being codisplayed; the exosomes in NPCs showed green fluorescence in the nucleus pulposus cytoplasm, suggesting that the exosomes have the ability of membrane fusion and can be ingested by NPCs (Figure 1(l)).

*3.2. BMSC-Exo Inhibits NPC Apoptosis by Promoting Autophagy.* To induce the apoptosis of NPCs, we cultured the NPCs with LPS gradient concentration (0, 100, 200, 500, and 1000 $\mu$g/ml). The CCK-8 results showed that after being treated with 500 $\mu$g/ml LPS, the integrated optical density (IOD) values decreased significantly ($P < 0.01$) (Figure 2(a)); we therefore established the apoptosis model by treating NPCs with 500 $\mu$g/ml LPS. After being treated with BMSC-Exo gradient concentration (12, 16, 20, and 30 $\mu$g/ml) for 48 h, the viability of NPCs increased gradually (Figure 2(b)). Compared with the control group, the mRNA expression of COL2A1 significantly decreased, while the expression of Beclin-1 and IL-1$\beta$ significantly increased in the model group (treated with 500 $\mu$g/ml LPS) ($P < 0.01$); compared with the model group, the mRNA expression of COL2A1 and Beclin-1 increased significantly, while the expression of IL-1$\beta$ decreased in the exosome treatment group (treated with 500 $\mu$g/ml LPS and 20 $\mu$g/ml BMSC-Exo) ($P < 0.01$); compared with the exosome treatment group, the mRNA expression of COL2A1 and Beclin-1 decreased significantly, while the expression of IL-1$\beta$ increased significantly in the autophagy inhibition group (treated with 500 $\mu$g/ml LPS, 20 $\mu$g/ml BMSC-Exo, and 10 mM 3-MA) ($P < 0.01$) (Figure 2(c)). Furthermore, we detected the autophagy and apoptosis-related protein (Col2a1, Baxter, LC3, Beclin-1, and Cleaved Caspase-3) expression with Western blot analysis and the release of IL-1$\beta$ and TNF-$\alpha$ with ELISA, which was consistent with the mRNA expression (Figures 2(d)–2(g)). In summary, these results demonstrated that BMSC-Exo inhibits NPC apoptosis by promoting autophagy.

*3.3. BMSC-Exo Promotes Autophagy by Inhibiting the Akt-mTOR Pathway.* To elucidate the mechanism by which exosomes promote autophagy, NPCs were divided into three groups: degeneration group, exosome group, and pathway activation group. The relative expressions of autophagy pathway-related proteins like p-Akt, p-mTOR, and LC3 II/I in NPCs were detected by Western-blot. The results showed that compared with the degeneration group, p-Akt/Akt and p-mTOR/mTOR were significantly reduced, and LC3 II/I was significantly increased in the exosome group. Compared with the exosome group, p-Akt/Akt and p-mTOR/mTOR were significantly increased, while LC3 II/I was significantly decreased in the pathway activation group (Figure 3(a)). Thus, exosomes could significantly reduce the relative expression of p-Akt and p-mTOR; however, when the Akt-mTOR pathway was activated, the levels of p-mTOR and p-Akt were recovered and autophagy levels were reduced, suggesting that exosomes facilitate autophagy by inhibiting the Akt-mTOR pathway in LPS-induced degeneration of NPCs.

*3.4. BMSC-Exo Promotes Autophagy to Alleviate Disc Degeneration through Inhibition of the Akt-mTOR Pathway in the Rat IDD Model.* In further studies, we established a rat model of intervertebral disc degeneration to observe the therapeutic effect of BMSC-Exo on the degeneration. MRI scans were performed on all of the rats. The results showed a significant decrease in the exosome group in terms of the T2-weighted phase of Thompson scores at the 8th week of treatment ($P < 0.05$) compared with the other two groups (Figures 4(a) and 4(c)). Staining in the control and pathway activation groups showed a reduction in the disc nucleus and the number of nucleus cell number and also a damage in disc annulus fibrosus. However, more nucleus pulposus cells and annulus fibrosus were intact in the exosome treatment group (Figures 4(b) and 4(d)). The function of the disc was

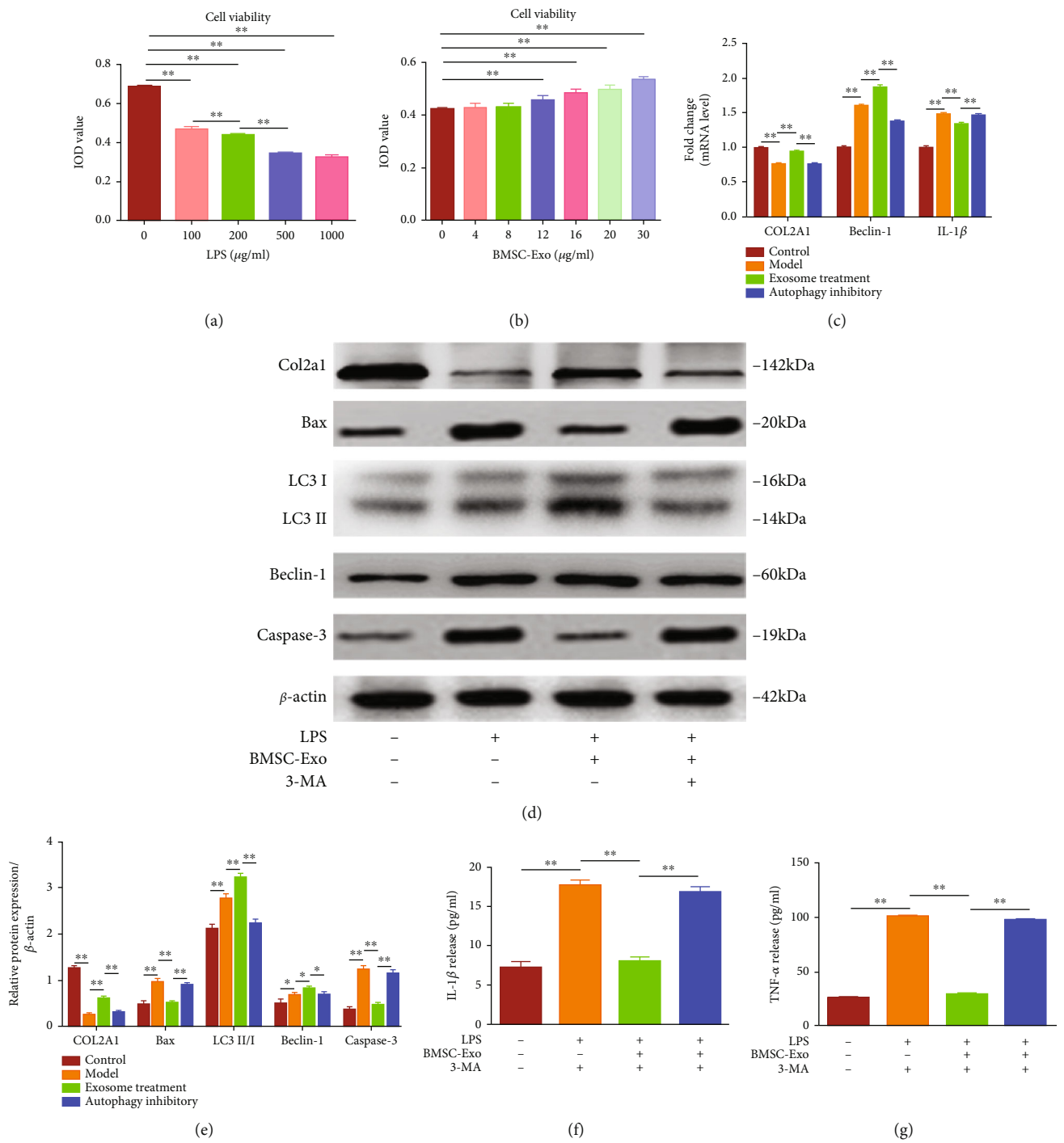


Figure 2: BMSC-Exo inhibits NPC apoptosis by promoting autophagy: (a) the integrated optical density (IOD) of NPCs treated with LPS gradient concentration; (b) IOD of NPCs treated with BMSC-Exo gradient concentration; (c) the mRNA expression of NPCs after incubation with LPS, BMSC-Exo, or 3-MA; (d–g) protein levels of autophagy and apoptosis-related protein (Col2a1, Baxter, LC3, Beclin-1, and Cleaved Caspase-3) in NPCs after being treated with LPS, BMSC-Exo, or 3-MA. $n = 6$. Data are presented as mean ± SD. Statistical analysis was performed with Student's $t$-test and one-way ANOVA followed by Tukey's multiple comparisons test. $^{*}P < 0.05$; $^{**}P < 0.01$.

determined by collagen II. Administration of exosomes resulted in increased expression of type II collagen compared to the control and pathway activation groups (Figure 4(e)). This suggests that exosomes can contribute to the recovery of the structure and function of disc degeneration and effectively promote the synthesis and secretion of the major matrix components in disc degeneration, which is achieved through the activation of the Akt-mTOR pathway.

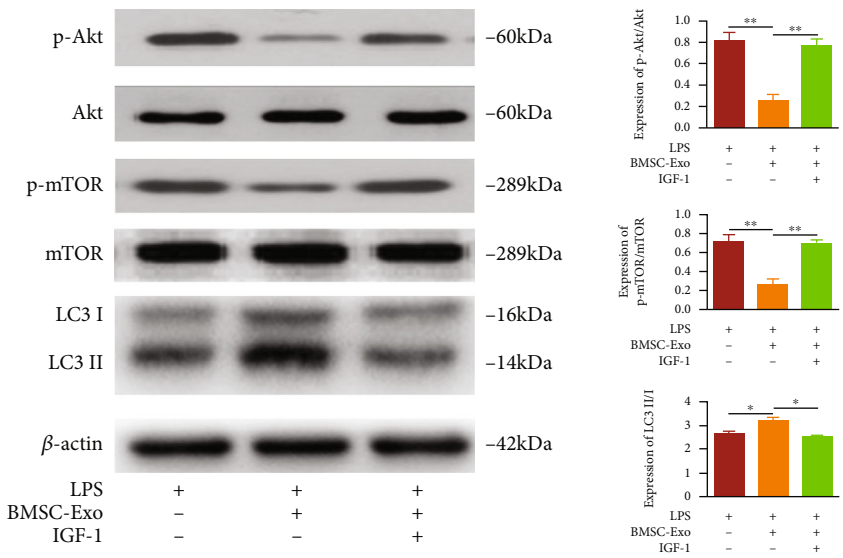


Figure 3: Western blot detects the relative expression changes of p-Akt, Akt, p-mTOR, mTOR, and LC3 in each group. $n = 6$. $^{*}P < 0.05$; $^{**}P < 0.01$.

## 4. Discussion

The pathogenesis of IDD is unknown, and evidence has been established that the pathological process of disc degeneration is strongly associated with increased oxidative stress, inflammatory factors, apoptosis, and increased matrix metalloproteinases [12]. The inflammation is most closely related to the NPCs, and the inflammatory factors play an essential role [14, 15]. Proinflammatory factors not only inhibit the synthesis of the extracellular matrix but also induce apoptosis, leading to a decrease in the number of the NPCs, which further aggravates IDD [12]. It has been shown that MSC-derived exosomes can inhibit the inflammatory response in the disc and thus reduce the apoptotic response of NPCs, but the mechanism is not clear. Therefore, it is necessary to investigate the mechanism of MSC-derived exosomes in the disc inflammatory response and apoptosis.

Exosomes are microvesicles measuring around 40–100 nm in diameter and contain a variety of biologically active substances [16]. Studies have shown that exosomes play an important role in cellular communication and metabolic regulation [17]. BMSC-Exo inhibits the activation of inflammatory mediators and reduces nucleus pulposus cell apoptosis [11]. Exosome separation and extraction methods predominantly include ultracentrifugation, polymer precipitation, ultrafiltration, immunoaffinity, and microfluidic separation technology. Ultracentrifugation is the "gold standard" and the most widely used [18]. The method was used to extract exosomes in this study. The International Society for Extracellular Vesicles stipulates that the identification of exosomes must include particle size, morphology, and protein molecular markers [19]. The extracted exosomes were identified by observing the particle size with a nanoparticle tracking analyzer and detecting surface markers with immunoblotting assays, and using immunofluorescence assay, it was confirmed that they could be ingested by NPCs. We found that the apoptosis in the exosome group was blindingly evident by flow cytometry, suggesting that BMSC-Exo can be ingested by NPCs and reduce their apoptosis.

LPS is an important proinflammatory factor in the human body that can induce strong inflammation in NPCs leading to apoptosis, reducing extracellular matrix synthesis, and plays an important role in IDD [12]. LPS can activate the inflammatory response to promote apoptosis [12]. Therefore, LPS was selected as the induction medium in our study; it was found in the CCK-8 experiment that the *A* value gradually decreased with the increase of LPS concentration, it was positively correlated with cell viability, and there was no significant difference in this value between the groups tested with LPS 500 $\mu$g/ml and 1000 $\mu$g/ml. Therefore, we used LPS 500 $\mu$g/ml concentration to establish the cell apoptosis model and detect the apoptosis rate by flow cytometry; it was observed that LPS effectively induced the apoptosis of NPCs.

It was shown that disc degeneration could produce a large number of inflammatory factors, such as TNF-$\alpha$ and IL-1$\beta$ [20]. As an initiation factor of inflammation, TNF-$\alpha$ can stimulate the expression of other inflammatory factors, and there is also a synergy between TNF-$\alpha$ and the stimulated inflammatory factors, such as IL-1$\beta$, showing a "positive feedback" effect [21]. It was found that the extracellular matrix degradation was increased after stimulation of NPCs by IL-1$\beta$, advancing the development of IDD [22]. Therefore, the inflammatory state of the cells can be understood by the detection of TNF-$\alpha$ and IL-1$\beta$. In this experiment, we examined the expression of IL-1$\beta$ mRNA by RT-qPCR and found that the expression of IL-1$\beta$ mRNA was significantly increased in NPCs after LPS-induced degeneration, and that of IL-1$\beta$ mRNA was significantly decreased after the treatment with exosome. The detection of the concentrations of TNF-$\alpha$ and IL-1$\beta$ concentrations in the supernatant for each group by ELISA showed that the concentrations in the model group increased apparently compared with the those in the control group, and those in

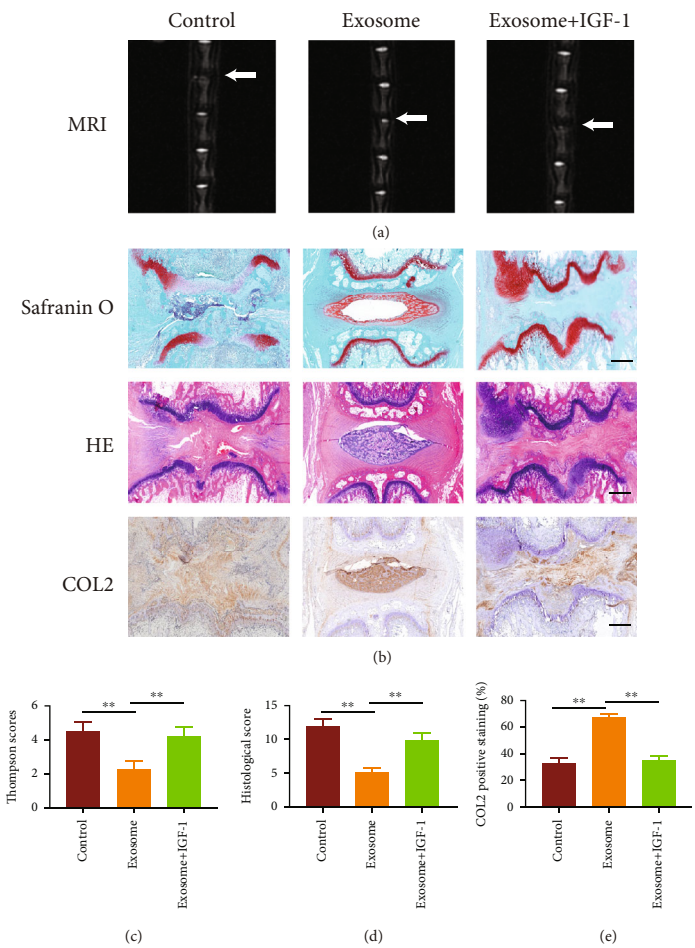


Figure 4: Results of the experiments in live animals. (a) MRI findings after injection of exosomes and IGF-1 into the caudal disc of a rat. (b) Histological analysis of HE and S/O staining discs. Immunohistochemical staining of type II collagen showed the presence of type II collagen in the exosome group, but little in the control and exosome+IGF-1 groups. Scale bar: 100 $\mu$m. (c) Thompson scores of three groups. The score of the exosome group is lower than that of the other groups. (d) Histological score showed significant imaging improvement at week 8 of the therapy with exosome, but higher in the control and exosome+IGF-1 groups; (e) Immunohistochemical staining of type II collagen area (%). $^{**}P < 0.01$.

the exosome group were significantly lower compared with those the model group. All of the results suggested that LPS promoted the inflammatory response of NPCs but exosomes inhibited it.

Autophagy, which is a key adaptive response, is a cellular self-protective process that can degrade and recycle intracellular damaged organelles and proteins [23]. It plays a key role in the pathogenesis of degenerative diseases (such as osteoarthritis and Alzheimer disease) [24]. Xu et al. found that autophagy attenuated the catabolic effect of NPCs in rats [25]. Therefore, we hypothesized that the inhibitory and antiapoptotic effects of the MSC-derived exosome may also be linked to autophagy.

LC3 protein is known to be important throughout autophagy. In the process of autophagy, the newly synthesized carbon terminal of LC3 is hydrolyzed by cysteine protease to generate LC3I. With the progression of the autophagy process, LC3I covalently binds phosphatidylethanolamine to form LC3II catalyzed by a ubiquitin-like reaction enzyme [23]. The ratio of LC3II/LC3I, as the end product of autophagy, is positively associated with the level of autophagy. Beclin-1 was the first identified mammalian autophagy-related gene, and it is considered a positive regulatory molecule of autophagy [24]. Therefore, the occurrence of autophagy can be reflected by detecting the content of LC3II/LC3I and Beclin-1. By measuring the Beclin-1 mRNA expression using RT-qPCR, it was found that the expression in the model group was significantly higher than that of the control group, and the Beclin-1 mRNA expression was further increased in the exosome group compared with the model group. Similar results were found in the detection of protein expression of LC3II/LC3I and Beclin-1 in each group by Western blot. The protein expression of LC3II/LC3I and Beclin-1 in the model group was increased significantly compared with that in the control group, whereas the expression was further increased in the exosome group compared to the model group. All of the results indicated that exosomes could promote autophagy in nucleus pulposus cells.

To investigate the relationship between the antiapoptotic effect of BMSC-Exo on nucleus pulposus cells and

autophagy, we employed the autophagy pathway inhibitor 3-MA which can prevent the formation of autophagosome by inhibiting phosphoinositide 3-kinase (PI3K) and thus fundamentally inhibit autophagy from the source. We examined the expression of IL-1$\beta$ mRNA by RT-qPCR after inhibiting autophagy using 3-MA and found that the expression of IL-1$\beta$ mRNA increased again. However, the TNF-$\alpha$ and IL-1$\beta$ content of supernatants in each group also found that the TNF-$\alpha$ and IL-1$\beta$ contents were significantly increased in the autophagy inhibition group compared with the exosome group. All the results suggest that the inhibitory effect of exosomes is reversed after autophagy is inhibited, suggesting that exosomes may produce the effect of inhibiting inflammation by promoting autophagy. The flow cytometry showed that exosomes could inhibit apoptosis of nucleus pulposus cells due to LPS, while the rate of apoptosis increased again after inhibition of autophagy using 3-MA. Additionally, we examined the nucleus myelocytes Bax, Cleaved Caspase-3, and type II collagen by Western blot. Bax is an important factor in the regulation of apoptosis and mainly resides in the cytoplasm, which mediates the release of downstream apoptotic molecules and triggers apoptosis [26, 27]. The apoptosis may occur when Bax expression is upregulated [28, 29]. Caspase-3 is a key molecule for performing apoptosis, and as an activated form of Caspase-3, the formation of Cleaved Caspase-3 marks irreversible apoptosis [30]. Type II collagen is an important component of the disc, and it is found that this collagen in the disc is significantly decreased in IDD patients [31]. Therefore, the expression of type II collagen in nucleus pulposus cells is positively correlated with the degree of degeneration. Results are shown: the expression of Cleaved Caspase-3, Bax, and type II collagen was decreased significantly in the model group compared with the control group. In comparison with the model group, the expression of type II collagen was increased and that of Cleaved Caspase-3 and Bax decreased significantly in the exosome group. Compared with the exosome group, Cleaved Caspase-3 and Bax showed an evident increase, and that of type II collagen was significantly decreased in the autophagy inhibition group. In this experiment, we also investigated the expression of type II collagen by RT-qPCR experiments for each group, and the results showed that the expression of mRNA in the model group was significantly reduced compared with that in the control group, whereas that of the mRNA in the exosome group of collagen mRNA expression was significantly increased compared with that in the model group, and that of the collagen was decreased in the autophagy inhibition group as compared to the exosome group. All the results indicate that exosomes can inhibit nucleus pulposus cell apoptosis, but its antiapoptotic effect is basically reversed after autophagy is inhibited, suggesting that BMSC-Exo may exert an antiapoptotic effect by promoting autophagy.

Numerous studies have shown that the Akt-mTOR signaling pathway is an important pathway to regulate the biological functions of various cells [32–34], including the regulation of the biological function of NPCs [35–37]. The Akt-mTOR signaling pathway is also involved in the progression of various human degenerative diseases, including the degeneration of nucleus pulposus cells [38]. As a typical autophagy signaling pathway, the Akt-mTOR pathway shows a negative role in the regulation of autophagy. We therefore hypothesized that BMSC-Exo would probably produce anti-inflammatory and antiapoptotic effects by inhibiting Akt-mTOR signaling to promote the autophagy of nucleus pulposus cells.

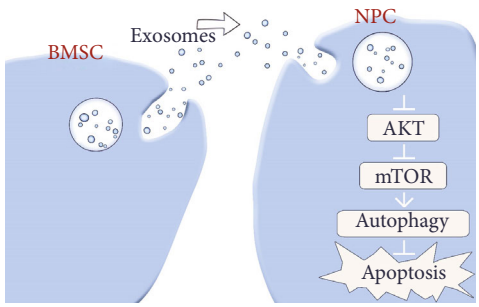


Figure 5: MSC-derived exosomes mitigate apoptosis against LPS-induced apoptosis by promoting nucleus pulposus cell autophagy, which is achieved through the Akt-mTOR signaling pathway.

To prove this hypothesis, we applied the pathway activator IGF-1 on degenerative nucleus pulposus cells after exosome treatment. We examined the activation of the Akt-mTOR pathway by Western blot to test the phosphorylation-activated mTOR (p-mTOR) and phosphorylation-activated Akt (p-Akt) and investigated the changes in LC3/LC3I expression as well as the activation of autophagy. It was found that the autophagy protein LC3II/LC3I increased markedly and the pathway proteins p-mTOR and p-Akt showed a decline in the exosome group, while the expression of autophagy-related protein LC3II/LC3I was significantly decreased in the pathway activation group, and the expressions of p-Akt and p-mTOR protein were significantly higher than the exosome group ($P < 0.05$), suggesting that the Akt-mTOR signaling pathway was involved in the exosome-regulated autophagy process in nucleus pulposus cells.

Taken together, MSC-derived exosomes mitigate apoptosis against LPS-induced apoptosis by promoting nucleus pulposus cell autophagy, which is achieved through the Akt-mTOR signaling pathway (Figure 5). This study reveals the likely mechanism of exosomes alleviating LPS-induced inflammatory damage and apoptosis, which will provide a new direction for the treatment of IDD. However, it should be noted that all the current studies on exosomes are still in the basic research stage, and there are still many problems to be solved. The first thing is that there are certain differences between people and animals. Secondly, exosomes cannot be mass-produced, which also limits their clinical application [39]. Additionally, exosomes isolated from biofluid are impure and highly variable. Moreover, subsets of exosomes and the specific mechanisms underlying their effects on receptor cells remain poorly defined. Therefore, despite some achievements made in the treatment of IDD with exosomes, there is still a long way to go before it can be put into clinical application. It is believed that with the progress of the research, the treatment with exosomes will eventually become a new regimen for the clinical treatment of IDD.

## Data Availability

The data used to support the findings of this study are available from the corresponding author upon request.

## Conflicts of Interest

The authors declare that they have no conflicts of interest.

## Authors' Contributions

Quan Xiao, Yun Teng, and Zhe Zhao collected the data. Quan Xiao, Lungang Wu, and Jinlong Wang performed the experiments. Quan Zhou, Sumei Chen, and Zhe Zhao analyzed data and interpreted them. Yun Teng, Hongjun Xu, and Lungang Wu searched the literature and completed picture processing. Quan Zhou, Quan Xiao, and Zhe Zhao wrote the paper. Quan Zhou and Quan Xiao designed and funded the studies. All authors read and approved the final manuscript. Quan Xiao, Zhe Zhao, and Yun Teng contributed equally to this work.

## Acknowledgments

This work was supported by Scientific Research Project of Jiangsu Provincial Health Commission (M2020103) and Huai'an Natural Science Research Plan (HAB201953).

## References

[1] M. T. Modic and J. S. Ross, "Lumbar degenerative disk disease," *Radiology*, vol. 245, no. 1, pp. 43–61, 2007.

[2] B. Pennicooke, Y. Moriguchi, I. Hussain, L. Bonssar, and R. Hartl, "Biological treatment approaches for degenerative disc disease: a review of clinical trials and future directions," *Cureus*, vol. 8, no. 11, article e892, 2016.

[3] F. Ding, Z. W. Shao, and L. M. Xiong, "Cell death in intervertebral disc degeneration," *Apoptosis*, vol. 18, no. 7, pp. 777–785, 2013.

[4] G. Xu, Q. Mei, D. Zhou, J. Wu, and L. Han, "Vitamin D receptor gene and aggrecan gene polymorphisms and the risk of intervertebral disc degeneration - a meta-analysis," *PLoS One*, vol. 7, no. 11, article e50243, 2012.

[5] J. W. Chen, B. B. Ni, B. Li, Y. H. Yang, S. D. Jiang, and L. S. Jiang, "The responses of autophagy and apoptosis to oxidative stress in nucleus pulposus cells: implications for disc degeneration," *Cellular Physiology and Biochemistry*, vol. 34, no. 4, pp. 1175–1189, 2014.

[6] J. Liu, P. Yu, F. Dai, H. Jiang, and Z. Ma, "Tetrandrine reduces oxidative stress, apoptosis, and extracellular matrix degradation and improves intervertebral disc degeneration by inducing autophagy," *Bioengineered*, vol. 13, no. 2, pp. 3944–3957, 2022.

[7] Z. Zheng, Z. G. Wang, Y. Chen et al., "Spermidine promotes nucleus pulposus autophagy as a protective mechanism against apoptosis and ameliorates disc degeneration," *Journal of Cellular and Molecular Medicine*, vol. 22, no. 6, pp. 3086–3096, 2018.

[8] M. Quan, M. W. Hong, M. S. Ko, and Y. Y. Kim, "Relationships between disc degeneration and autophagy expression in human nucleus pulposus," *Orthopaedic Surgery*, vol. 12, no. 1, pp. 312–320, 2020.

[9] C. Y. Gong and H. H. Zhang, "Autophagy as a potential therapeutic target in intervertebral disc degeneration," *Life Sciences*, vol. 273, article 119266, 2021.

[10] W. Li, S. Zhang, D. Wang et al., "Exosomes immunity strategy: a novel approach for ameliorating intervertebral disc degeneration," *Frontiers in Cell and Developmental Biology*, vol. 9, article 822149, 2021.

[11] C. Xia, Z. Zeng, B. Fang et al., "Mesenchymal stem cell-derived exosomes ameliorate intervertebral disc degeneration via anti-oxidant and anti-inflammatory effects," *Free Radical Biology & Medicine*, vol. 143, pp. 1–15, 2019.

[12] W. Yi, Y. Wen, F. Tan et al., "Impact of NF-$\kappa$B pathway on the apoptosis-inflammation-autophagy crosstalk in human degenerative nucleus pulposus cells," *Aging*, vol. 11, no. 17, pp. 7294–7306, 2019.

[13] Q. Xiao, C. Xu, Y. Wang, and Q. Zhou, "Exosomes derived from bone mesenchymal stem cells regulate NF-$\kappa$B signaling pathway to inhibit apoptosis of nucleus pulposus cells," *Southeast National Defense Medicine*, vol. 22, no. 5, pp. 449–455, 2020.

[14] C. Cunha, A. J. Silva, P. Pereira, R. Vaz, R. M. Goncalves, and M. A. Barbosa, "The inflammatory response in the regression of lumbar disc herniation," *Arthritis Research & Therapy*, vol. 20, no. 1, p. 251, 2018.

[15] F. J. Lyu, H. Cui, H. Pan et al., "Painful intervertebral disc degeneration and inflammation: from laboratory evidence to clinical interventions," *Bone Research*, vol. 9, no. 1, p. 7, 2021.

[16] C. Han, X. Sun, L. Liu et al., "Exosomes and their therapeutic potentials of stem cells," *Stem Cells Int.*, vol. 2016, article 7653489, 11 pages, 2016.

[17] Z. Li, Y. Wang, K. Xiao, S. Xiang, Z. Li, and X. Weng, "Emerging role of exosomes in the joint diseases," *Cellular Physiology and Biochemistry*, vol. 47, no. 5, pp. 2008–2017, 2018.

[18] B. Zhang, L. Shen, H. Shi et al., "Exosomes from human umbilical cord mesenchymal stem cells: identification, purification, and biological characteristics," *Stem Cells International*, vol. 2016, Article ID 1929536, 11 pages, 2016.

[19] S. Gurunathan, M. H. Kang, M. Jeyaraj, M. Qasim, and J. H. Kim, "Review of the isolation, characterization, biological function, and multifarious therapeutic approaches of exosomes," *Cells*, vol. 8, no. 4, p. 307, 2019.

[20] A. Tekari, A. Marazza, K. Crump, P. Bermudez-Lekerika, and B. Gantenbein, "Inhibition of the extracellular signal-regulated kinase pathway reduces the inflammatory component in nucleus pulposus cells," *Journal of Orthopaedic Research*, 2022.

[21] H. Kang, Y. Dong, R. Peng et al., "Inhibition of IRE1 suppresses the catabolic effect of IL-1$\beta$ on nucleus pulposus cell and prevents intervertebral disc degeneration in vivo," *Biochemical Pharmacology*, vol. 197, article 114932, 2022.

[22] L. Kang, C. Yang, H. Yin et al., "MicroRNA-15b silencing inhibits IL-1$\beta$-induced extracellular matrix degradation by targeting SMAD3 in human nucleus pulposus cells," *Biotechnology Letters*, vol. 39, no. 4, pp. 623–632, 2017.

[23] Y. Matsuzawa-Ishimoto, S. Hwang, and K. Cadwell, "Autophagy and inflammation," *Annual Review of Immunology*, vol. 36, no. 1, pp. 73–101, 2018.

[24] M. Filfan, R. E. Sandu, A. D. Zavaleanu et al., "Autophagy in aging and disease," *Romanian Journal of Morphology and Embryology*, vol. 58, no. 1, pp. 27–31, 2017.

[25] K. Xu, W. Chen, X. Wang et al., "Autophagy attenuates the catabolic effect during inflammatory conditions in nucleus pulposus cells, as sustained by NF-κB and JNK inhibition," *International Journal of Molecular Medicine*, vol. 36, no. 3, pp. 661–668, 2015.

[26] R. T. Uren, M. O'Hely, S. Iyer et al., "Disordered clusters of Bak dimers rupture mitochondria during apoptosis," *Elife*, vol. 6, 2017.

[27] R. Phonarknguen, S. Nobsathian, and K. Assawasuparerk, "Effect of Betulinic acid extraction from guava (Psidium guajava Linn.) leaves against human cholangiocarcinoma cells," *Asian Pacific Journal of Cancer Prevention*, vol. 23, no. 2, pp. 583–590, 2022.

[28] N. Cil, E. O. Oguz, E. Mete, A. Cetinkaya, and G. A. Mete, "Effects of umbilical cord blood stem cells on healing factors for diabetic foot injuries," *Biotechnic & Histochemistry*, vol. 92, no. 1, pp. 15–28, 2017.

[29] J. Yuan, M. Chen, Q. Xu et al., "Effect of the diabetic environment on the expression of MiRNAs in endothelial cells: Mir-149-5p restoration ameliorates the high glucose-induced expression of TNF-α and ER stress markers," *Cellular Physiology and Biochemistry*, vol. 43, no. 1, pp. 120–135, 2017.

[30] M. Brentnall, L. Rodriguez-Menocal, R. L. De Guevara, E. Cepero, and L. H. Boise, "Caspase-9, caspase-3 and caspase-7 have distinct roles during intrinsic apoptosis," *BMC Cell Biology*, vol. 14, article 32, 2013.

[31] S. Rajasekaran, D. C. R. Soundararajan, and C. Tangavel, "Sri Vijay Anand K. S., Sharon Miracle Nayagam, Monica Steffi Matchado, Raveendran Muthurajan, Ajoy Prasad Shetty, Rishi Mugesh Kanna, K. DharmalingamProteomic signature of nucleus pulposus in fetal intervertebral disc," *Asian Spine Journal*, vol. 14, no. 4, pp. 409–420, 2020.

[32] K. Xu, F. Wu, K. Xu et al., "NaHS restores mitochondrial function and inhibits autophagy by activating the PI3K/Akt/mTOR signalling pathway to improve functional recovery after traumatic brain injury," *Chemico-Biological Interactions*, vol. 286, pp. 96–105, 2018.

[33] M. Choi, S.-M. Moon, S. Lee et al., "Adenosine induces intrinsic apoptosis via the PI3K/Akt/mTOR signaling pathway in human pharyngeal squamous carcinoma FaDu cells," *Oncology Letters*, vol. 15, no. 5, pp. 6489–6496, 2018.

[34] G. Liu, X. Zhao, J. Zhou, X. Cheng, Z. Ye, and Z. Ji, "LncRNA TP73-AS1 promotes cell proliferation and inhibits cell apoptosis in clear cell renal cell carcinoma through repressing KISS1 expression and inactivation of PI3K/Akt/mTOR signaling pathway," *Cellular Physiology and Biochemistry*, vol. 48, no. 1, pp. 371–384, 2018.

[35] Y. Xu, H. Yao, P. Li et al., "Dynamic compression promotes the matrix synthesis of nucleus pulposus cells through up-regulating N-CDH expression in a perfusion bioreactor culture," *Cellular Physiology and Biochemistry*, vol. 46, no. 2, pp. 482–491, 2018.

[36] W. Wang, P. Li, J. Xu et al., "Resveratrol attenuates high glucose-induced nucleus pulposus cell apoptosis and senescence through activating the ROS-mediated PI3K/Akt pathway," *Bioscience Reports*, vol. 38, no. 2, 2018.

[37] J. Gao, Q. Zhang, and L. Song, "Resveratrol enhances matrix biosynthesis of nucleus pulposus cells through activating autophagy via the PI3K/Akt pathway under oxidative damage," *Bioscience Reports*, vol. 38, no. 4, 2018.

[38] D. Zhan, M. Lin, J. Chen et al., "Hypoxia-inducible factor-1α regulates PI3K/AKT signaling through microRNA-32-5p/PTEN and affects nucleus pulposus cell proliferation and apoptosis," *Experimental and Therapeutic Medicine*, vol. 21, no. 6, p. 646, 2021.

[39] T. Yamashita, Y. Takahashi, and Y. Takakura, "Possibility of exosome-based therapeutics and challenges in production of exosomes eligible for therapeutic application," *Biological & Pharmaceutical Bulletin*, vol. 41, no. 6, pp. 835–842, 2018.

Hindawi
Stem Cells International
Volume 2022, Article ID 9179111, 9 pages
https://doi.org/10.1155/2022/9179111

*Review Article*

# Mechanical Cues Regulate Histone Modifications and Cell Behavior

**Buwei Hu**,[1,2] **Dandan Zhou**,[3] **Haoming Wang**,[4] **Ning Hu**,[1] **and Weikang Zhao**[1]

[1]*Department of Orthopedics, The First Affiliated Hospital of Chongqing Medical University, Chongqing 40042, China*
[2]*Zhejiang Provincial Laboratory of Life Sciences and Biomedicine, School of Life Sciences, Westlake University, Hangzhou, Zhejiang 310024, China*
[3]*Department of Gastroenterology, The People's Hospital of Jiulongpo District, Chongqing 400050, China*
[4]*Department of Orthopedics, Chongqing University Three Gorges Hospital, Chongqing 404100, China*

Correspondence should be addressed to Haoming Wang; wanghaoming1227@163.com, Ning Hu; huncqjoint@yeah.net, and Weikang Zhao; weikangzhao90@hospital.cqmu.edu.cn

Received 16 November 2021; Accepted 19 March 2022; Published 11 May 2022

Academic Editor: Zhaoji Pan



Change of biophysical factors in tissue microenvironment is an important step in a chronic disease development process. A mechanical and biochemical factor from cell living microniche can regulate cell epigenetic decoration and, therefore, further induce change of gene expression. In this review, we will emphasize the mechanism that biophysical microenvironment manipulates cell behavior including gene expression and protein decoration, through modifying histone amino acid residue modification. The influence given by different mechanical forces, including mechanical stretch, substrate surface stiffness, and shear stress, on cell fate and behavior during chronic disease development including tumorigenesis will also be teased out. Overall, the recent work summarized in this review culminates on the hypothesis that a mechanical factor stimulates the modification on histone which could facilitate disease detection and potential therapeutic target.

## 1. Introduction

In the development of chronic disease, cells are exposed to many stimuli that require distinct response mechanisms to injury and tissue repair. During these processes, cells often exhibit extraordinary cell behavior and activities under change of regular living microenvironment. Cell behavior includes cytoskeleton reorganization, protein activity regulation, gene expression pattern change, and management of posttranscriptional regulation [1–3]. Posttranscriptional regulation requires the recruitment of microRNA and long noncoding RNA (lncRNA), both of them are involved in chronic disease development [4, 5].

Chronic disease is a long-term tissue injury process, resulting in microenvironmental cues that can manipulate cell status. Elegant control of cell behavior is important to reduce the impact given by chronic disease [6]. Furthermore, the change of cell living microenvironment could lead to both biochemical rewiring and physical reshaping of all cellular compartments on both short and long timescales.

Suffering from a long-term tissue injury process, the mechanical factors in the cell microenvironment, including compression, substrate stiffness, stretch, and shear stress, have changed and influenced cell properties [7, 8]. These forces can induce nuclear deformation or activate biochemical pathways and thus regulate the epigenetic state in a mechanotransduction-dependent manner (shown in Figure 1) [9]. Additionally, the chemical and physical signals induced by mechanical stimuli are shaping the cell gene expression pattern based on chromatin remodeling enzymes and the transcriptional machinery [10]. At the same time, epigenetic regulation could manipulate chromosome structure including heterochromatin with limited transcription activity and less condensed, transcription active euchromatin regions. This process is achieved based on the decoration on amino acid residues of histone and their variants,

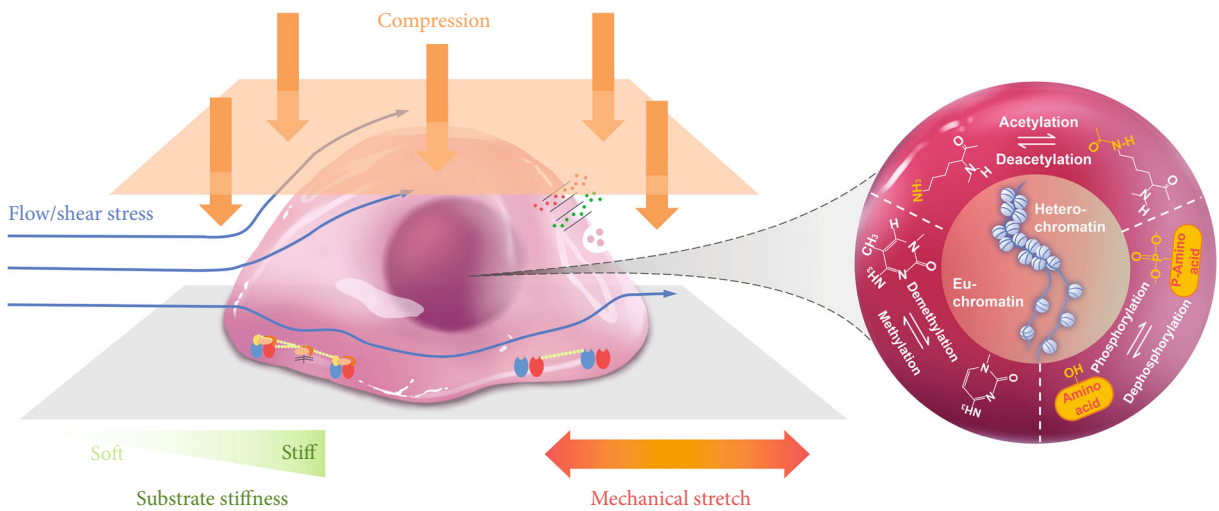


Figure 1: Mechanical cues regulate histone modifications to modulate cell fate. Various mechanical stimuli, including substrate stiffness, mechanical stretch, topological substrate, shear stress, compression, and squeezing, modulate histone modifications, which regulate chromatin reorganization and cell plasticity.

including methylation and acetylation [11, 12]. The acetylation/deacetylation of histones controls global chromatin structure and influences the gene active transcription area [13]. Methylation/demethylation of DNA is also involved in modulating chromatin condensation, and this process is highly correlated with cell metabolism and behavior [14]. Overall, these epigenetic modifications could be caused by the change of mechanical microenvironment and impact cell gene expression and, therefore, further promote chronic disease development and set barriers to patient recovery. In this review, we will discuss how various mechanical cues modulate cell behavior based on histone modification.

## 2. Extracellular Matrix Stiffness

Many studies have shown that the tissue fibrosis escalates the stiffness of the extracellular matrix (ECM) playing an influential role in tumor development and atherosclerosis [1, 3]. The ECM of tumor consists of collagen I, elastin, fibronectin, hyaluronan, and sulfated glycosaminoglycan. The cancer-associated fibroblast (CAF) secretes the majority of ECM components and facilitates tumor microenvironment construction [1]. Increasing ECM stiffness further manages fibroblast ECM secretion and macrophage cytokine production, induces cancer cell proliferation, and promotes metastasis [2].

During lung cancer development, the epigenetic modification on an oncogene promoter facilitates the construction of mechanical microenvironment. Under stimulation, the Yes-associated protein (YAP) aggregates in the nucleus of the human lung adenocarcinoma cell (H1299), which is induced by RASFF1A promoter methylation and promotes prolyl 4-hydroxylase alpha-2 (P4HA2) expression. The expression of P4HA2 further induces collagen production and makes the substrate stiffer [15]. Similarly, in gastric cancer, YAP reciprocally interacts with DNA methylation inhibitors GRHL2, TET2, and KMT2A to prevent YAP promoter methylation, causing oncogenic activation of YAP [16]. On the soft substrate, Liu et al. reported CDC42 accumulation in the cell nucleus and promote Tet2 expression, which demethylates the promoter of P21 and P27 to shift the cancer cell to dormancy status, which helps cancer cells overcome harsh conditions [17]. Under similar conditions, tumor-repopulating cells (TRC) preserve their plasticity through downregulating G7a to reduce histone3 lysine residue 9 (H3K9) methylation and result in Sox2 expression [18]. Based on these mechanisms, cancer cells can preserve their plasticity and halt their proliferation progress until reaching appropriate position for tumor regeneration.

Not only cancer but also tissue fibrosis process happening on different organs can manipulate cell epigenetic change and result in organ pathological damage. The lung epithelial cell during idiopathic pulmonary fibrosis escalates desmoplakin (DSP) expression due to demethylation of its promoter. Accumulation of DSP increases cell-cell adhesion force and promotes lung fibrosis [19]. Furthermore, H3K9me decoration maintains lung fibroblast under activation status to produce collagen during lung fibrosis. The G9a and CBX5 histone methyltransferase is activated in a stiffer matrix and mediates histone methylation to induce ECM protein overexpression [20]. Similar to lung fibroblast, stiffness of the substrate also can regulate vascular smooth muscle cell (VSMC) epigenetic modification. On higher stiffness ECM, VSMC downregulates the expression of DMNT1 and reduces the general methylation status. Xie et al. reported that DMNT1 can manipulate the promoter of SM22a and SMA, both of them were involved in SMC functional contractility and induce vascular disease [21]. Altogether, these studies demonstrate that matrix stiffness can modulate the epigenome to facilitate disease development and impact the cell gene expression pattern (Table 1).

Table 1: Summary of the effects of matrix stiffness on histone modifications in cell plasticity.

| Cell type | Stiffness tested | Epigenetic modification | Function | Ref. |
|---|---|---|---|---|
| H1299 | 0.5-25 kPa | DNA methylation | RASSF1A promoter methylation | [15] |
| MDA-MB-231 | 0.5-50 kPa | Histone demethylation | ECM stiffness regulates histone demethylase JMJD1a nuclear aggregation | [22] |
| Fibroblast | 0.2-64 kPa | H3K9me2/3 | Stiff matrices increase global H3K9me2/3 | [20] |
| A549 | 1-20 kPa | DNA hypomethylation/ demethylation | Observed DNA hypomethylation/demethylation under stiff matrix conditions | [19] |
| MEFs | 0.5-100 kPa | Histone deacetylation | HDAC4 expression increased | [23] |
| HUASMCs | 2.16-16.75 kPa | DNA methylation | Substrate stiffening downregulation of DNMT1 and DNA methylation | [21] |
| AGS | 0.5-7 kPa | DNA methylation | Stiffer substrate induces reduction in global methylation | [16] |
| TRC | 50-1050 Pa | DNA methylation | Soft surface demethylates p21 and 27 promoters | [17] |
| DLD-1 | 0.4-25.6 kPa | H3K4me3 | Reduction of H3K4me3 on softer matrices | [19] |
| TRC | 50-1050 Pa | H3K9me | Softening of the matrix reduces H3K9 methylation | [18] |
| MEF | 0.5-20 kPa | Microtubule acetylation | Soft matrix modulates microtubule acetylation | [24] |

MSCs: mesenchymal stem cells; HSCs: hepatic stellate cells; hMSCs: human mesenchymal stem cells; MCF10A: mammary epithelial cells; A549: human alveolar epithelial adenocarcinoma cells; DLD-1: colorectal adenocarcinoma cells; MEFs: mouse embryonic fibroblasts; HUASMCs: human umbilical artery smooth muscle cell; H1299: human lung adenocarcinoma cell; MDA-MB-231: breast cancer cell; AGS: human gastric cancer cell; TRC: tumor repopulating cell; HDAC: histone deacetylase.

## 3. Mechanical Strain

Mechanical stretch is another biophysical factor that can influence cell gene expression, disease development, and tissue regeneration. Cells in the vascular wall and lung tissue are permanently exposed to cyclic or stain mechanical stretch. Under high blood pressure, cyclic strain on vascular cell increases vascular wall thickness and facilitates reactive oxygen species (ROS) generation [25]. Similar to the vessel, cyclic stretch in the lung stimulates local fibroblast and macrophage change biochemical microenvironment [26]. In addition to the influence on cell physiological status, mechanical strain is also involved in the tissue regeneration process.

Cyclic strain has already shown potential to mediate tissue regeneration including the osteogenesis process [27]. With strain stimulation, the epigenetic status of cell is changed and regulates cell differentiation. DNA methylation is a common epigenetic modification that is modulated during cell differentiation. Human adipose tissue multipotential stromal cell (hAT-MSCs) promote osteogenic induction by cyclic stretch-induced DNA demethylation on the CpG of the GNAS gene[28].

In addition to DNA methylation, the modification of histones is another epigenetic mechanism that is influenced by mechanical stretch. HDACs regulate histone acetylation, thereby modulating the chromatin state and gene expression. In lung endothelial dysfunction, cyclic stretch induces HDAC6 activation and is downregulated in endothelial cells (EC) and results in a-tubulin deacetylation[29]. However, instead of changes in tubulin modification, HDAC4 translocation from the cytoplasm to the nucleus in murine chondrocytes after stretch repressed RUNX-2 expression [30]. In chondrocytes, cyclic stretch also stimulates the expression of ADAMTS-5 which could induce osteoarthritis. The inhibitor of HDAC could reduce the expression of ADAMTS-5 and provide a potential solution for osteoarthritis [31]. Although numerous studies have shown that mechanical stretch can regulate HDAC expression, further research into the mechanism of this HDAC regulation is still required.

Recent studies demonstrating the mechanism of post-transcriptional regulation, including microRNA and lncRNA, in the cell under strain can provide some valuable insight into the direction for future research. Interestingly, in human chondrocytes, miR-365 levels decreased after stretch, which led to a downregulation of ACAN gene expression and cartilage degeneration [32]. Also, after stretch, HPMEC expressed lncRNA mainly enriched in response to hypoxia and inflammatory response. This result provides a research clue on ventilator-induced lung injury [33]. Therefore, it may be possible that mechanical strain induces specific microRNAs in different cell types to influence the expression of histone modification marks and as a result mediate the epigenetic state and cell gene expression.

Cell proliferation is also involved in disease development progress. Cell division could be facilitated through histone 3 phosphorylation (H3P), which can produce a loosen chromatin region for active gene expression. In response to mechanical strain, the activation of the Piezo1 ion channel induced H3P and promoted cell proliferation [34]. Similarly, in neointimal hyperplasia, cell proliferation is facilitated by vascular stretch, and microRNA-33 expression repressed to facilitate cell division [35, 36].

Taken together, these studies demonstrate that mechanical stretch regulates DNA methylation, histone phosphorylation, acetylation, and methylation to modulate cell behavior. Furthermore, both static and cyclic strains can influence HDAC expression directly or through miRNA and lncRNA regulation. Currently, most research has been focused on respiratory and cardiovascular disease. Yet, how

mechanical forces, such as compression and strain, affect epigenetic mechanisms in cancer remains unclear. A summary of the effects of mechanical stretch on the epigenetic state and cell behavior discussed in this section can be found in Table 2.

## 4. Shear Stress

Shear stress can also directly regulate histone-modifying enzymes, which play a critical role in cardiovascular disease development, including atherosclerosis. The increase in shear stress mediates endothelial cell gene expression and regulates the local immune microenvironment [7]. The spreading of the nucleus caused by cytoskeleton reorganization led to the accommodation of more signaling molecules and transcription factors. Previous researches have illustrated that HDACs are significantly involved in regulating hemodynamic-induced EC function and dysfunction (Table 3). Bazou et al. [37] reported that the interstitial flow increased HDAC1 phosphorylation which promotes endothelial morphogenesis and matrix metalloproteinase-14 (MMP14) expression. Activated vascular ECs showed higher growth and migration capabilities, which could contribute to angiogenesis. The involvement of HDAC6 facilitates endothelial cell migration and could potentially induce an atherosclerosis lesion [38]. In addition, low fluid shear stress and EGR-KLF2 cooperatively regulated the transcriptional expression of anticoagulant thrombomodulin (TM) [39]. ERG binding to the TM promoter recruits p300 and induces H3K27 acetylation, which directly drives the exposure of the TM promoter region further inducing TM expression in ECs.

On the contrary, high shear stress (65-85 dyn/cm$^2$) also could affect cell plasticity, possibly even leading to disease. For example, through attenuating the HDAC5 nuclear export, high laminar shear stress modulates the interaction between HDAC5 and KLF2 in HUVEC (human umbilical vein cell). Furthermore, pulsatile shear stress (PS) is believed to prevent atherosclerosis by maintaining cell homeostasis [40, 41]. The key regulator KLF4 can regulate PS-mediated H3K27ac, which contributes to the $Ca^{2+}$-dependent eNOS activation and EC homeostasis [42].

A recent study found that shear stress can modulate the expression of the polycomb methyltransferase EZH2 [43]. Xu et al. [44] reported that 20 dynes/cm$^2$ laminar shear stress could decrease the expression of EZH2 through the mechanosensitive microRNA miR101 in ECs. The downregulation of EZH2 expression concurrently further decreases methylation on H3K27, which limits endothelial inflammatory factor expression. This research has revealed that in atheroprotective flow, the reduction of H3K27me3 is the potential histone-based mechanism to augment anti-inflammatory gene expression in the endothelium. Moreover, through EZH2, high uniform shear stress also could induce cell quiescence through limiting the expression of cell cycle-related genes.

In addition to histone modifications, shear forces can also modulate cell behavior through DNA modifications. Monocyte adhesion on the HUVEC surface was decreased when the DNMT1 inhibitor 5-Aza was administered, indicating that DNMT1 regulated the inflammation of ECs. Moreover, arteriogenic capacity and arterial vascular remodeling also can be regulated by DNMT1. Heuslein et al. [41] determined that nonreversed flow collateral segments exhibited general *in vivo* DNA hypermethylation. Furthermore, ECs exposed to the nonreversed waveform escalate DNMT1 expression, which induces hypermethylation of the promoters of significantly regulated genes and a DNMT1-dependent reduction in proatherogenic monocyte adhesion [45].

Other mechanical forces, such as pressure, can also regulate histone modifiers to influence cell function. For example, mechanical forces play a fundamental role in regulating cartilage morphogenesis and maintenance. HDAC4 is a transcriptional regulatory protein involved in regulating the cell cycle, cartilage development, and endochondral ossification [46]. Cheleschi et al. demonstrated the beneficial role of cyclic hydrostatic pressure, suggesting the involvement and regulation of HDAC4 activation in osteoarthritis chondrocytes [47]. Moreover, some diseases lead to increased pressure in local tissues that alter the epigenetic state. For example, in the fetal lamb model, persistent pulmonary hypertension reorganized the epigenetic characteristics in pulmonary artery ECs, especially the nitric oxide synthase gene [48]. This process was mediated through a decrease in H4K12ac and an increase in H3K9me3, which are active and repressive marks that were found at the binding site of Sp1 in the eNOS promoter region, respectively. In a retinal ischemia-reperfusion (IR) injury mouse model, elevated intraocular pressure activated glial cells as a result of increased HDAC2 activity [49].

Altogether, findings from these studies suggest that methylation and acetylation of histones can be modulated by shear stress and therefore affect cell plasticity, including stem cell differentiation, cellular transitions (e.g., EMT and EndMT), and EC function. In some cases, high shear stress was able to induce stem cell differentiation and protect ECs from inflammation whereas low or oscillating shear stress induced EC inflammation and promoted arteriosclerosis. Furthermore, DNA methylation can also be regulated by fluid shear forces to affect cellular behavior. Apart from fluid shear force, local high pressure under pathological and physiological conditions also plays a role in regulating histone modifiers that affect cellular plasticity.

## 5. Nanotopography and Nanostructure

Surface nanotopography, structure, and pattern are important factors to influence cell behavior and differentiation, and a summary of the effects can be found in Table 4. Under pathological condition, the tumor will have a special surface pattern, which can be used as a criterion to give diagnosis [50]. In the tissue engineering area, material nanotopography influences cell differentiation and reprogramming had been widely discussed. In bone regeneration research, $TiO_2$ is a widely used material to support osteogenesis. Based on the previous research, a $TiO_2$ nanotube array was found to have the ability to promote hASC osteogenic differentiation.

Table 2: Summary or examples of the effects of mechanical stretch on histone modifications.

| Cell type | Stretch parameters | Epigenetic modification | Function | Ref |
|---|---|---|---|---|
| SMC | Cyclic strain, 10% elongation, 1.25 Hz | MicroRNA 33 | Stretch represses miR33 expression | [35] |
| Epithelial cell | 10-33% elongation | Histone H3P | Promoted cell proliferation | [34] |
| hAT-MSC | 2.5-15% elongation, 1 Hz | DNA demethylation | GNAS CpG demethylation | [28] |
| HC | 10% elongation, 0.5 Hz | miR-365 reduced HDAC4 | Cartilage degeneration, downregulated ACAN | [32] |
| MLVEC | Cyclic stretch, 20% elongation, 30 cycles/min | HDAC6 | Activated HDAC6 induces deacetylation of a-tubulin | [29] |
| HC | Cyclic stretch, 10% elongation, 0.5 Hz | HDAC | HDAC inhibitor downregulates RUNX-2, ADAMTS-5, and MMP-3 expression | [31] |
| HPMEC | Cyclic stretch, 20% elongation | Differentially expressed lncRNA (DEL) | lncRNA might regulate inflammation and fibrosis | [33] |
| C2C12 | Cyclic stretch, 5% elongation | MicroRNA 146a | Increasing miR-146 expression which downregulates Numb | [36] |
| MC | 0.25 Hz 6% elongation | HDAC4, histone 3 deacetylation | Promoted collagen II and repressed RUNX2 expression | [30] |

MSC: mesenchymal stem cells; hAT-MSC: human adipose tissue multipotential stromal cell; SMC: smooth muscle cell; HC: human chondrocyte; MLVEC: mouse lung vascular endothelial cell; HPMEC: human pulmonary microvascular endothelial cell; C2C12: mouse myoblast; MC: murine chondrocyte.

Table 3: Examples of shear stress-regulated histone modifications.

| Cell type | Shear stress | Histone/gene | Function | Ref. |
|---|---|---|---|---|
| VSMC | 15 dynes/cm$^2$ | HDAC6 | Shear stress increases HDAC6 and 5downregulates acetylated tubulin | [38] |
| ECs | Interstitial flow | HDAC1 | Increased morphogenesis, MMP14, and angiogenesis | [37] |
| HUVECs | 5 dynes/cm$^2$ shear stress | H3K4Me3, H3K27Ac | Increased thrombomodulin expression | [39] |
| HUVECs | 12 ± 4 dynes/cm$^2$ pulsatile shear stress | H3K27ac | $Ca^{2+}$-dependent eNOS activation, EC homeostasis | [42] |
| ECs | 20 dynes/cm$^2$ laminar shear stress | EZH2 | Deceased cell cycle and promoted quiescence | [43] |
| HUVECs | 12 dynes/cm$^2$ laminar flow | H3K27me3 | Confer an anti-inflammatory response | [44] |
| HUVECs | 15-30 dynes/cm$^2$ shear stress | DNMT1 | Exhibited DNA hypermethylation | [45] |
| Chondrocytes | 0.5 MPa hydrostatic pressure | HDAC4 | Downregulate MMP-13, ADAMTS-5, and HDAC4 | [47] |
| ECs | Pulmonary hypertension | H4K12ac, H3K9me3 | Decreased expression of eNOS | [48] |
| GC | Intraocular pressure | HDACs | Enhanced glial activation following IR injury | [49] |

ECs: endothelial cells; ESCs: embryonic stem cells; HUVECs: human umbilical vein cells; VSMC: vascular smooth muscle cell; GC: glial cell.

On the nanotube array, HDAC expression was downregulated and induces histone acetylation and promotes KDM3E gene expression, which facilitates bone regeneration [51]. Also, through mimicking the physiological tissue constraint, a three-dimensional synthesizing matrix promotes fibroblast rejuvenation through facilitating chromatin decondensation [52]. These phenomena illustrated the importance on nanotopography and structure in tissue regeneration and cell reprogramming.

Microgroove is a fundamental model used to investigate influence given by surface topography. On microgrooves, the reprogramming efficiency of fibroblast will be influenced through histone modification. In IPSC reprogramming, microgroove could reduce HDAC expression and increase the H3 methytransferase subunit, WDR5, and expression. This process increases histone acetylation and H3K4 methylation and facilitates the cell to perform stemness [53]. Under a similar mechanism, it was also found that microgroove can facilitate induced dopaminergic neuron reprogramming from the fibroblast [54]. Related researches also had been done on the stem cell. In BMSC, it was also found that due to the nuclear shape change given by microgrooves, the force applied on the nucleus deformed the lamin A/C around the cell nucleus, which could be stimulated and

Table 4: Examples of nanotopography-regulated histone modifications.

| Cell type | Nanotopography | Epigenetic modification | Function | Ref |
|---|---|---|---|---|
| hASC | Nanotube array | HDAC | Promote osteogenic differentiation | [51] |
| Fibroblast | Microgroove | HDAC | Facilitate IPSC reprogramming | [53] |
| BMSC | Microgroove | HDAC | Not tested in research | [55] |
| Fibroblast | Microgroove | H3K4me3 | Promote induced dopaminergic neuron reprogramming | [54] |
| MSC | Micropatterning | H3K9ac, H3K9me3, H3K36me3 | Increase MSC proangiogenic activity and increase angiogenesis | [57] |
| MCF7 | Micropatterning | H3K9ac, H3K4me3, K27me3 | Induce transcriptome change and nuclear reprogramming, increase cell stemness | [58] |
| Fibroblast | Tissue 3D constraints | HDAC and H3K9ac | Increase cell sensitivity to mechanostimulation, promote essential processes for cell rejuvenation | [52] |
| MIC | Micropatterning | H3K4me2 and H3K9ac | Upregulate PRDM14 gene and influence melanoma heterogeneity | [59] |
| Cardiac progenitors | Microgroove | Histone acetylation | Increase myocardin, tbx5, and mef2c expression | [56] |

hASC: human adipose tissue-derived stem cell; BMSC: bone marrow mesenchymal stem cells; MIC: malignant melanoma-initiating cell.

modulate the epigenetic modification, including HDAC activity and histone acetylation [55]. The cardiac progenitor cell also found that under similar stimulation, histone acetylation is upregulated and promotes mycardin and Tbx5 gene expression to promote cardiovascular differentiation [56]. Similar with microgrooves, the micropattern also could regulate cell differentiation and tissue regeneration. It was found that the micropattern which decreases the cell nuclear area downregulates H3K9ac and increases H3K9me3. This process increases MSC proangiogenic activity and promotes angiogenesis [57].

For the cancer cell, current research is more focused on the impact given by the micropattern. In breast cancer, micropatterning can facilitate cancer cell gain stemness through increasing H3K9ac and prohibiting H3K27me3. This result also found mouse embryonic fibroblast [58]. Similarly, micropattern curvature can manipulate histone methylation and increase tumor cell heterogenesis [59]. However, microgrooves can influence cancer cell proliferation and migration and may be involved in metastasis [60–62]. The research on how this factor impacts cancer cell epigenetic modification is still under investigation. The research on how the nanotopographical pattern in the tumor influences cancer cell epigenetic activity could provide another insight into cancer therapy development.

## 6. Conclusions and Future Directions

Chronic disease change of tissue mechanical microenvironment continuously stimulates local or recruited cell populations via mechanotransduction pathways. In arteriovenous malformation caused by hereditary hemorrhagic telangiectasia, shear stress stimulates type I/II serine/threonine kinase receptor (ALKs) on the endothelial cell surface and regulates interaction between the receptor and bone morphogenetic proteins 9 and 10 (BMP9 and BMP10). This cascade can regulate heat development though change expression of SMAD protein [63]. Also, change of matrix stiffness during atherosclerosis development regulates ECs through the RhoA/ROCK pathway and MAPK pathway [64]. Similarly, ECM stiffness regulates epidermal cell proliferation, migration, and differentiation based on the Rho/ROCK pathway through integrin stimulation [65]. Additionally, the mechanical properties of cell, including cell stiffness, could become potential therapeutic target for cancer chemotherapy and immune therapy [66, 67].

Different mechanical cues can initiate distinct epigenetic modifications, even on the same histone, such as HDAC family members which have varied responses to shear stress and mechanical stretch, and modifications of H3K9 in response to matrix stiffness and shear stress are distinctive as well. All of these processes involve numerous complex systems which include not only the cytoskeleton-nuclear skeleton-chromatin pathway but also mechanical-chemical coupling. Current work has put most attention on investigating the epigenetic modification under pathological mechanical stimulation. The knowledge in this area provides another opportunities to develop more effective therapies for tissue repair and cancer treatment. However, the relationship between the cell signaling pathway and change of epigenetic status still needs further investigation.

Interestingly, the relationship between mechanical microenvironment factors and epigenetic modification for immune cells including macrophages still remains blank. It is known that macrophages can sense stiffness, shear stress, cyclic stretch, and microgroove pattern and induce macrophage polarization and cytokine expression [68, 69]. Also, epigenetic modification is related to cytokine secretion and macrophage biochemical microenvironment construction [70, 71]. However, how mechanical factors influence macrophage epigenetic modification remains to be elucidated. The mechanism that pathological biophysical microenvironment regulates macrophage histone modification still needs further investigation.

Although a large number of studies have provided insights into the mechanism by which mechanical cues affect histone modifications and regulate cell gene expression, some questions still remain unclear. Mechanical stimuli, such as cyclic stretch, can induce more than one epigenetic modification process. However, the priority of types of

epigenetic modification in different cell types and which mechanical stimuli have a dominant impact on different diseases still need further investigation. Similarly, whether mechanical-chemical coupling is involved during the modulation of histone modifications should be further examined. All of these questions require further investigation and will provide incisive understanding on pathological influence given by mechanical microenvironment change in disease development and provide new therapeutic targets.

## Data Availability

The data used to support the findings of this study are available from the corresponding author upon request.

## Conflicts of Interest

The authors declare that they have no conflicts of interest.

## Authors' Contributions

Buwei Hu and Dandan Zhou contributed equally to this work and should be regarded as co-first authors.

## Acknowledgments

This work was supported by grants from the Natural Science Foundation of China (Nos. 82072443 and 82102571) the Natural Science Foundation of Chongqing, China (Nos. cstc2020jscx-msxmX0094 and cstc2021jcyj-msxmX0569) and Science and Health Foundation of Chongqing(2019ZDXM014).

## References

[1] M. Kalli and T. Stylianopoulos, "Defining the role of solid stress and matrix stiffness in cancer cell proliferation and metastasis," *Frontiers in Oncology*, vol. 8, pp. 55–55, 2018.

[2] B. Emon, J. Bauer, Y. Jain, B. Jung, and T. Saif, "Biophysics of tumor microenvironment and cancer metastasis - a mini review," *Computational and Structural Biotechnology Journal*, vol. 16, pp. 279–287, 2018.

[3] C. Palombo and M. Kozakova, "Arterial stiffness, atherosclerosis and cardiovascular risk: pathophysiologic mechanisms and emerging clinical indications," *Vascular Pharmacology*, vol. 77, pp. 1–7, 2016.

[4] R.-Z. He, D.-X. Luo, and Y.-Y. Mo, "Emerging roles of lncRNAs in the post-transcriptional regulation in cancer," *Genes & Diseases*, vol. 6, no. 1, pp. 6–15, 2019.

[5] W. Filipowicz, S. N. Bhattacharyya, and N. Sonenberg, "Mechanisms of post-transcriptional regulation by microRNAs: are the answers in sight?," *Nature Reviews Genetics*, vol. 9, no. 2, pp. 102–114, 2008.

[6] L. Bejarano, M. J. C. Jordão, and J. A. Joyce, "Therapeutic targeting of the tumor microenvironment," *Cancer Cell*, vol. 11, no. 4, pp. 933–959, 2021.

[7] A. Yurdagul Jr., A. C. Finney, D. Woolard Matthew, and A. W. Orr, "The arterial microenvironment: the where and why of atherosclerosis," *Biochemical Journal*, vol. 473, no. 10, pp. 1281–1295, 2016.

[8] Q. Liu, Q. Luo, Y. Ju, and G. Song, "Role of the mechanical microenvironment in cancer development and progression," *Cancer Biology & Medicine*, vol. 17, no. 2, pp. 282–292, 2020.

[9] L. W. Lv, Y. M. Tang, P. Zhang, Y. S. Liu, X. S. Bai, and Y. S. Zhou, "Biomaterial cues regulate epigenetic state and cell functions-a systematic review," *Tissue Engineering Part B-Reviews*, vol. 24, no. 2, pp. 112–132, 2018.

[10] C. Uhler and G. V. Shivashankar, "Chromosome intermingling: mechanical hotspots for genome regulation," *Trends in Cell Biology*, vol. 27, no. 11, pp. 810–819, 2017.

[11] R. C. Allshire and H. D. Madhani, "Ten principles of heterochromatin formation and function," *Nature Reviews Molecular Cell Biology*, vol. 19, no. 4, pp. 229–244, 2018.

[12] A. Janssen, S. U. Colmenares, and G. H. Karpen, "Heterochromatin: guardian of the genome," *Annual Review of Cell and Developmental Biology*, vol. 34, no. 1, pp. 265–288, 2018.

[13] T. Narita, B. T. Weinert, and C. Choudhary, "Author correction: functions and mechanisms of non-histone protein acetylation," *Nature Reviews Molecular Cell Biology*, vol. 20, no. 8, pp. 508–508, 2019.

[14] X. J. Wu and Y. Zhang, "TET-mediated active DNA demethylation: mechanism, function and beyond," *Nature Reviews Genetics*, vol. 18, no. 9, pp. 517–534, 2017.

[15] D. Pankova, Y. Jiang, M. Chatzifrangkeskou et al., "RASSF1A controls tissue stiffness and cancer stem-like cells in lung adenocarcinoma," *The EMBO Journal*, vol. 38, no. 13, pp. e100532–e100532, 2019.

[16] M. Jang, J. An, S. W. Oh et al., "Matrix stiffness epigenetically regulates the oncogenic activation of the Yes-associated protein in gastric cancer," *Nature Biomedical Engineering*, vol. 5, no. 1, pp. 114–123, 2021.

[17] Y. Liu, J. Lv, X. Liang et al., "Fibrin stiffness mediates dormancy of tumor-repopulating cells via a Cdc42-driven Tet2 epigenetic program," *Cancer Research*, vol. 78, no. 14, pp. 3926–3937, 2018.

[18] Y. Tan, A. Tajik, J. Chen et al., "Matrix softness regulates plasticity of tumour-repopulating cells via H3K9 demethylation and Sox2 expression," *Nature Communications*, vol. 5, no. 1, p. 4619, 2014.

[19] J. Qu, L. Y. Zhu, Z. J. Zhou et al., "Reversing mechanoinductive DSP expression by CRISPR/dCas9-mediated epigenome editing," *American Journal of Respiratory and Critical Care Medicine*, vol. 198, no. 5, pp. 599–609, 2018.

[20] G. Ligresti, N. Caporarello, J. A. Meridew et al., "CBX5/G9a/H3K9me-mediated gene repression is essential to fibroblast activation during lung fibrosis," *Insight*, vol. 4, no. 12, 2019.

[21] S.-A. Xie, T. Zhang, J. Wang et al., "Matrix stiffness determines the phenotype of vascular smooth muscle cell in vitro and in vivo: role of DNA methyltransferase 1," *Biomaterials*, vol. 155, pp. 203–216, 2018.

[22] K. G. Birukov, "Cyclic stretch, reactive oxygen species, and vascular remodeling," *Antioxidants & Redox Signaling*, vol. 11, no. 7, pp. 1651–1667, 2009.

[23] J. Pugin, I. Dunn-Siegrist, J. Dufour, P. Tissières, P. E. Charles, and R. Comte, "Cyclic stretch of human lung cells induces an acidification and promotes bacterial growth," *American Journal of Respiratory Cell and Molecular Biology*, vol. 38, no. 3, pp. 362–370, 2008.

[24] J. Gao, S. Fu, Z. Zeng et al., "Cyclic stretch promotes osteogenesis-related gene expression in osteoblast-like cells

through a cofilin-associated mechanism," *Molecular Medicine Reports*, vol. 14, no. 1, pp. 218–224, 2016.

[25] A. M. Vlaikou, D. Kouroupis, A. Sgourou et al., "Mechanical stress affects methylation pattern of GNAS isoforms and osteogenic differentiation of hAT-MSCs," *Biochimica et Biophysica Acta (BBA) - Molecular*, vol. 1864, pp. 1371–1381, 2017.

[26] Y. Wang, Y.-J. Liu, D.-F. Xu et al., "DRD1 downregulation contributes to mechanical stretch-induced lung endothelial barrier dysfunction," *Theranostics*, vol. 11, no. 6, pp. 2505–2521, 2021.

[27] C. Chen, X. Wei, Z. Lv et al., "Cyclic equibiaxial tensile strain alters gene expression of chondrocytes via histone deacetylase 4 shuttling," *PLoS One*, vol. 11, no. 5, p. e0154951, 2016.

[28] T. Saito, K. Nishida, T. Furumatsu, A. Yoshida, M. Ozawa, and T. Ozaki, "Histone deacetylase inhibitors suppress mechanical stress-induced expression of RUNX-2 and ADAMTS-5 through the inhibition of the MAPK signaling pathway in cultured human chondrocytes," *Osteoarthritis and Cartilage*, vol. 21, no. 1, pp. 165–174, 2013.

[29] Q. Zheng, X. X. Li, L. Xiao et al., "MicroRNA-365 functions as a mechanosensitive microRNA to inhibit end plate chondrocyte degeneration by targeting histone deacetylase 4," *Bone*, vol. 128, article 115052, 2019.

[30] D. Wang, C. Dai, X. Zhang et al., "Identification and functional analysis of long non-coding RNAs in human pulmonary microvascular endothelial cells subjected to cyclic stretch," *Frontiers in Physiology*, vol. 12, 2021.

[31] S. A. Gudipaty, J. Lindblom, P. D. Loftus et al., "Mechanical stretch triggers rapid epithelial cell division through Piezo1," *Nature*, vol. 543, no. 7643, pp. 118–121, 2017.

[32] K. Huang, H. Bao, Z.-Q. Yan et al., "MicroRNA-33 protects against neointimal hyperplasia induced by arterial mechanical stretch in the grafted vein," *Cardiovascular Research*, vol. 113, no. 5, pp. 488–497, 2017.

[33] D. Bazou, M. R. Ng, J. W. Song, S. M. Chin, N. Maimon, and L. L. Munn, "Flow-induced HDAC1 phosphorylation and nuclear export in angiogenic sprouting," *Scientific Reports*, vol. 6, no. 1, article 34046, 2016.

[34] Y. H. Wang, Z. Q. Yan, Y. X. Qi et al., "Normal shear stress and vascular smooth muscle cells modulate migration of endothelial cells through histone deacetylase 6 activation and tubulin acetylation," *Annals of Biomedical Engineering*, vol. 38, no. 3, pp. 729–737, 2010.

[35] C. Peghaire, N. P. Dufton, M. Lang et al., "The transcription factor ERG regulates a low shear stress-induced antithrombotic pathway in the microvasculature," *Nature Communications*, vol. 10, no. 1, p. 5014, 2019.

[36] N. E. Ajami, S. Gupta, M. R. Maurya et al., "Systems biology analysis of longitudinal functional response of endothelial cells to shear stress," *Proceedings of the National Academy of Sciences of the United States of America*, vol. 114, no. 41, pp. 10990–10995, 2017.

[37] B. Gongol, T. Marin, J. Zhang et al., "Shear stress regulation of miR-93 and miR-484 maturation through nucleolin," *Proceedings of the National Academy of Sciences of the United States of America*, vol. 116, no. 26, pp. 12974–12979, 2019.

[38] M. He, T. S. Huang, S. Li et al., "Atheroprotective flow upregulates ITPR3 (inositol 1,4,5-trisphosphate receptor 3) in vascular endothelium via KLF4 (Krüppel-like factor 4)-mediated histone modifications," *Arteriosclerosis, Thrombosis, and Vascular Biology*, vol. 39, no. 5, pp. 902–914, 2019.

[39] M. Maleszewska, B. Vanchin, M. C. Harmsen, and G. Krenning, "The decrease in histone methyltransferase EZH2 in response to fluid shear stress alters endothelial gene expression and promotes quiescence," *Angiogenesis*, vol. 19, no. 1, pp. 9–24, 2016.

[40] S. Xu, Y. Xu, M. Yin et al., "Flow-dependent epigenetic regulation of IGFBP5 expression by H3K27me3 contributes to endothelial anti-inflammatory effects," *Theranostics*, vol. 8, no. 11, pp. 3007–3021, 2018.

[41] J. L. Heuslein, C. M. Gorick, J. Song, and R. J. Price, "DNA methyltransferase 1-dependent DNA hypermethylation constrains arteriogenesis by augmenting shear stress set point," *Journal of the American Heart Association*, vol. 6, no. 12, 2017.

[42] X. Yang, Y. Guan, S. Tian, Y. Wang, K. Sun, and Q. Chen, "Mechanical and IL-1$\beta$ responsive miR-365 contributes to osteoarthritis development by targeting histone deacetylase 4," *International Journal of Molecular Sciences*, vol. 17, no. 4, pp. 436–436, 2016.

[43] S. Cheleschi, A. De Palma, A. Pecorelli et al., "Hydrostatic pressure regulates microRNA expression levels in osteoarthritic chondrocyte cultures via the Wnt/$\beta$-catenin pathway," *International Journal of Molecular Sciences*, vol. 18, no. 1, p. 133, 2017.

[44] X. Ke, H. Johnson, X. Jing et al., "Persistent pulmonary hypertension alters the epigenetic characteristics of endothelial nitric oxide synthase gene in pulmonary artery endothelial cells in a fetal lamb model," *Physiological Genomics*, vol. 50, no. 10, pp. 828–836, 2018.

[45] M. S. Sung, H. Heo, G. H. Eom et al., "HDAC2 regulates glial cell activation in ischemic mouse retina," *International Journal of Molecular Sciences*, vol. 20, no. 20, p. 5159, 2019.

[46] K. Tanaka, H. Toyoda, S. Kadowaki et al., "Surface pattern classification by enhanced-magnification endoscopy for identifying early gastric cancers," *Gastrointestinal Endoscopy*, vol. 67, no. 3, pp. 430–437, 2008.

[47] L. Lv, Y. Liu, P. Zhang et al., "The epigenetic mechanisms of nanotopography-guided osteogenic differentiation of mesenchymal stem cells via high-throughput transcriptome sequencing," *International Journal of Nanomedicine*, vol. Volume 13, pp. 5605–5623, 2018.

[48] B. Roy, L. Yuan, Y. Lee, A. Bharti, A. Mitra, and G. V. Shivashankar, "Fibroblast rejuvenation by mechanical reprogramming and redifferentiation," *Proceedings of the National Academy of Sciences*, vol. 117, no. 19, pp. 10131–10141, 2020.

[49] T. L. Downing, J. Soto, C. Morez et al., "Biophysical regulation of epigenetic state and cell reprogramming," *Nature Materials*, vol. 12, no. 12, pp. 1154–1162, 2013.

[50] J. Yoo, M. Noh, H. Kim, N. L. Jeon, B.-S. Kim, and J. Kim, "Nanogrooved substrate promotes direct lineage reprogramming of fibroblasts to functional induced dopaminergic neurons," *Biomaterials*, vol. 45, pp. 36–45, 2015.

[51] Y. Li, S. Chu Julia, K. Kurpinski et al., "Biophysical regulation of histone acetylation in mesenchymal stem cells," *Biophysical Journal*, vol. 100, no. 8, pp. 1902–1909, 2011.

[52] C. Morez, M. Noseda, M. A. Paiva, E. Belian, M. D. Schneider, and M. M. Stevens, "Enhanced efficiency of genetic programming toward cardiomyocyte creation through topographical cues," *Biomaterials*, vol. 70, pp. 94–104, 2015.

[53] A. A. Abdeen, J. Lee, Y. Li, and K. A. Kilian, "Cytoskeletal priming of mesenchymal stem cells to a medicinal phenotype,"

*Regenerative Engineering and Translational Medicine*, vol. 3, no. 1, pp. 5–14, 2017.

[54] B. Roy, S. Venkatachalapathy, P. Ratna et al., "Laterally confined growth of cells induces nuclear reprogramming in the absence of exogenous biochemical factors," *Proceedings of the National Academy of Sciences*, vol. 115, no. 21, p. E4741, 2018.

[55] J. Lee, T. G. Molley, C. H. Seward et al., "Geometric regulation of histone state directs melanoma reprogramming," *Communications Biology*, vol. 3, no. 1, p. 341, 2020.

[56] P. P. Provenzano, K. W. Eliceiri, J. M. Campbell, D. R. Inman, J. G. White, and P. J. Keely, "Collagen reorganization at the tumor-stromal interface facilitates local invasion," *BMC Medicine*, vol. 4, no. 1, p. 38, 2006.

[57] P. K. Chaudhuri, C. Q. Pan, B. C. Low, and C. T. Lim, "Topography induces differential sensitivity on cancer cell proliferation via rho-ROCK-myosin contractility," *Scientific Reports*, vol. 6, no. 1, p. 19672, 2016.

[58] A. Beliveau, G. Thomas, J. Gong, Q. Wen, and A. Jain, "Aligned nanotopography promotes a migratory state in glioblastoma multiforme tumor cells," *Scientific Reports*, vol. 6, no. 1, p. 26143, 2016.

[59] Y. Mahendra, M. He, M. A. Rouf et al., "Progress and prospects of mechanotransducers in shear stress-sensitive signaling pathways in association with arteriovenous malformation," *Clinical Biomechanics*, vol. 88, article 105417, 2021.

[60] V. Vania, L. Wang, M. Tjakra et al., "The interplay of signaling pathway in endothelial cells–matrix stiffness dependency with targeted-therapeutic drugs," *Biochimica et Biophysica Acta (BBA) - Molecular Basis of Disease*, vol. 1866, no. 5, article 165645, 2020.

[61] Y. Wang, G. Wang, X. Luo, J. Qiu, and C. Tang, "Substrate stiffness regulates the proliferation, migration, and differentiation of epidermal cells," *Burns*, vol. 38, no. 3, pp. 414–420, 2012.

[62] X. Chen, Y. Fan, J. Sun et al.et al., "Nanoparticle-mediated specific elimination of soft cancer stem cells by targeting low cell stiffness," *Acta Biomaterialia*, vol. 135, pp. 493–505, 2021.

[63] K. Lei, A. Kurum, M. Kaynak et al., "Cancer-cell stiffening via cholesterol depletion enhances adoptive T-cell immunotherapy," *Nature Biomedical Engineering*, vol. 5, no. 12, pp. 1411–1425, 2021.

[64] J. Li, Y. Li, B. Gao et al., "Engineering mechanical microenvironment of macrophage and its biomedical applications," *Nanomedicine (London, England)*, vol. 13, no. 5, pp. 555–576, 2018.

[65] S. Singh, D. Awuah, H. M. Rostam et al., "Unbiased analysis of the impact of micropatterned biomaterials on macrophage behavior provides insights beyond predefined polarization states," *ACS Biomaterials Science & Engineering*, vol. 3, no. 6, pp. 969–978, 2017.

[66] S. Chen, J. Yang, Y. Wei, and X. Wei, "Epigenetic regulation of macrophages: from homeostasis maintenance to host defense," *Cellular & Molecular Immunology*, vol. 17, no. 1, pp. 36–49, 2020.

[67] I. Lodewijk, S. P. Nunes, R. Henrique, C. Jerónimo, M. Dueñas, and J. M. Paramio, "Tackling tumor microenvironment through epigenetic tools to improve cancer immunotherapy," *Clinical Epigenetics*, vol. 13, no. 1, p. 63, 2021.

[68] R. Kaukonen, A. Mai, M. Georgiadou et al., "Normal stroma suppresses cancer cell proliferation via mechanosensitive regulation of JMJD1a-mediated transcription," *Nature Communications*, vol. 7, no. 1, p. 12237, 2016.

[69] Y. F. Li, C. B. Tang, and K. A. Kilian, "Matrix mechanics influence fibroblast-myofibroblast transition by directing the localization of histone deacetylase 4," *Cellular and Molecular Bioengineering*, vol. 10, no. 5, pp. 405–415, 2017.

[70] E. You, Y. H. Huh, A. Kwon et al., "SPIN90 depletion and microtubule acetylation mediate stromal fibroblast activation in breast cancer progression," *Cancer Research*, vol. 77, no. 17, pp. 4710–4722, 2017.

[71] W. Kuang, J. Tan, Y. Duan et al., "Cyclic stretch induced miR-146a upregulation delays C2C12 myogenic differentiation through inhibition of Numb," *Biochemical and Biophysical Research Communications*, vol. 378, no. 2, pp. 259–263, 2009.

Hindawi
Stem Cells International
Volume 2022, Article ID 5719077, 16 pages
https://doi.org/10.1155/2022/5719077

*Research Article*

# High-Throughput Sequencing Reveals CXCR4 and IGF1 Behave Different Roles in Weightlessness Osteoporosis

**Dong Wang,[1,2] Weihang Li,[1] Ziyi Ding,[1] Quan Shi,[1,2] Shilei Zhang,[1] Zhuoru Zhang,[3] Zhibin Liu,[2] Xiaocheng Wang,[3,4] and Ming Yan[1]**

[1]*Department of Orthopedic Surgery, Xijing Hospital, Air Force Medical University, Xi'an, China*
[2]*Department of Orthopaedics, Affiliated Hospital of Yanan University, Yanan 716000, China*
[3]*Center of Clinical Aerospace Medicine, School of Aerospace Medicine, Air Force Medical University, Xi'an 710032, China*
[4]*Department of Aviation Medicine, The First Affiliated Hospital, Air Force Medical University, Xi'an 710032, China*

Correspondence should be addressed to Zhibin Liu; liuzhibin1997@126.com, Xiaocheng Wang; wxcnose@126.com, and Ming Yan; yanming_spine@163.com

Dong Wang, Weihang Li, and Ziyi Ding contributed equally to this work.

Received 3 March 2022; Accepted 24 March 2022; Published 18 April 2022

Academic Editor: Qiang Zhou



*Objective*. This study is aimed at screening the differential expression profiles of mRNA under weightlessness osteoporosis through high-throughput sequencing technology, as well as investigating the pathogenesis of weightlessness osteoporosis at the molecular level especially in bone marrow mesenchymal stem cells (BMSCs). *Methods*. The mouse bone marrow mesenchymal stem cell line was divided into ground group and simulated microgravity (SMG) group. BMP-2 was used to induce osteogenic differentiation, and SMG group was placed into 2D-gyroscope to simulate weightless condition. Transcriptome sequencing was performed by Illumina technology, DEGs between ground and SMG group was conducted using the DEseq2 algorithm. Molecular functions and signaling pathways enriched by DEGs were then comprehensively analyzed via multiple bioinformatic approaches including but not limited to GO, KEGG, GSEA, and PPI analysis. *Results*. A total of 263 DEGs were identified by comparing these 2 groups, including 186 upregulated genes and 77 downregulated genes. GO analysis showed that DEGs were enriched in osteoblasts, osteoclasts cell proliferation, differentiation, and apoptosis; KEGG analysis revealed that DEGs were significantly enriched in the TNF signaling pathway and FoxO signaling pathway; the enrichment results from Reactome database displayed that DEGs were mainly involved in the transcription of Hoxb3 gene, RUNX1 recruitment KMT2A gene, and activation of Hoxa2 chromatin signaling pathway. The four genes, IL6, CXCR4, IGF1, and PLOD2, were identified as hub genes for subsequent analysis. *Conclusions*. This study elucidated the significance of 10 hub genes in the development of weightlessness osteoporosis. In addition, the results of this study provide a theoretical basis and novel ideas for the subsequent research of the pathogenesis and clinical treatment of weightlessness osteoporosis.

## 1. Introduction

Osteoporosis, a systemic degenerative bone disease, is characterized by systemic bone loss and hypoplasia; reduced bone density, thinning, and fracture of osteophytic bone trabeculae; and increased risk of fracture [1]. At present, antiosteoporosis drugs are clinically classified into two main categories: bone resorption inhibiting drugs and bone formation promoting drugs [2], which have achieved good results in clinical practice. However, some studies have reported [3] that astronauts suffered from weightlessness osteoporosis due to the lack of physiological mechanical load stimulation under special weightless environment of space, thus, it is almost difficult for the commonly used antiosteoporosis drugs to alleviate the progression of osteoporosis in astronauts [4], which seriously threatens the physical and mental health of astronauts and the smooth execution of flight missions. These reasons are mainly attributed to the

lack of exploration in the pathogenesis and treatment of weightlessness osteoporosis.

Bone marrow mesenchymal stem cells (BMSCs) are a class of adult stem cells with self-renewal and multidirectional differentiation potential [5], which can differentiate into a host of cells including osteoblasts, such as adipocytes, chondroblasts, muscle cells, and nerve cells. Moreover, it plays an important regulatory role in maintaining normal physiological activities of the body. Studies have shown that BMSCs are important regulators in maintaining the content of osteocytes and myoblasts in vivo. Relevant scholars [6, 7] found that the differentiation of BMSCs into osteoblasts was inhibited, and adipocyte differentiation was promoted under weightlessness, which can lead to the symptoms of muscular system atrophy and osteoporosis. Therefore, studying the mechanism of BMSCs and the expression of related target genes under weightlessness environment has become the key to the prevention of weightlessness osteoporosis.

Spaceflight data [8] manifested that weightlessness-induced bone mineral density decreases at an average rate of 1.0% ~1.6% per month, which were 10~15 times faster than the rate of bone loss in postmenopausal women. Therefore, in order to ensure the astronauts successfully complete space missions in long-term spaceflight, this study is aimed at investigating the pathogenic genes and possible mechanisms of weightlessness osteoporosis, as well as providing reference for subsequent clinical drug targets.

In recent years, with the rapid development of high-throughput sequencing (HTS) technology, its characteristics of high throughput, short time, and high sensitivity make it applied to several biomedical science fields [9]. HTS technology could figure out gene sets that play important regulatory roles in various diseases. Therefore, the study firstly constructed an osteoporosis cell model under weightlessness and analyzed differentially expressed genes (DEGs) through HTS technology, followed by analysis of Gene Otology (GO) and Kyoto Encyclopedia of Genes and Genomes (KEGG) of DEGs to unveil their pathogenesis. Then, protein-protein interaction (PPI) network was constructed to explore the relationship between proteins that contribute to weightlessness osteoporosis. This will provide a strong basis for the molecular mechanism in the occurrence and development of weightlessness osteoporosis and potential drug therapy targets. Based on the findings, this study would provide effective means for early detection, diagnosis, and treatment of weightlessness osteoporosis in astronauts and make corresponding contributions to the aerospace industry ultimately.

## 2. Materials and Methods

*2.1. Cell Culture and Experimental Conditions.* Bone marrow mesenchymal stem cells (BMSCs, C3H10T1/2) were purchased from Procell Life Science & Technology Co., Ltd. (PLS, CHN) and routinely incubated in high-glucose Dulbecco's modified Eagle's medium (DMEM, Procell, CHN) containing 10% head-inactivated fetal bovine serum (FBS, Gemini, USA) at 37°C and 5% $CO_2$ saturated humidity incubator. On the day before simulated weightlessness, the cells were inoculated on 2.55 cm × 2.15 cm coverslips at a density of $1 \times 10^5$ pcs/piece and incubated overnight in six-well plates. After the cells reached 30% density on the coverslips, the coverslips of inoculated cells were inserted into the slot of the stainless steel bracket of the rotator and placed into the preheated rotary chamber filled with high-sugar DMEM medium containing 10%FBS, and osteogenic differentiation solution BMP-2 was added for osteogenic induction. After the bubbles were drained, the slides were placed on the rotating arm of a 2D-clinostat (2D-RWV, Rotating Wall Vessel, manufactured by China Astronaut Research and Training Center) [10]. The cells were rotated at 24 r/min for 48 h in the cell incubator. The ground group was placed next to the gyroscope and incubated for the same time. After simulated weightlessness, the cells were collected into a centrifuge tube for subsequent RNA extraction. The structure of 2D-clinostat and simulated microgravity device is shown in Figure 1.

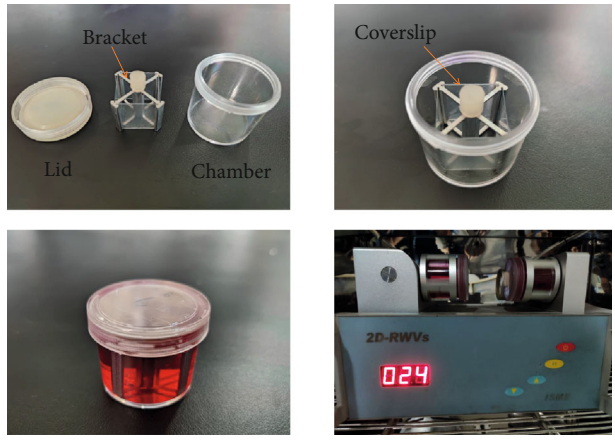


Figure 1: The structure of 2D-clinostat and simulated microgravity device.

*2.2. Illumina High-Throughput Sequencing Database.* Trizol kit (Invitrogen, Carlsbad, CA, USA) was utilized to extract total RNA from ground group and SMG group cell samples, respectively. Agilent 2100 biological analyzer was used to evaluate the quality of the extracted total RNA. After enrichment of eukaryotic mRNA with polyA tails by magnetic beads with Oligo (dT), the mRNA was interrupted by buffer. The fragmented mRNA was used as a template and random oligonucleotides as primers to synthesize the first strand of cDNA in the M-MuLV reverse transcriptase system, followed by degradation of the RNA strand with RNaseH and synthesis of the second strand of cDNA with dNTPs under the DNA polymerase I system. The purified double-stranded cDNAs were end-repaired, A-tailed, and connected to sequencing connectors, the cDNAs of about 200 bp were screened by AMPure XP beads, PCR amplification was performed, and the PCR products were purified again with AMPure XP Beads. Finally, the library was obtained and amplified and sequenced with Illumina Novaseq6000 sequencer.

*2.3. Quality Control of Gene Expression Matrix.* The generated matrices were analyzed for gene expression values to

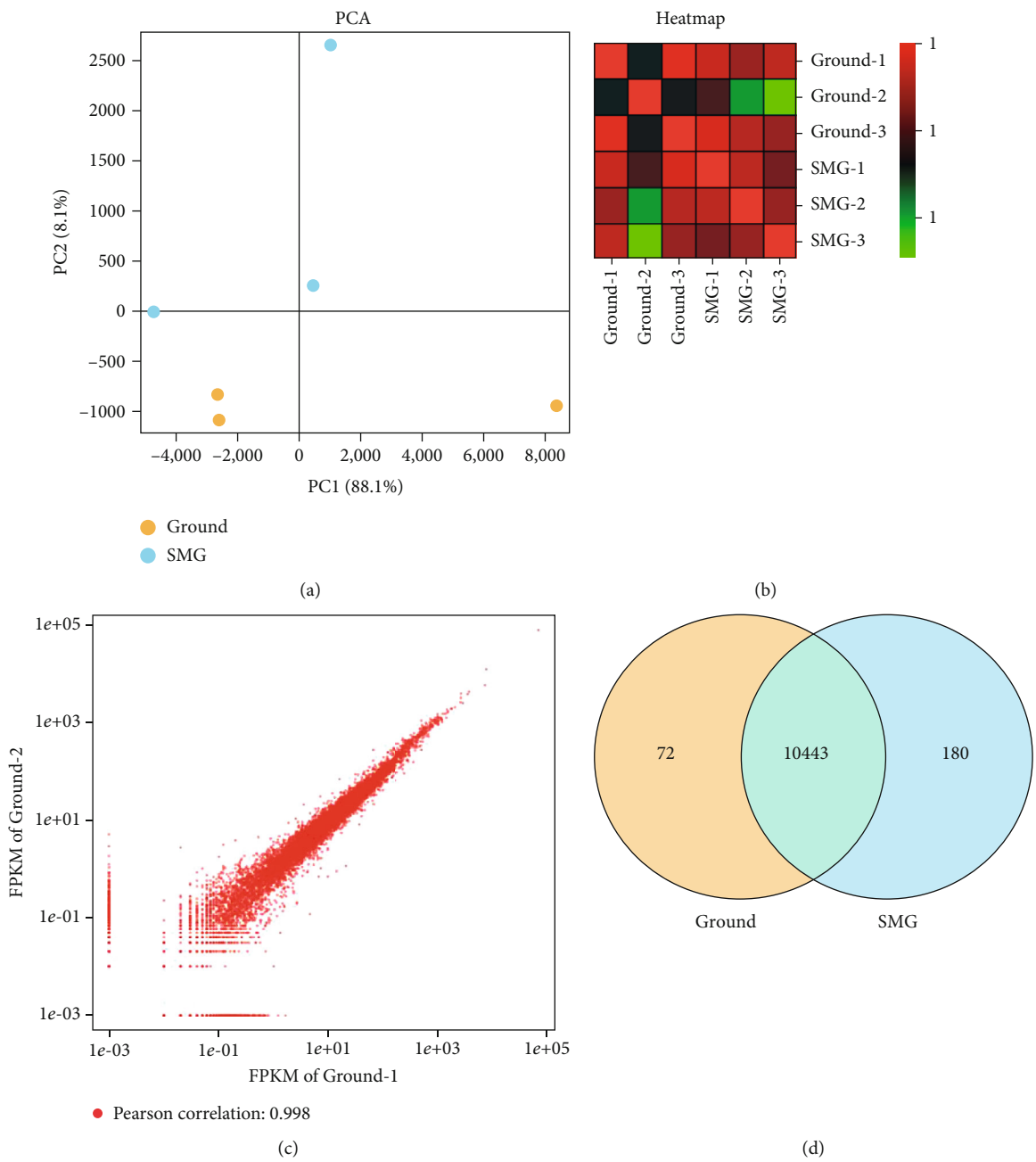


Figure 2: Continued.

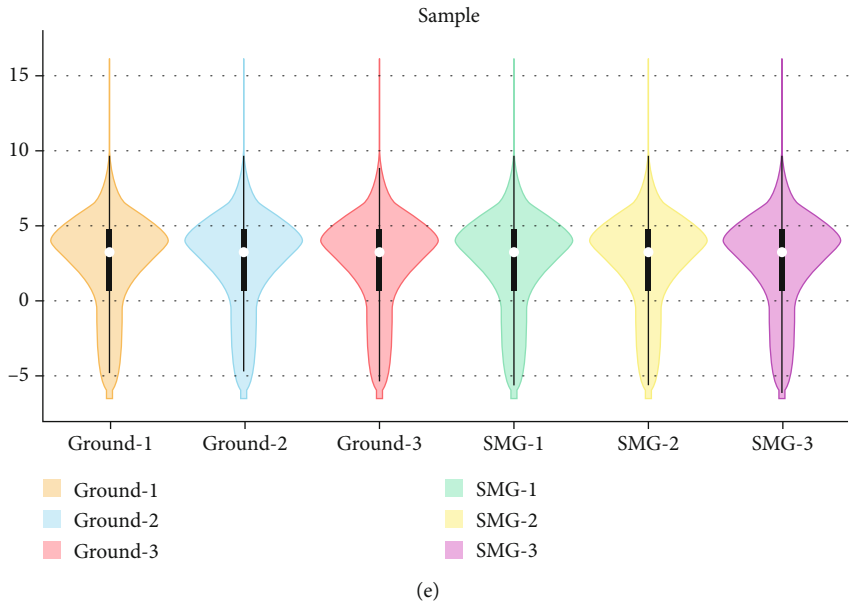


Figure 2: Sample relationship and data analysis. (a) Principal component analysis, (b) heatmap analysis, (c) repeatability scatter plot analysis, (d) Venn plot analysis, and (e) violin diagram of sample of ground group and SMG group.

clarify the differences between groups and whether they were suitable for subsequent analysis. Principal component analysis (PCA) and correlation heat map were utilized to show the difference between these 2 groups. The genes obtained by sequencing of the two groups were conducted by Venn diagram analysis for subsequent analysis. Additionally, the violin diagram of expression values of 6 samples was visualized by *R*, which displayed the data density within each sample.

*2.4. Screening of DEGs in Weightlessness Osteoporosis.* DEseq2 algorithm was utilized to analyze the significant difference between ground group and SMG group cell samples. The screening threshold of DEGs was defined as $|\mathrm{FC}\,(\text{fold change})| > 1.5$ and $P < 0.05$, which was considered as statistically significant difference. The samples and genes were further performed for clustering analysis, and the heat map of DEGs was drawn by R ("pheatmap" package) to display the expression magnitude and change pattern of DEGs in each group.

*2.5. Function and Signal Pathway Enrichment Analysis of DEGs in Weightlessness Osteoporosis.* DEGs were uploaded into DAVID (http://david.abcc.ncifcrf.gov/, gene functional annotation online database tools) [11] and *R* to perform GO (Gene Ontology) and KEGG (Kyoto Encyclopedia of Genes and Genomes) analysis, and Reactome database enrichment analysis and GSEA analysis were further conducted to explore the biological significance of DEGs at the molecular level. GO is an international standard classification system for gene functions, which mainly includes cellular component (CC), molecular function (MF), and biological process (BP). KEGG is the main public database of signaling pathways, allowing information on signaling pathways related to DEGs. The Reactome database covers the reactions and biological signaling pathways of some species, more significantly enriched pathways could be found in DEGs. Gene Set Enrichment Analysis (GSEA) further explores the dominant cellular signaling pathways of DEGs.

*2.6. Protein-Protein Interaction (PPI) Network Analysis.* The STRING is a database for analyzing the interaction relationship between proteins expressed by different genes. The selected common DEGs were used to construct the interaction network using STRING database, and the obtained gene networks were imported into Cytoscape 3.8.0 software for further analysis, and then the most closely interactive subnetworks were further screened based on MCC algorithm. Studies [12] have shown that MCC algorithm is aimed at identifying the most relevant key targets and subnetworks from the complex and huge interaction network, which is one of the most effective methods to identify target genes. This contributes to study the molecular mechanisms of diseases and new targets of drugs from a more comprehensive perspective.

*2.7. Western Blotting Assay.* Western blotting assay was primarily used to detect the expression levels of related proteins. BMSCs were inoculated in T25 culture flasks, and after inducing osteogenic differentiation, the samples of SMG group were subjected to simulated weightless experiment. Then, total proteins were extracted from BMSCs of the two groups separately using phenylmethylsulfonyl fluoride (PMSF) cell lysis buffer. The Pierce BCA protein assay kit (Beyotime Biotechnology, China) was utilized to determine the protein standard curves and the protein concentrations of both samples. Then, the protein samples were mixed with buffer solution and boiled at 100°C. Proteins were isolated by 10% sodium dodecyl sulphate-polyacrylamide gel electrophoresis (SDS-PAGE) and then transferred onto

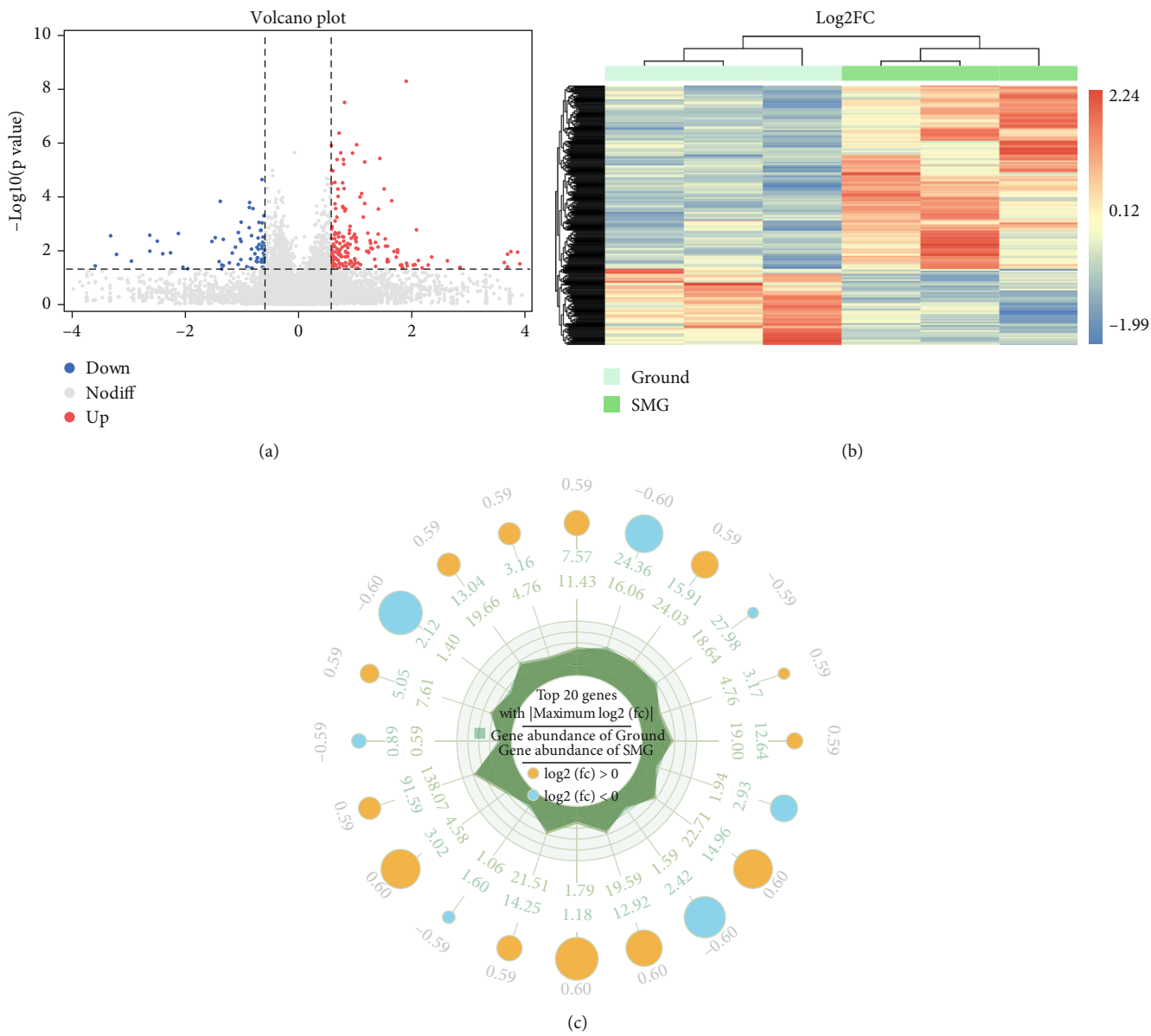


Figure 3: DEG screening and expression level analysis of different samples. (a) Volcano plot analysis of selected DEGs from Ground group and SMG group. (b) Heatmap of hierarchical clustering analysis of selected DEGs from ground group and SMG group. (c) Radar plot analysis of selected DEGs from ground group and SMG group.

polyvinylidene fluoride (PVDF) membrane via semidry transfer method. The membrane was sealed at room temperature for 2 hours with 5% skim milk, TRIS buffer brine and Tween 20 (TBST) buffer; primary antibodies including CXCR4, IGF1, and GAPDH (Abcam, UK) were diluted and incubated overnight at 4°C. And the membranes were incubated by goat anti-rabbit horseradish peroxidase conjugate (Abcam, UK) at room temperature for 1 h. Finally, protein signals were detected with an enhanced chemiluminescence kit, and band density was measured using the Viber Bio imaging tool.

*2.8. Statistical Analysis.* All numerical data were expressed as mean ± standard deviation of three independent replicate experiments. The results were statistically compared using the Student's $T$-test. $P < 0.05$ was considered a statistically significant difference. All statistical analyses were conducted by SPSS19.0 software (SPSS Company, USA).

## 3. Results

*3.1. Data Preprocessing of Expression Matrix.* According to the results of Illumina sequencing instrumentation, relationships between sample and the obtained data were conducted to get a comprehensive assessment. PCA analysis revealed that the ground and SMG group were distinguishable on the PC2 axis (Figure 2(a)); correlation heat map analysis showed a strong correlation between the two groups, which was valuable for subsequent analysis (Figure 2(b)); repeatability scatter plot indicated that the data distribution within

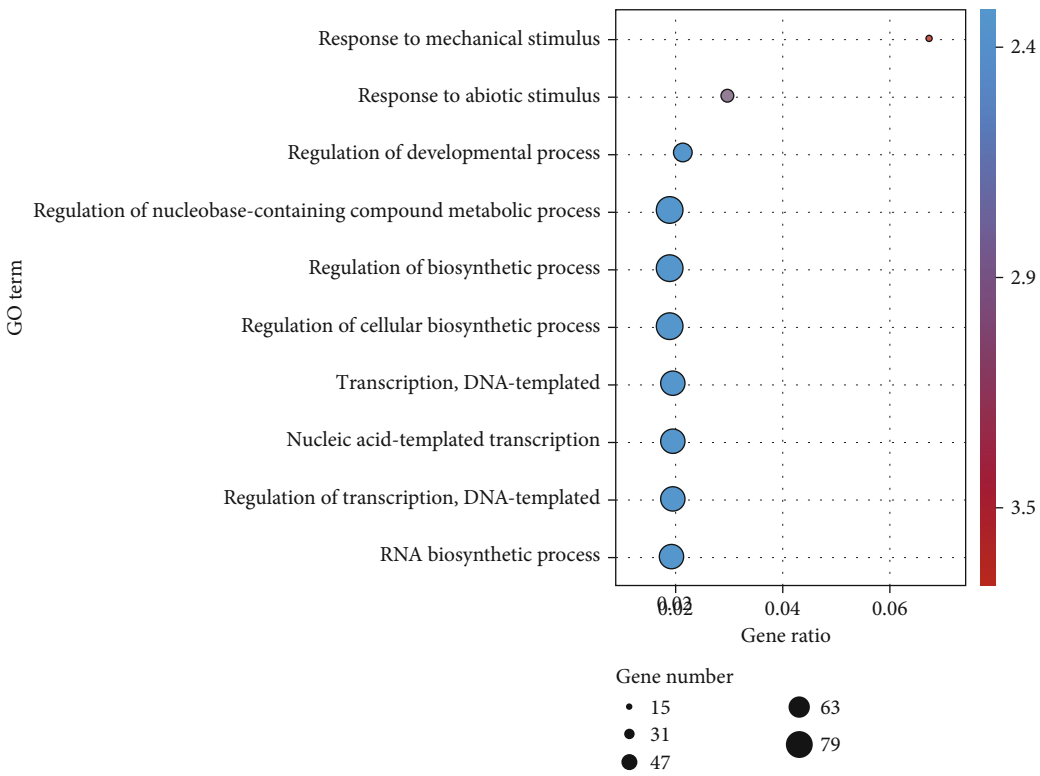


(a)

Figure 4: Continued.

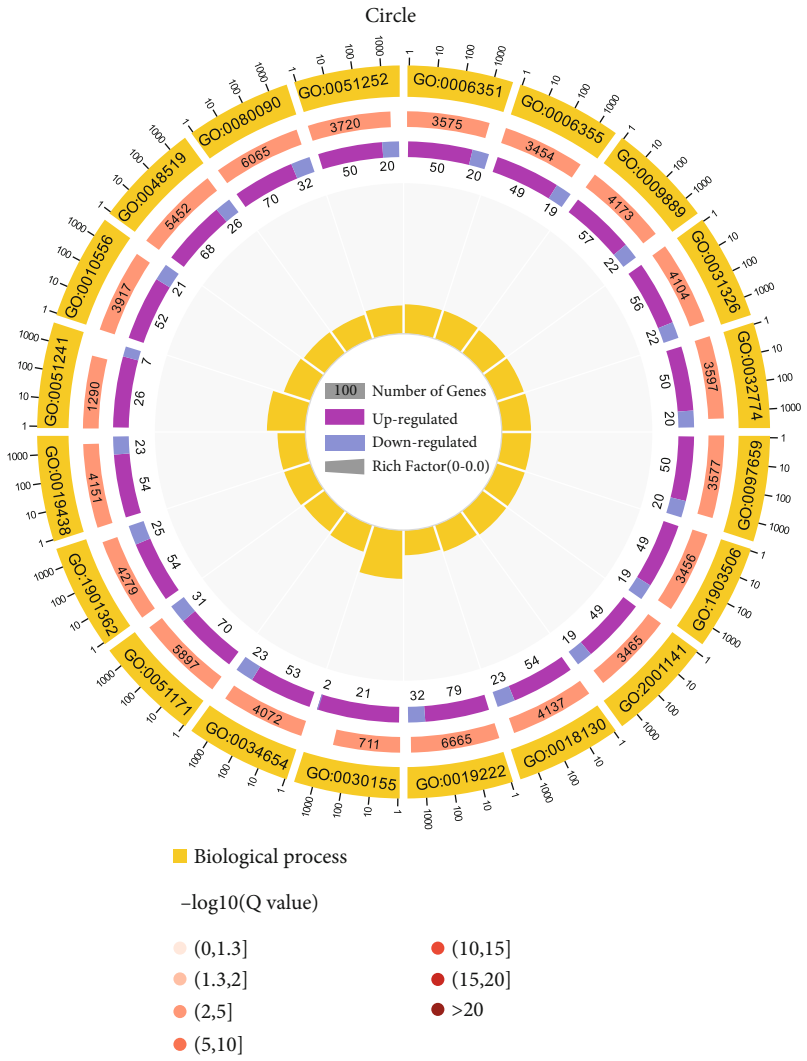


Biological process

–log10(Q value)

- (0,1.3]
- (1.3,2]
- (2,5]
- (5,10]
- (10,15]
- (15,20]
- >20

(b)

Figure 4: Continued.

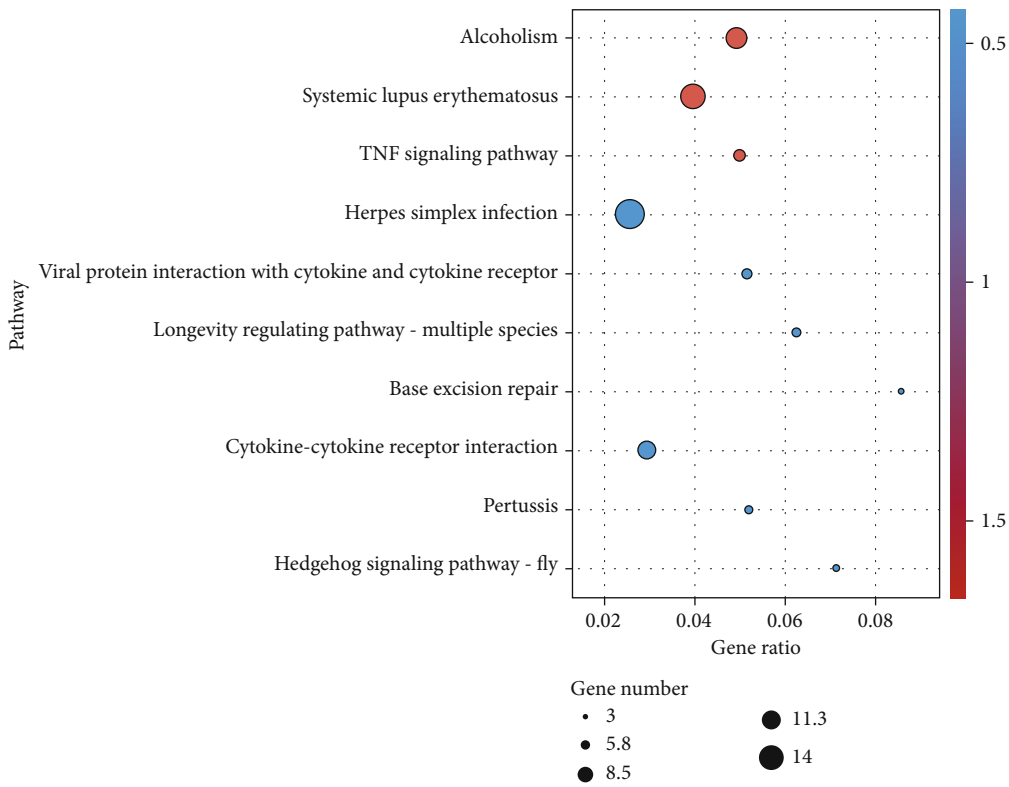


(c)

Figure 4: Continued.

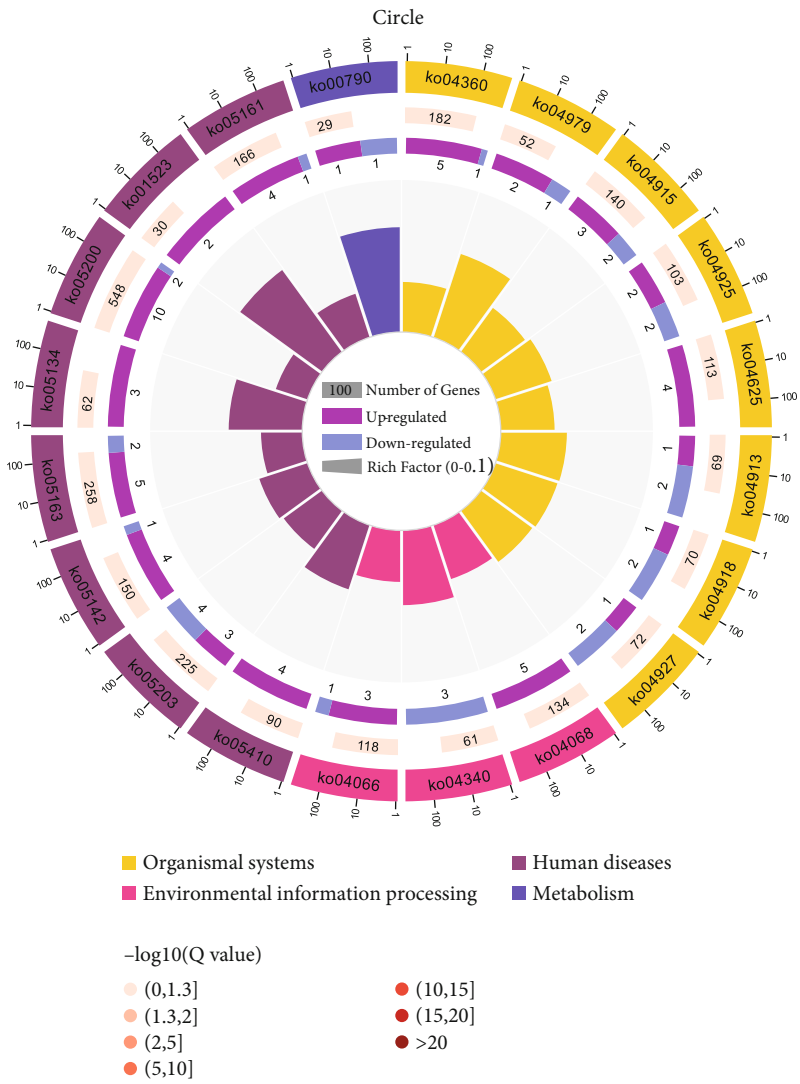


(d)

Figure 4: Continued.

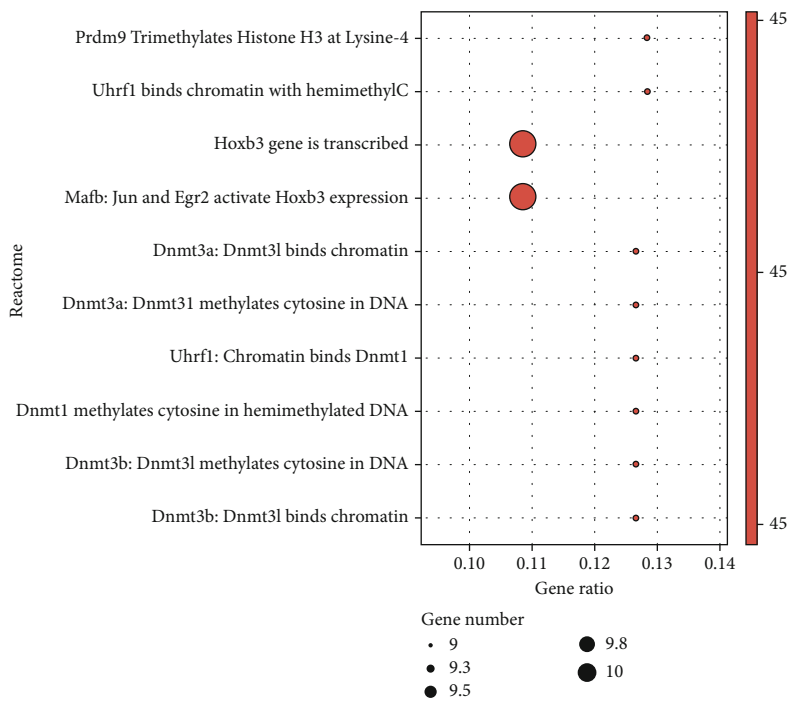


(e)

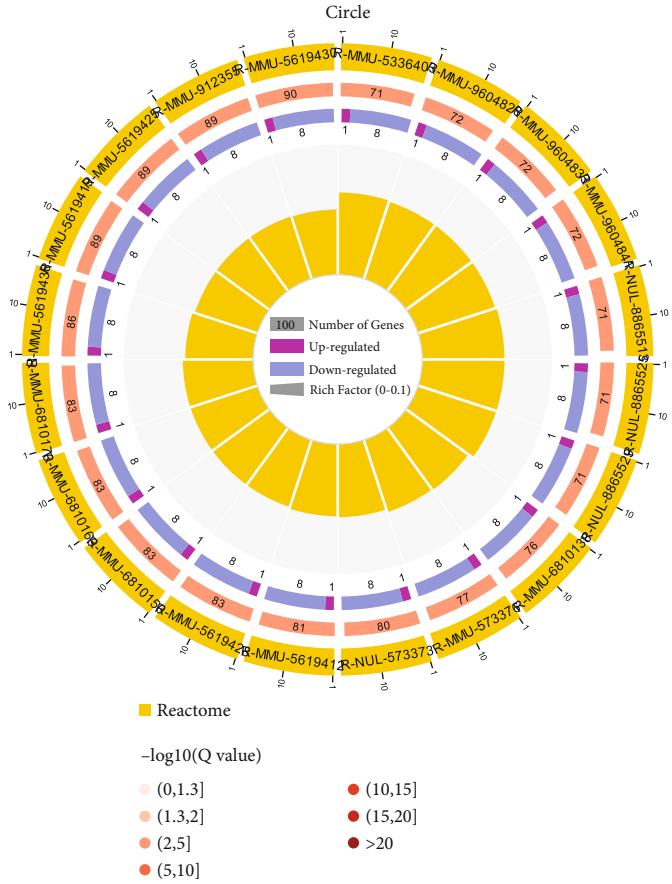


(f)

Figure 4: GO, KEGG, and Reactome analysis results of DEGs. (a) Bubble diagram and (b) circle diagram exhibited GO enrichment analysis results of the DEGs. (c) Bubble diagram and (d) circle diagram showed KEGG enrichment analysis results of the DEGs. (e) Bubble diagram and (f) circle diagram displayed Reactome pathway analysis results of the DEGs.

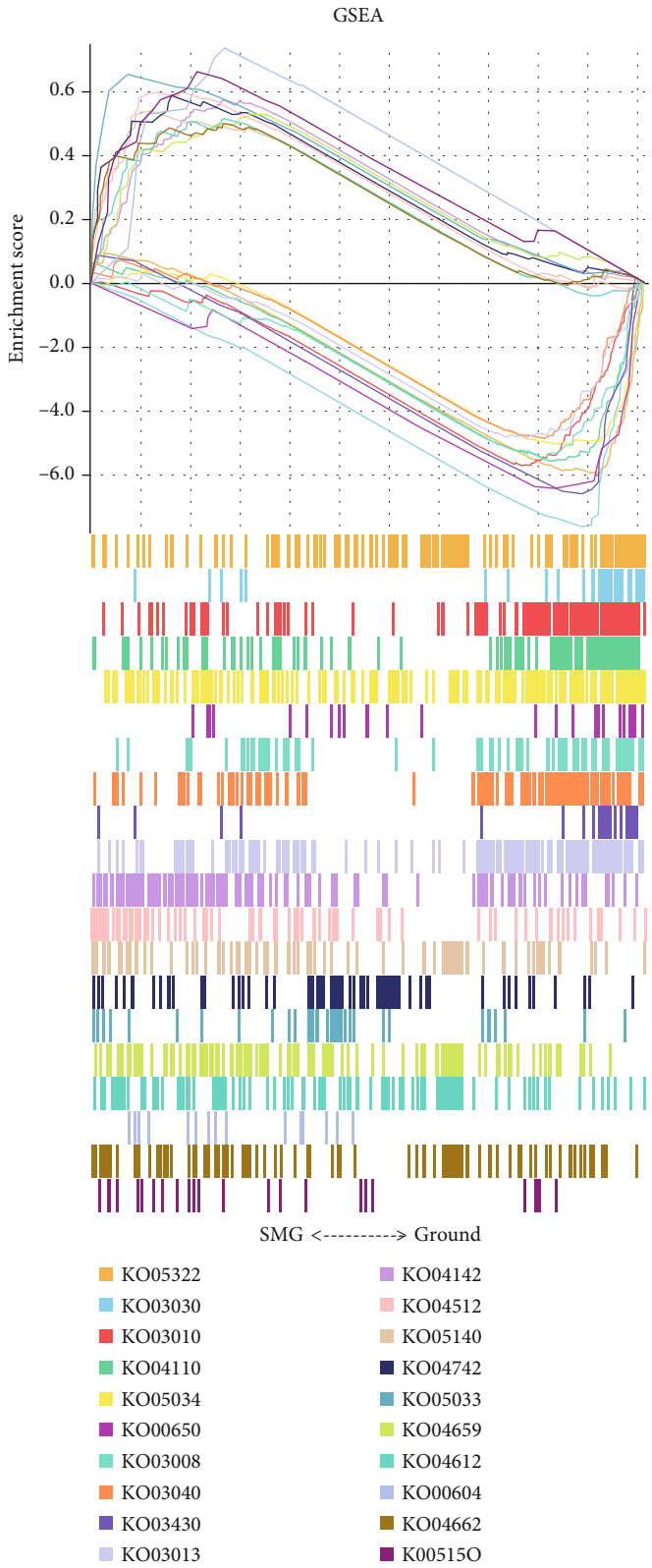


Figure 5: GSEA analysis results of DEGs.

the group was positively correlated (Figure 2(c)). Venn plot demonstrated that there were 10,443 genes that simultaneously correspond to both groups after sequencing (Figure 2(d)); the violin diagram displayed that the expression of six samples conformed to normal distribution (Figure 2(e)).

*3.2. Expression Analysis of DEGs in Weightlessness Osteoporosis.* By setting the threshold of |FC (fold change)| > 1.5 and $P < 0.05$, the sequencing results of ground and SMG groups showed that a total of 263 DEGs were detected, including 186 upregulated genes and 77 downregulated genes, and their specific gene distribution was shown in the volcano plot (Figure 3(a)), at the same time, the results of hierarchical clustering analysis demonstrated that the expression levels of common DEGs between ground group and SMG group were significantly different (Figure 3(b)). This study further exhibited the expression of the top 20 DEGs, as shown in the radar plot (Figure 3(c)). The specific coupregulated and codownregulated genes are shown in Supplementary Table 1.

*3.3. Functional Enrichment Analysis of DEGs.* The screened DEGs were uploaded into the DAVID database and *R* for GO functional enrichment analysis in weightlessness osteoporosis. Results of GO elucidated that the upregulated DEGs in BP were mainly involved in the negative regulation of multicellular biological processes, ribonucleic acid biosynthesis process, and cell-cell adhesion; in MF, they were chiefly associated with the regulation of cell differentiation, antioxidant activity, and regulation of cellular value-added; in CC, they were primarily enriched in the extracellular matrix containing collagen, synapses, and Golgi vesicles. Downregulated DEGs multicellular biological processes, MSC migration, and mitotic cell cycle phase transition were mainly involved in BP; regulation of nucleobase-containing compound metabolism and ATPase activator activity was principally associated with MF; and supramolecular complexes, intracellular membrane-bound organelles, and chromatin were mainly enriched in CC. Furthermore, bubble plots displayed the top 10 terms with the most significant differences from the results of GO, as shown in Figure 4(a), and the next 20 terms with significant differences were shown in chord plots (Figure 4(b)). In addition, the enrichment results of GO with all specific thresholds $P < 0.05$ are shown in supplementary Table 2.

*3.4. Signaling Pathway Enrichment Analysis of DEGs.* The screened DEGs were uploaded into the DAVID database and *R* for KEGG, Reactome, and GSEA signal pathway enrichment analysis in weightlessness osteoporosis. Enrichment analysis of KEGG revealed that DEGs was primarily involved in the interaction between cytokines, TNF signaling pathway, and FoxO signaling pathway. The top 10 signaling pathways with the strongest correlation were selected and displayed as bubble diagrams (Figure 4(c)), and the next 20 signaling pathways with strong correlation were selected to draw chord plot, as shown in Figure 4(d). Further pathway enrichment analysis was also performed in the Reactome database to explore the specific signaling pathways. Moreover, enrichment analysis of Reactome signal pathway further suggested that DEGs were mainly enriched in the transcription of Hoxb3 gene, RUNX1 recruitment of KMT2A gene, and activation of Hoxa2 chromatin signaling pathways. The top 10 most relevant signaling pathways were displayed as bubble diagrams (Figure 4(e)), and the next 20 signaling pathways with the most correlation were shown in chord diagrams (Figure 4(f)). In addition, the enrichment results of KEGG and Reactome with all specific thresholds $P < 0.05$ are shown in supplementary Tables 3 and 4, respectively. GSEA analysis in this study further indicated that the upregulated pathways primarily included ribosomal biogenesis, gene replication, and RNA transport in eukaryotes, while downregulated pathways mainly include ECM receptor interaction, Th17 cell differentiation, and B cell receptor signaling pathway (Figure 5).

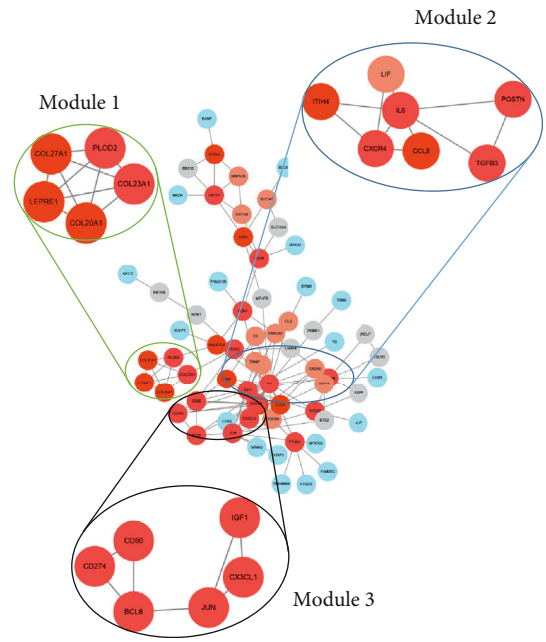


Figure 6: Interaction between DEGs in weightless osteoporosis. PPI network analysis of DEGs as well as the top 3 modules from PPI network. Every edge represented the interaction between two genes.

*3.5. Protein-Protein Interaction Network Analysis (PPI).* After analyzing the functions and aberrant signaling pathways, the common DEGs were then applied to construct PPI networks using the STRING database, and the generated gene networks were imported into Cytoscape 3.8.0 software for further analysis. The MCC algorithm was utilized to identify subnetworks with the closest interactions within gene networks, and totally, 3 subnetworks were generated. The top 10 genes calculated by MCC values were as follows: IL6, CXCR4, IGF1, JUN, CD80, CD274, BCL6, CX3CL1, COL23A1, and PLOD2. The detailed results were shown in Figure 6, and the darker color indicated the more significant role of the genes in the progression of weightlessness osteoporosis.

*3.6. Validation Results of Western Blotting.* The expression of CXCR4 and IGF1 was detected by Western blotting analysis. As shown in Figures 7(a) and 7(b), CXCR4 was highly expressed in the weightless environment, while IGF1 was lowly expressed. This is consistent with the findings of this study.

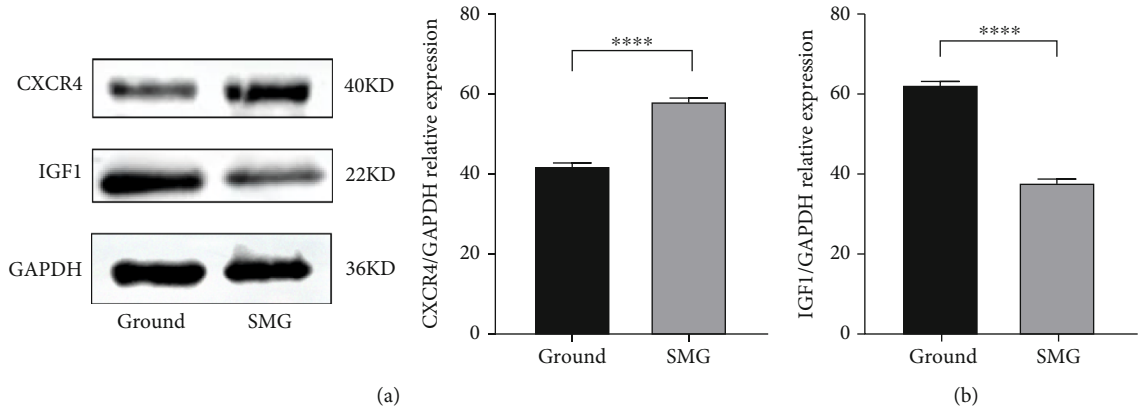


Figure 7: Validation of hub genes under weightlessness osteoporosis. Western blotting analysis of CXCR4 (a) and IGF1 (b) protein expression level in BMSCs after 48 h simulated microgravity. Data are presented as mean ± SD.

## 4. Discussion

Osteoporosis, currently recognized as the most prevalent systemic degenerative bone disease around the world, is mainly caused by the functional imbalance between osteoblasts and osteoclasts. It is mainly divided into primary and secondary osteoporosis, and secondary osteoporosis [13] primarily includes endocrine metabolic diseases that affect bone metabolism, drug-related, disuse, and other osteoporosis with clear etiology. Among which weightlessness osteoporosis caused by space flight is a special kind of disuse osteoporosis [14]. Some studies have shown [15] that the dominant reason is bone loss due to reduced skeletal loading and mechanical forces under weightlessness. Some scholars have also found [16] that weightlessness osteoporosis is associated with the redistribution of body fluids throughout the body after mankind enter the space. Nevertheless, there are few researches focusing on the molecular targets that contribute to the occurrence of weightlessness osteoporosis. In order to find effective potential therapeutic targets, it is necessary to further explore the pathogenesis of weightlessness osteoporosis.

In recent years, with the rapid development of HTS technology together with bioinformatics, it has been widely applied to study the occurrence and development of diseases and further analyze the disease-related causative genes and their biological significance [17–19]. Besides, the novel drug screening based on hub genes has also been reported [20]. Thus, this study is aimed at investigating the regulatory mechanisms and primary functions of pathogenic genes in the occurrence and development of weightlessness osteoporosis, aiming at providing novel ideas for the pathogenesis of osteoporosis and subsequent therapeutic targets.

GO enrichment analysis showed that the downregulated DEGs were mainly involved in the negative regulation of biological processes, MSC migration, mitotic cell cycle phase change, and osteoclast maturation, which indicated that osteoblasts were prone to osteoporosis progression under weightless condition; enrichment analysis of KEGG signal pathway revealed that the upregulated DEGs were mainly involved in cytokine interactions, TNF signaling pathway, and FoxO signaling pathway. Previous research reported that TNF mediated the development of postmenopausal osteoporosis and osteoporosis in systemic lupus erythematosus (SLE) patients, which is consistent with the results in this study that TNF signaling pathway also mediated osteoporosis in weightlessness condition; enrichment analysis of Reactome signal pathway elucidated that DEGs were primarily involved in Hoxb3 gene transcription, RUNX1 recruitment of KMT2A gene, and Hoxa2 chromatin activation signaling pathway, suggesting that Hoxb3 and RUNX1 related signaling pathways also played a crucial role in weightlessness osteoporosis. GSEA analysis further indicated that DEGs are mainly involved in ribosome biogenesis, gene replication and RNA transport, ECM receptor interaction, Th17 cell differentiation, and B cell receptor signaling pathway in eukaryotes. These functions may have a certain impact on bone tissue, mainly including regulation of osteoblast differentiation, bone development, bone mineralization, regulation of bone resorption, intramembranous bone growth, and regulation of bone remodeling. The abovementioned functions and signaling pathways related to DEGs are the key pathogenesis that mediated weightlessness osteoporosis.

The occurrence and development of weightlessness osteoporosis are the result of the joint action of multiple genes and signaling pathways. In this study, PPI network was further constructed to identify and authenticate synergistic genes, and the top 10 genes were calculated using the MCC algorithm, namely, IL6, CXCR4, IGF1, JUN, CD80, CD274, BCL6, COL23A1, and PLOD2. Among them, IL6, CXCR4, IGF1, and PLOD2 were finally included in this study for follow-up analysis, because the relationships between these genes and weightlessness osteoporosis remained unclear, which was worth further analyzing. Therefore, these gene sets would provide new ideas for understanding the pathogenesis of weightlessness osteoporosis.

IL6 is a multibiological characteristic cytokine located on human chromosome 7p21, which is not only widely presented in various types of inflammations as a common inflammatory factor but also played important roles in multiple stages and systems of biology, such as cirrhosis [21].

Related scholars have found that IL6 could promote the formation and absorption of bone cells [22–24]. A clinical study showed [25] that IL6 mRNA was highly expressed in bone explants of patients with pyramidal fractures due to osteoporosis. It has also been found [26] that some inflammatory factors such as IL6 may upregulate the expression of RANKL in osteoblasts and accelerate RANKL signaling transduction, which directly resulted in bone destruction. Our study further confirmed that IL6 is closely associated with the progression of osteoporosis in weightlessness. CXC chemokine receptor type 4 (CXCR4) is a 7-transmembrane G-protein-coupled receptor [27], which is widely expressed in peripheral blood and other organ tissues, including hematopoietic stem cells, endothelial cells, lymphocytes, and cancer cells [28], and mainly participates in chemotaxis in the immune and hematopoietic systems [29]. Studies [30] have shown that SDF-1/CXCR4 played a significant role in the occurrence and development of bone differentiation, bone regeneration, and orthopedic diseases, such as neovascularization, BMSC migration, and cytokine secretion. In addition, SDF-1/CXCR4 could also promote BMSCs bone regeneration and differentiation through MAPK signaling pathway [31]. However, our findings revealed that CXCR4 was highly expressed in weightlessness osteoporosis, which may contradict the low expression state in normal osteoporosis. Combined with the previous finding that vascular endothelial cells tend to apoptosis in weightlessness condition via SDF-1/CXCR4 signaling pathway [32], this study deduced that the SDF-1/CXCR4 pathway mainly mediated the apoptotic process of vascular endothelial cells rather than bone differentiation under weightlessness condition. Procollagen-lysine, 2-oxoglutate 5-dioxygenase (PLOD2) is one of the members of the PLOD family. Studies [33–35] showed that PLOD2 was mediated by HIF-1$\alpha$, TGF-$\beta$, and microRNA-26a/b to promote the occurrence and development of gliomas. Meanwhile, PLOD2 induced the differentiation of bone marrow stromal cells [36], and the abnormal expression of PLOD2 could result in Bruck syndrome [37], which is manifested as osteogenesis imperfection, bone fragility, and brittle fracture. This study firstly found that PLOD2 played a momentous role in mediating the progression of weightlessness osteoporosis. IGF1, namely, insulin-like growth factor I, is also a protein encoded by human gene and an important product of multiple cells through autocrine and paracrine secretion. It has been shown that IGF1 promoted metastasis of melanoma cells and also promoted migration and invasion of hepatocellular carcinoma cells through upregulating the expression of EGR1. IGF1 also played a vital anabolic role in skeletal development [38], and low expression of IGF1 could induce risk of osteoporosis fracture, which was consistent with the conclusion in this study.

## 5. Conclusions

In conclusion, finding new drug targets to prevent or slow down weightlessness osteoporosis is one of the major issues that need to be urgently addressed in spaceflight. In this study, DEGs were identified by high-throughput sequencing by weightlessness osteoporosis model, and the synergistic relationships between their DEGs were analyzed to further explore the regulatory mechanisms affecting the occurrence of weightlessness osteoporosis. IL6, CXCR4, IGF1, and PLOD2 played crucial roles in weightlessness osteoporosis, which provided a theoretical basis for the pathogenic mechanism and treatment of weightlessness osteoporosis.

## Data Availability

The raw data of Bulk-RNA sequencing used to support the findings of this study are deposited at the NCBI with the accession ID SUB11153018, which would be released on Jan 1, 2023, on NCBI due to some conflicts of interest and the importance of our experimental data. Alternatively, the same raw data could also be found at Figshare, and the URLs are as follows. Gene matrix data used to support the findings of this study are available from the corresponding author upon request. We uploaded a total of 6 files to Figshare, and the URLs are as follows: https://figshare.com/s/74eb3ca1839318a2b249https://figshare.com/s/ef0cd053ad787107410dhttps://figshare.com/s/a02ce47840e7ecef1af6https://figshare.com/s/6093aec3ae70d11e9af6https://figshare.com/s/6fe3d14cbdbd9820a3adhttps://figshare.com/s/8adf677a50441fb43b92

## Consent

All contributing authors have agreed with the publication of this article.

## Conflicts of Interest

All authors declared no conflicts of interests related to this manuscript, and all authors have approved the publication of this work.

## Authors' Contributions

This study was completed with teamwork. Each author had made corresponding contribution to the study. Ming Yan, Zhibin Liu, and Dong Wang conceived the idea. Dong Wang, Weihang Li, and Ziyi Ding wrote the main manuscript. Dong Wang, Weihang Li, and Ziyi Ding used the software. Ziyi Ding, Quan Shi, Shilei Zhang, and Zhuoru Zhang downloaded and collected data. Dong Wang, Weihang Li, Xiaocheng Wang, and Shilei Zhang analyzed the data. Zhibin Liu, Ming Yan, and Dong Wang prepared figures. Ming Yan, Weihang Li, Dong Wang, and Xiaocheng Wang redressed the manuscript. Xiaocheng Wang, Zhibin Liu, Ziyi Ding, and Shilei Zhang reviewed the manuscript. Dong Wang, Weihang Li, and Ziyi Ding contributed equally as the co-first authors. Dong Wang, Weihang Li, and Ziyi Ding contributed equally to this work.

## Acknowledgments

This study was supported by grants from the National Natural Science Foundation of China (no. 82072475).

## Supplementary Materials

The specific coupregulated and codownregulated genes are shown in supplementary Table 1. The detailed enrichment results of GO, KEGG, and Reactome with all specific thresholds $P < 0.05$ are shown in supplementary Tables 2, 3, and 4, respectively. *(Supplementary Materials)*

## References


[1] T. Coughlan and F. Dockery, "Osteoporosis and fracture risk in older people," *Clinical Medicine (London, England)*, vol. 14, no. 2, pp. 187–191, 2014.

[2] K. M. Prestwood, C. C. Pilbeam, and L. G. Raisz, "Treatment of osteoporosis," *Annual Review of Medicine*, vol. 46, no. 1, pp. 249–256, 1995.

[3] W. Qin, X. Li, Y. Peng et al., "Sclerostin antibody preserves the morphology and structure of osteocytes and blocks the severe skeletal deterioration after motor-complete spinal cord injury in rats," *Journal of Bone and Mineral Research*, vol. 30, no. 11, pp. 1994–2004, 2015.

[4] R. J. White and M. Averner, "Humans in space," *Nature*, vol. 409, no. 6823, pp. 1115–1118, 2001.

[5] P. Bianco, M. Riminucci, S. Gronthos, and P. G. Robey, "Bone marrow stromal stem cells: nature, biology, and potential applications," *Stem Cells*, vol. 19, no. 3, pp. 180–192, 2001.

[6] Z. Q. Dai, R. Wang, S. K. Ling, Y. M. Wan, and Y. H. Li, "Simulated microgravity inhibits the proliferation and osteogenesis of rat bone marrow mesenchymal stem cells," *Cell Proliferation*, vol. 40, no. 5, pp. 671–684, 2007.

[7] M. Zayzafoon, W. E. Gathings, and J. M. McDonald, "Modeled microgravity inhibits osteogenic differentiation of human mesenchymal stem cells and increases adipogenesis," *Endocrinology*, vol. 145, no. 5, pp. 2421–2432, 2004.

[8] Z. Hu, Y. Wang, Z. Sun et al., "miRNA-132-3p inhibits osteoblast differentiation by targeting Ep300 in simulated microgravity," *Scientific Reports*, vol. 5, no. 1, article 18655, 2015.

[9] Z. Liu and J. H. Xu, "The application of the high throughput sequencing technology in the transposable elements," *Yi Chuan*, vol. 37, no. 9, pp. 885–898, 2015.

[10] Y. Pan, C. F. Li, Y. Gao, Y. C. Wang, and X. Q. Sun, "Effect of miR-27b-5p on apoptosis of human vascular endothelial cells induced by simulated microgravity," *Apoptosis*, vol. 25, no. 1-2, pp. 73–91, 2020.

[11] G. J. Dennis, B. T. Sherman, D. A. Hosack et al., "DAVID: database for annotation, visualization, and integrated discovery," *Genome Biology*, vol. 4, no. 5, p. P3, 2003.

[12] C. H. Chin, S. H. Chen, H. H. Wu, C. W. Ho, M. T. Ko, and C. Y. Lin, "cytoHubba: identifying hub objects and subnetworks from complex interactome," *BMC Systems Biology*, vol. 8, Supplement 4, 2014.

[13] E. Stein and E. Shane, "Secondary osteoporosis," *Endocrinology and Metabolism Clinics of North America*, vol. 32, no. 1, pp. 115–134, 2003.

[14] S. Takata and N. Yasui, "Disuse osteoporosis," *The Journal of Medical Investigation*, vol. 48, no. 3-4, pp. 147–156, 2001.

[15] P. M. Loomer, "The impact of microgravity on bone metabolism in vitro and in vivo," *Critical Reviews in Oral Biology and Medicine*, vol. 12, no. 3, pp. 252–261, 2001.

[16] B. Zhu, H. Guo, X. J. Hao, Q. Fu, and S. M. Hu, "Mechanism of weightlessness osteoporosis and preventive and therapeutic effect of traditional Chinese medicine," *Zhongguo Gu Shang*, vol. 25, no. 7, pp. 611–616, 2012.

[17] W. Li, Y. Zhao, D. Wang et al., "Transcriptome research identifies four hub genes related to primary myelofibrosis: a holistic research by weighted gene co-expression network analysis," *Aging (Albany NY)*, vol. 13, no. 19, pp. 23284–23307, 2021.

[18] W. Li, Z. Ding, D. Wang et al., "Ten-gene signature reveals the significance of clinical prognosis and immuno-correlation of osteosarcoma and study on novel skeleton inhibitors regarding MMP9," *Cancer Cell International*, vol. 21, no. 1, 2021.

[19] W. Li, B. Yuan, Y. Zhao et al., "Transcriptome Profiling Reveals Target in Primary Myelofibrosis Together with Structural Biology Study on Novel Natural Inhibitors Regarding JAK2," *Aging*, vol. 13, no. 6, pp. 8248–8275, 2021.

[20] W. Li, Z. Ding, Y. Zhao et al., "Novel natural inhibitors targeting enhancer of Zeste homolog 2: a comprehensive structural biology research," *Oncology*, vol. 11, 2021.

[21] K. Yamaguchi, Y. Itoh, C. Yokomizo et al., "Blockade of interleukin-6 signaling enhances hepatic steatosis but improves liver injury in methionine choline-deficient diet-fed mice," *Laboratory Investigation*, vol. 90, no. 8, pp. 1169–1178, 2010.

[22] T. Kishimoto, M. Hibi, M. Murakami, M. Narazaki, M. Saito, and T. Taga, "The molecular biology of interleukin 6 and its receptor," *Ciba Foundation Symposium*, vol. 167, 2007.

[23] Y. O. Ishimi, C. H. Miyaura, C. H. Jin et al., "IL-6 is produced by osteoblasts and induces bone resorption," *Journal of Immunology*, vol. 145, no. 10, pp. 3297–3303, 1990.

[24] A. J. Littlewood, J. Russell, G. R. Harvey, D. E. Hughes, R. G. G. Russell, and M. Gowen, "The modulation of the expression of IL-6 and its receptor in human osteoblasts in vitro," *Endocrinology*, vol. 129, no. 3, pp. 1513–1520, 1991.

[25] S. H. Ralston, "Do genetic markers aid in risk assessment?," *Osteoporosis International*, vol. 8, Supplement 1, pp. S37–S42, 1998.

[26] J. R. Arron and Y. Choi, "Bone versus immune system," *Nature*, vol. 408, no. 6812, pp. 535-536, 2000.

[27] T. Pozzobon, G. Goldoni, A. Viola, and B. Molon, "CXCR4 signaling in health and disease," *Immunology Letters*, vol. 177, pp. 6–15, 2016.

[28] D. Rossi and A. Zlotnik, "The biology of chemokines and their receptors," *Annual Review of Immunology*, vol. 18, no. 1, pp. 217–242, 2000.

[29] Y. R. Zou, A. H. Kottmann, M. Kuroda, I. Taniuchi, and D. R. Littman, "Function of the chemokine receptor CXCR4 in haematopoiesis and in cerebellar development," *Nature*, vol. 393, no. 6685, pp. 595–599, 1998.

[30] H. Qin, X. Zhao, Y. J. Hu et al., "Inhibition of SDF-1/CXCR4 axis to alleviate abnormal bone formation and angiogenesis could improve the subchondral bone microenvironment in osteoarthritis," *BioMed Research International*, vol. 2021, Article ID 8852574, 13 pages, 2021.

[31] Y. Xiang, Y. Li, L. Yang, Y. He, D. Jia, and X. Hu, "miR-142-5p as a CXCR4-targeted microRNA attenuates SDF-1-induced chondrocyte apoptosis and cartilage degradation via inactivating MAPK signaling pathway," *Biochemistry Research International*, vol. 2020, Article ID 4508108, 14 pages, 2020.

[32] H. Zhang, P. Wang, X. Zhang, W. Zhao, H. Ren, and Z. Hu, "SDF1/CXCR7 signaling axis participates in angiogenesis in degenerated discs via the PI3K/AKT pathway," *DNA and Cell Biology*, vol. 38, no. 5, pp. 457–467, 2019.

[33] E. B. Rankin and A. J. Giaccia, "Hypoxic control of metastasis," *Science*, vol. 352, no. 6282, pp. 175–180, 2016.

[34] A. Tsezou, "Osteoarthritis year in review 2014: genetics and genomics," *Osteoarthritis and Cartilage*, vol. 22, no. 12, pp. 2017–2024, 2014.

[35] K. Miyamoto, N. Seki, R. Matsushita et al., "Tumour-suppressive *miRNA-26a-5p* and *miR-26b-5p* inhibit cell aggressiveness by regulating *PLOD2* in bladder cancer," *British Journal of Cancer*, vol. 115, no. 3, pp. 354–363, 2016.

[36] M. Valtavaara, C. Szpirer, J. Szpirer, and R. Myllylä, "Primary structure, tissue distribution, and chromosomal localization of a novel isoform of lysyl hydroxylase (lysyl hydroxylase 3)∗," *The Journal of Biological Chemistry*, vol. 273, no. 21, pp. 12881–12886, 1998.

[37] R. Ha-Vinh, Y. Alanay, R. A. Bank et al., "Phenotypic and molecular characterization of Bruck syndrome (osteogenesis imperfecta with contractures of the large joints) caused by a recessive mutation in PLOD2," *American Journal of Medical Genetics. Part A*, vol. 131A, no. 2, pp. 115–120, 2004.

[38] J. L. Fowlkes, J. S. Nyman, R. C. Bunn et al., "Osteo-promoting effects of insulin-like growth factor I (IGF-I) in a mouse model of type 1 diabetes," *Bone*, vol. 57, no. 1, pp. 36–40, 2013.

Hindawi
Stem Cells International
Volume 2022, Article ID 2190447, 15 pages
https://doi.org/10.1155/2022/2190447

*Research Article*

# Platelet-Derived Growth Factor-Functionalized Scaffolds for the Recruitment of Synovial Mesenchymal Stem Cells for Osteochondral Repair

**Yuan Luo,[1,2] Xiaodong Cao,[2] Junfeng Chen,[2] Jianwei Gu,[2] Hao Yu,[1] Junying Sun,[1] and Jun Zou[1]**

[1]*Department of Orthopedic, The First Affiliated Hospital of Soochow University, Suzhou, Jiangsu, China*
[2]*Department of Orthopedic, Taicang Affiliated Hospital of Soochow University, Taicang, Jiangsu, China*

Correspondence should be addressed to Jun Zou; jzou@suda.edu.cn

Received 6 December 2021; Accepted 11 January 2022; Published 27 January 2022

Academic Editor: Qiang Zhou



Cartilage regeneration is still a challenge for clinicians because of avascularity, denervation, load-bearing, synovial movement, and the paucity of endogenous repair cells. We constructed a multilayered osteochondral bionic scaffold and examined its repair capacity using a rabbit osteochondral defect model. The cartilage phase and interface layer of the scaffold were prepared by freeze-drying, whereas the bone phase of the scaffold was prepared by high-temperature sintering. The three-phase osteochondral bionic scaffold was formed by joining the hydroxyapatite (HAp) and silk fibroin (SF) scaffolds using the repeated freeze-thaw method. Different groups of scaffolds were implanted into the rabbit osteochondral defect model, and their repair capacities were assessed using imaging and histological analyses. The cartilage phase and the interface layer of the scaffold had a pore size of $110.13 \pm 29.38$ and $96.53 \pm 33.72\,\mu$m, respectively. All generated scaffolds exhibited a honeycomb porous structure. The polydopamine- (PDA-) modified scaffold released platelet-derived growth factor (PDGF) for 4 weeks continuously, reaching a cumulative release of $71.74 \pm 5.38\%$. Synovial mesenchymal stem cells (SMSCs) adhered well to all scaffolds, but demonstrated the strongest proliferation ability in the HSPP (HAp-Silk-PDA-PDGF) group. Following scaffold-induced chondrogenic differentiation, SMSCs produced much chondrocyte extracellular matrix (ECM). In *in vivo* experiments, the HSPP group exhibited a significantly higher gross tissue morphology score and achieved cartilage regeneration at an earlier stage and a significantly better repair process compared with the other groups ($P < 0.05$). Histological analysis revealed that the new cartilage tissue in the experimental group had a better shape and almost filled the defect area, whereas the scaffold was nearly completely degraded. The new cartilage was effectively fused with the surrounding normal cartilage, and a substantial amount of chondrocyte ECM was formed. The SF/HAp three-layer osteochondral bionic scaffold exhibited favorable pore size, porosity, and drug sustained-release properties. It demonstrated good biocompatibility in vitro and encouraging repair effect at osteochondral defect site in vivo, thereby expected to enabling the repair and regeneration of osteochondral damage.

## 1. Introduction

Due to low cellularity and lack of vascularity and innervation, damaged articular hyaline cartilage often cannot repair itself spontaneously [1] and is prone to further degeneration when subjected to exercise and load, resulting in pain and dysfunction [2]. Damage to the articular cartilage can be divided into two types: partial-thickness damage and full-thickness damage. Among the most challenging aspects of clinical practice is the repair of full-thickness cartilage damage [3]. All available clinical treatment methods present problems, such as secondary injury and donor limitations, as well as difficulty in achieving long-term stable curative effects due to the inability to regenerate hyaline cartilage [4, 5]. Articular cartilage, subchondral bone, and bone together form a complete functional unit, exhibiting anatomical gradient and physiological specificity, while being closely connected in anatomical structure. In particular, the biomechanical properties,

metabolic characteristics, and material transport capabilities vary from one region to another. Therefore, research on bionic tissue engineering scaffolds has advanced significantly in recent years. Besides providing a frame for seed cells to adhere, proliferate, and differentiate, scaffolds can also serve as a carrier for the release of growth factors. In addition, they can also offer a mechanically stable environment to facilitate tissue regeneration [6–8]. SF is a natural polymer material, ideal for use as a scaffold in tissue engineering. The structure of SF is similar to that of collagen in normal tissues. Concomitantly, it also possesses favorable biocompatibility, mechanical properties, and a certain degree of biodegradability, making it a hot spot in regeneration research [9]. HAp is a calcium phosphate mineral that has gained widespread attention because of the similarity of its chemical composition and crystal structure to those of natural bone minerals. It has been successfully used in clinical bone repair and has produced satisfactory curative results [10].

The ability to differentiate into cartilage is the primary criteria used by researchers for the selection of seed cells and their reliable source, which is also an important factor for consideration. Recent studies have shown that SMSCs can efficiently proliferate and differentiate into cartilage and exist in a large number in the synovium around the joint, which makes it easy to obtain [3, 11]. In tissue engineering, growth factors are critical regulatory factors that control the proliferation rate, migration direction, and differentiation potential of cells. PDGF is a basic protein stored in platelet $\alpha$ particles. With cartilage injury, the coagulation mechanism helps to form many blood clots at the injury site, which contain platelets rich in PDGF [12]. However, macrophages that have migrated due to inflammation also synthesize large amounts of PDGF to promote the proliferation and differentiation of remaining chondrocytes nearby, achieving the local regeneration and repair of cartilage [13].

Many previous studies need to culture cells on scaffolds in advance, which has been damaged by multiple operations. The cell-free scaffold in this study can be implanted through one operation to avoid two-stage injuries and to recruit stem cells at the injured site for in situ repair. The structure, porosity, and pore size range of the scaffold material were examined under a scanning electron microscope (SEM). PDA was used to increase the active groups on the surface of the material, increasing the loading of PDGF to the scaffold material and achieving sustained release. The biological performance of cells on the scaffold material was also examined. Furthermore, scaffolds were implanted in rabbit osteochondral defect models, and the effects of osteochondral damage repair were assessed using imaging and histological indicators. Our study indicated that a cell-free tissue engineering scaffold can be constructed and growth factors within the scaffold can recruit SMSCs around the cartilage damage site to facilitate cartilage repair.

## 2. Materials and Methods

### *2.1. Construction and Characterization of the SF/HAp Three-Phase Scaffold [14]*

*2.1.1. Construction.* SF solutions from cocoons of *B. mori* (RudongXinsilu Co., Ltd., Jiangsu, China) were prepared using the following methods. SF was added to 0.5% $Na_2CO_3$ solution, boiled for 1 h, and dissolved in 9.3 mol/L lithium bromide solution (Strem Chemicals Inc., MA, USA). Repeated dialysis with ultrapure water and concentrating with ethylene glycol were performed to prepare SF solutions of different concentrations. HAp powder (Aladdin, Shanghai, China) was added to the 5% SF solution and sintered for 3 h; it was injected into a mold with a diameter of 4 mm and a length of 10 mm, placed in a refrigerator at -80°C overnight, and freeze-dried to obtain a scaffold. The scaffold was placed in a muffle furnace, and the temperature was raised to 90°C at 1.5°C/min, then to 200°C for 40 min, after it was risen further to 1250°C at 2°C/min, and sintered at this temperature for 4 h. The 5% SF solution was added to the mold and then placed in the refrigerator at -20°C overnight. The 20% SF solution was preheated to 45°C and dropped into the previous mold, which was then placed in the refrigerator at -80°C overnight. Subsequently, the HAp scaffold sample soaked in SF solution was preheated to 45°C and placed into the mold, then freezing overnight at -80°C. The SF/HAp three-layer osteochondral bionic scaffold was obtained by freeze-drying (Alpha 1e2 LD plus, Christ, Germany). After soaking in methanol for 30 min, the structure of SF was altered and an insoluble SF/HAp three-layer osteochondral bionic scaffold was obtained as illustrated in Figure 1.

*2.1.2. SEM Observation of Scaffold Structure.* The scaffold samples were cut to 2–3 mm thickness and adhered to the conductive adhesive on the sample stage. SEM samples were then sprayed with gold in the ion sputter coater for observation. Analysis of the pore size of the scaffold was performed using NanoMeasurer. Scaffold porosity was calculated using the liquid replacement method.

*2.2. Load and Release of PDGF on the Scaffold.* The above bionic scaffold was immersed in 2 mg/mL dopamine solution and shaken on a shaker at 20°C for 24 h. The scaffold was then ultrasonically cleaned with deionized (DI) water and dried overnight in a vacuum. The scaffold was sterilized by ultraviolet ($\lambda = 254$ nm) irradiation for 4 h before use. In the experimental design of this study, PDGF (Peprotech, USA) was only loaded on the cartilage-phase SF scaffold. Therefore, only the pure SF scaffold group (SP) and PDA-modified SF scaffold group (SP-PDA) were considered in this part of the study. *In vitro* PDGF release curves were measured using ELISA.

### *2.3. Evaluation of Biological Behaviors of Cells on the Scaffold*

*2.3.1. Cell Proliferation.* The scaffolds were first placed in 96-well plates according to groups. After irradiation sterilization, a 1 mL cell suspension (total of $2 \times 10^3$ cells) was dripped onto the scaffold and cultured in a 5% $CO_2$ incubator at 37°C with complete medium. The proliferation rate of cells in each group at different time points (1, 3, 5, and 7 d) was measured using the CCK-8 method, and the corresponding proliferation curves were plotted.

*2.3.2. Cell Migration.* A 24-well Transwell plate was selected, 150 $\mu$L cell suspension was added to the upper chamber, and 700 $\mu$L serum-free medium was added to the lower chamber. After 24 h of starvation, according to the added component, the lower chambers were set as the pure SF scaffold group

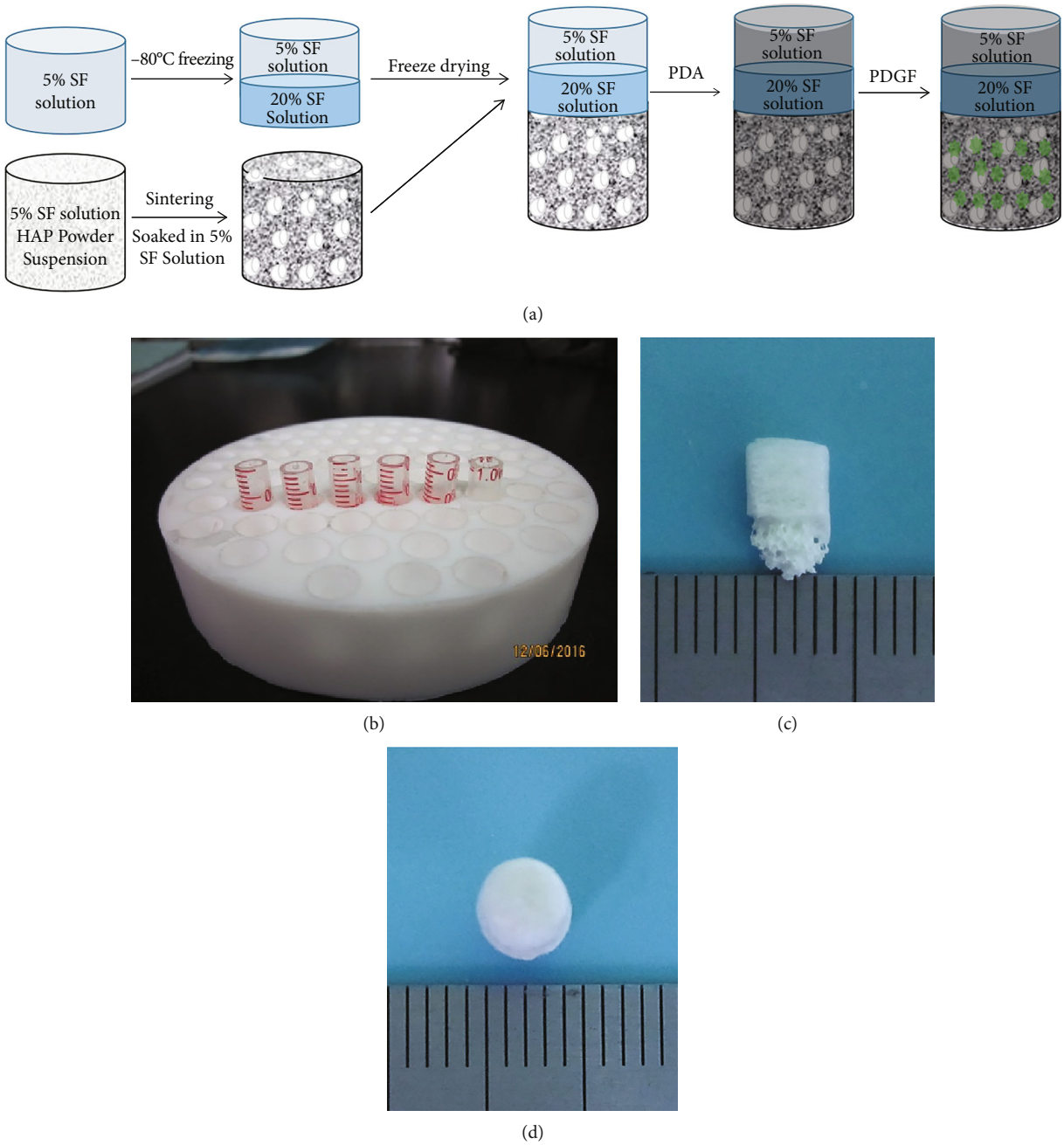


Figure 1: (a) Schematic illustration of the preparation of the three-phase scaffold. (b) Custom mold for making scaffold. The profile (c) and vertical (d) appearance of scaffold.

(SF), PDA-modified SF scaffold group (SP-2), PDA-modified and PDGF-loaded SF scaffold group (SPP), 50 ng/mL PDGF-supplemented DMEM group (DMEM+PDGF), and 5% FBS-supplemented DMEM group (DMEM+FBS). After overnight incubation, the upper chamber was taken out and the inner surface was scraped several times using cotton swabs. Only those cells that passed through the upper chamber and attached to the outer side of the membrane were retained. Cells were counted under a fluorescence microscope after staining with crystal violet.

*2.3.3. Pellet Culture.* The pellet culture was used to induce the differentiation of SMSCs into cartilage. P3 SMSCs were adjusted to $1 \times 10^5$/mL and 1 mL cell suspension taken for centrifugation to obtain SMSC agglomerates. Care was taken over the process to avoid blowing the agglomerates; they were gently transferred to an ultrafiltration centrifuge tube, and different group bionic scaffolds were placed in the inner chamber for pellet induction culture. The diameters of pellets in different groups were measured. After paraffin embedding, alcian blue, and toluidine blue staining were

applied to analyze the specific expression of ECM in pellets. In this part of the study, only the SP-2 group (PDA-modified SF scaffold) and the SPP group (PDA-modified and PDGF-loaded SF scaffold) were considered.

*2.3.4. Cytoskeleton Staining.* A Transwell culture was employed to induce cartilage formation, and the cytoskeleton and nuclei of cells were immunofluorescence stained to visualize the expression and arrangement of cytoskeleton proteins in each group.

*2.4. Construction of the Rabbit Osteochondral Defect Model and Implantation of the Three-Phase Scaffold.* New Zealand white rabbits were purchased from the Experimental Animal Center of Soochow University (Suzhou, China). The animal handling and surgical procedures were conducted in accordance with protocols approved by the Ethics Committee at the First Affiliated Hospital of Soochow University. A 4 mm diameter trephine was used to construct an osteochondral defect (4 mm in diameter and 5 mm in depth) at the trochlear part of the rabbit knee joint, where a scaffold was implanted. The following groups were set up: normal, blank, HSF, HSP-1, HSP-2, and HSPP as listed in Table 1.

*2.4.1. MRI.* We conducted magnetic resonance imaging (MRI) examinations at 6, 12, and 24 weeks after surgery. We used the 1.5 T GE Signa magnetic resonance imager (Signa HDe; GE) to perform a routine scan of the sagittal T2-weighted image (Sag 3D SPGR fat sat sequence) of rabbit's knee joint and scored according to the MOCART MRI evaluation standard.

*2.4.2. Staining.* Samples were harvested according to the set time points and evaluated based on International Cartilage Repair Society (ICRS) scores. After serial treatment, HE, Masson, and Safranin O/fast green staining, as well as immunohistochemical staining of aggrecan, Col-I, and Col-II, were conducted on the sections to analyze the cartilage regeneration status and specific ECM expressions.

*2.5. Statistics.* All samples were tested in triplicates (unless indicated), and values were expressed as the mean (M) ± standard deviation (SD). GraphPad Prism (GraphPad Software, Inc.; USA) were used for statistical analysis and plotting. Biohistochemical analysis and gene expression analysis were performed using one-way ANOVA and Tukey's test. Pairwise comparison between groups was performed using an independent sample $t$-test. $P < 0.05$ indicated a statistically significant difference between groups.

## 3. Results and Discussion

*3.1. Preparation and Characterization of the Osteochondral Bionic Scaffold.* In consideration of the tissue sections of normal rabbit knee joint and the requirements of tissue engineering scaffolds suitable for different cell growth, we selected the concentration of SF according to the pore size distribution and porosity under electron microscope. We finally selected the 5% SF solution for the cartilage phase, whereas the 20% SF solution was chosen as the working concentration for the interface layer. The constructed scaffold was approximately 4 mm in diameter and 5 mm in height, consistent with the dimensions of the critical defect reported in the literature [15].

Table 1: Sample abbreviations used in this study.

| Group | Composition |
|---|---|
| HSF | HAp+pure SF scaffold |
| HSP-1 | HAp+SF with physical adsorption of PDGF |
| HSP-2 | HAp+PDA-modified SF with no PDGF |
| HSPP | HAp+PDA-modified SF loaded with PDGF |

Note: the nomenclature with H corresponds to scaffolds that contain HAp bone phase.

The scaffold, which was cylindrical, was divided into three layers along its long axis. The height of cartilage layer was 1 mm, the interface layer 1 mm, and the subchondral bone, and bone phase was about 3 mm as shown in Figures 1(c) and 1(d). The pore size of the cartilage phase was in range of 60–177 $\mu$m, the interface layer 27–171 $\mu$m, and the bone phase 96–845 $\mu$m as shown in Figure 2. Interestingly, the pore size distribution of each layer was generally uniform. However, pore sizes within the cartilage phase, the interface layer, and the bone phase were not consistent, closely mimicking the normal anatomical structure. We also found that the porosity of each experimental group was not significantly changed compared to that of the blank group ($P > 0.05$), which was maintained at approximately 45%.

*3.2. Load and Release of PDGF.* Following the PDA modification of the scaffold, a uniform coating developed on its surface, resulting in a gray-black appearance like Figures 3(a) and 3(b). According to the minimum effective concentration, 50 ng PDGF was diluted into 100 $\mu$L solution and then dropped onto the physical adsorption group and PDA group. In this experiment, we only loaded PDGF on the SF scaffold of the cartilage phase; thus, only the HSP-1 and HSPP groups were investigated.

Because of the physical adsorption of PDGF, we observed a 52.5% burst release in the HSP-1 group on the first day. On the third day, the release reached 67.74%, whereas on the 28th day, the cumulative release reached approximately 73.41%. In comparison, we observed no burst release of PDGF in the HSPP group on the first day; instead, in this study, only 12.53% PDGF was released. However, on the seventh day, the gradual release reached 52.07%, whereas on the 28th day, the cumulative release reached 71.74% as shown in Figure 3(c).

*3.3. Evaluation of the Biological Behaviors of Cells on the Scaffold*

*3.3.1. Cell Adhesion and Proliferation Experiments.* For this experiment, we seeded P3 SMSCs onto each group of scaffolds and observed cells under a SEM microscope at the set time points. We observed that the PDGF-loaded SP-1, SPP, and DMEM+PDGF groups all demonstrated an obvious increase in the total content of cells, suggesting that PDGF had a significant promoting effect on cell proliferation

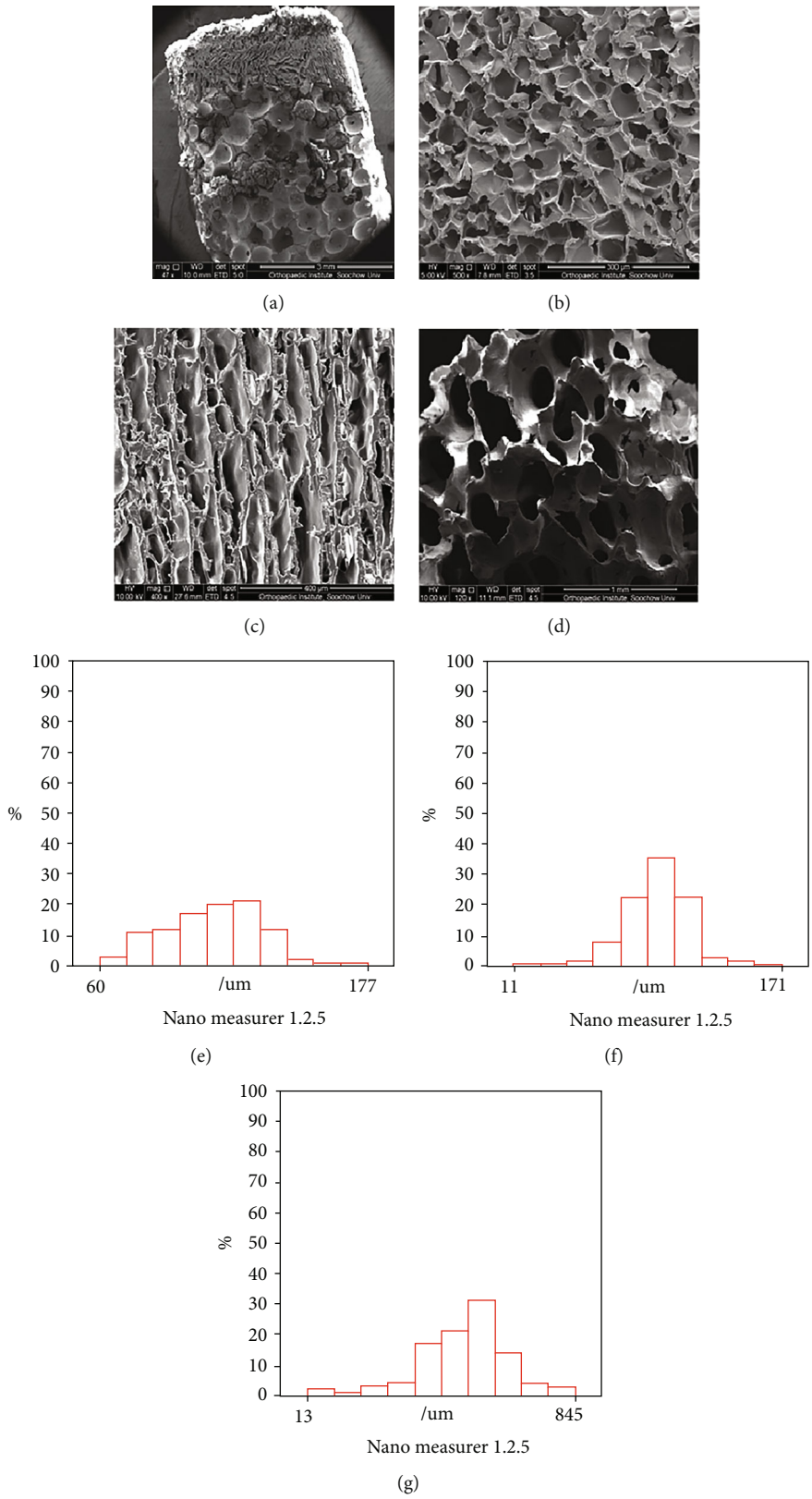


Figure 2: SEM image of porous structure of the scaffold ((a) scale bar = 3 mm) and the gradual porous structure of cartilage phase ((b) scale bar = 300 $\mu$m), interface layer ((c) scale bar = 400 $\mu$m), and bone phase ((d) scale bar = 1 mm). Pore size distribution of cartilage phase (e), interface layer (f), and bone phase (g) under nanomeasure.

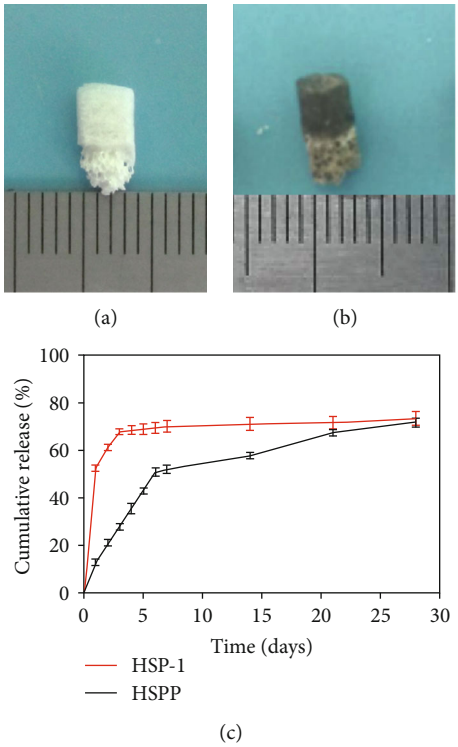


Figure 3: The appearance of scaffold treated (a) without and (b) with polydopamine and (c) *in vitro* release profiles of PDGF from HSP-1 and HSPP scaffold.

($P < 0.05$). Among all groups, the SPP group exhibited the most significant increase in the number of cells as shown in Figure 4($P < 0.05$).

*3.3.2. Migration Experiment.* We used Transwell culture plates in this experiment. We placed all scaffold samples in the lower chamber and seeded SMSCs in the upper chamber. After 24 h of coculture, cells adhering to the outside after penetrating the membrane were visualized using crystal violet and fluorescence staining. Five visual fields were selected for cell counting and plotting. The results in Figure 5 demonstrated that 5% FBS showed the strongest migration promoting effect ($P < 0.01$), and the simple DMEM + PDGF group was second only to the serum group, but there was no significant difference compared with the SPP group, indicating that the PDGF released by the scaffold could reach the effective working concentration of 50 ng/mL. There was no significant difference between SF group and SP-2 group ($P < 0.05$), indicating that PDA could not promote the migration of SMSCs.

*3.3.3. Chondrogenic Differentiation.* We performed the pellet culture experiment using the SP-2 and SPP groups to compare the differentiation-promoting effects of PDGF. After 14 d of culture, we embedded the scaffold samples in paraffin and stained the sections using alcian blue and toluidine blue. We observed that the pellet volume of the SPP group was slightly larger than the SP-2 group, and pellets were wrapped in a large amount of transparent ECM as shown in Figures 6(a) and 6(b). Observations of sections in Figure 6(c) revealed the SPP group displayed significantly better staining than the SP-2 group ($P < 0.05$), indicating that pellets contained large amounts of proteoglycan, hyaluronic acid, and epithelial acid mucin.

*3.3.4. Cytoskeleton Staining.* We also used Transwell plates for cell culture. We placed the scaffolds of each group in the upper chamber, whereas cells were seeded in the lower chamber. After 7 d, the number of cells in the SPP group was significantly higher than that in the SP-2 group ($P<0.05$), further demonstrating the promoting effect of PDGF on cell proliferation. By staining the cytoskeleton, furthermore, it changed from a short and wide shape into a long fusiform one. We further noticed that cells in the SPP group exhibited more orientation, and their skeleton proteins followed a more regular arrangement, with a tendency to fuse as shown in Figure 6(d). This finding was like the orderly arrangement of ECM in the superficial layer of cartilage, such as Col-II.

*3.4. Role of the Osteochondral Three-Layer Bionic Scaffold in Cartilage Repair in the Rabbit Osteochondral Defect Model.* To evaluate the effect of the scaffolds loaded with PDGF, as grafts to facilitate cartilage formation *in vivo*, we surgically created an osteochondral defect of 4 mm diameter and 5 mm depth in their femoral condyle using a trephine. Subsequently, we implanted scaffolds of the groups in the defect area as shown in Figure 7.

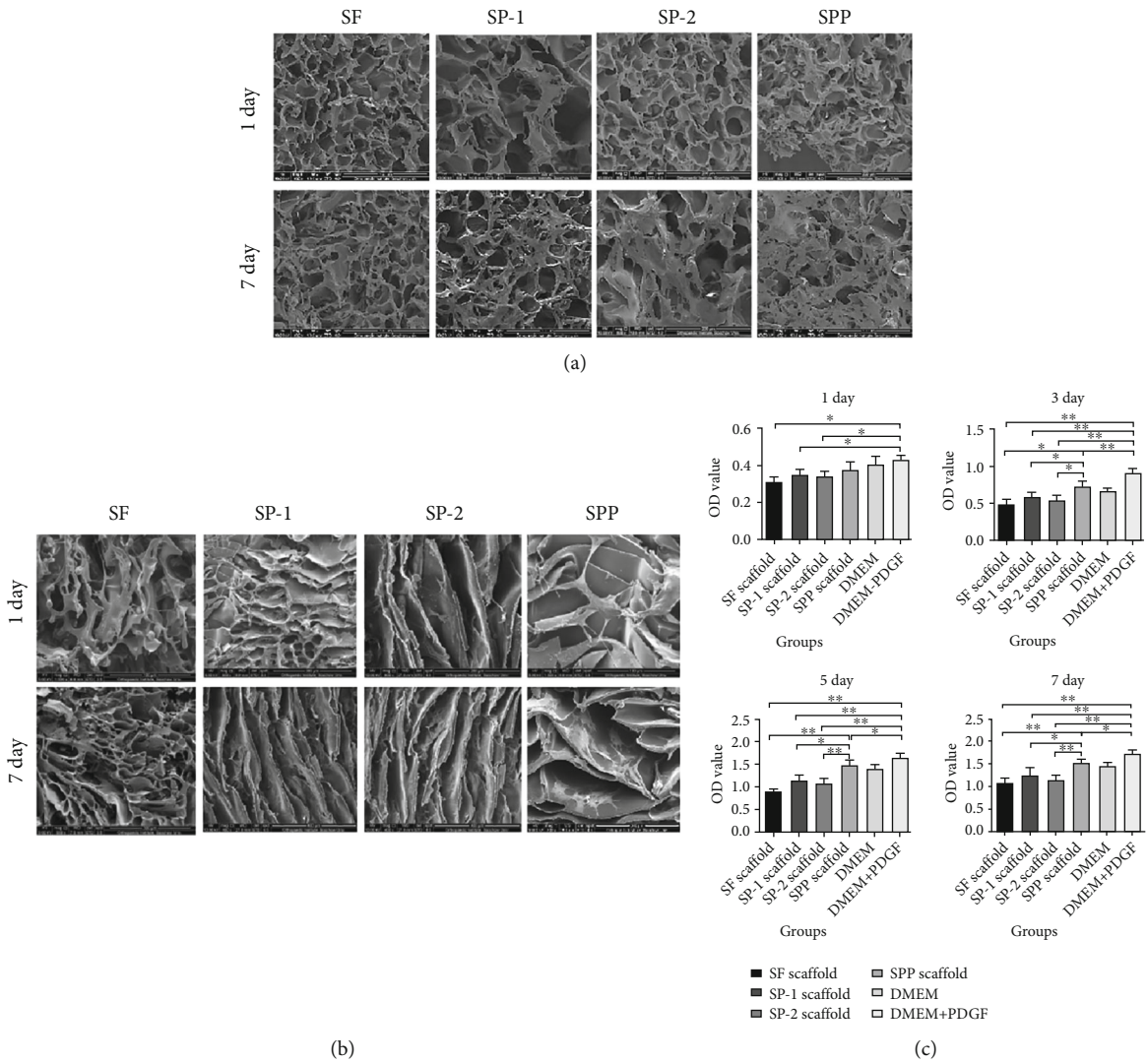


Figure 4: Cell adhesion and proliferation assays of different scaffolds. (a) SEM images of SMSCs adhesion on cartilage phase of scaffold loaded with or without PDGF or PDA after seeding for 1 d and 7 d. (b) SEM images of SMSC adhesion on interface layer of scaffold after seeding for 1 d and 7 d. (c) Cell proliferation of SMSCs cultured on different scaffolds after 1 d, 3 d, 5 d, and 7 d using a CCK-8 kit. Statistically significant differences are indicated with $^{*}P < 0.05$ and $^{**}P < 0.01$ compared with control.

*3.4.1. MRI Examinations of Scaffold Samples.* The sagittal scan of the T2 phase allows for a more intuitive visualization of the defect site, facilitating a better analysis of the reconstruction of the osteochondral tissue. By analyzing the MRI results, high signals were detected in the osteochondral defect area in the blank group at 6, 12, or 24 weeks, suggesting a lack of collagen filling in the local defect area. In contrast, water-like fillings were observed in the T2 phase. In comparison, the rest of the groups showed varying degrees of repair, with the surface producing cartilage-like tissues locally, including but not limited to fibrocartilage and hyaline cartilage as shown in Figure 8(a). We also noticed that the HSPP group had almost no high signal at 12 weeks, indicating the successful local tissue repair. We further observed that the 24-week MRI image was like that of a normal knee joint, suggesting that the regeneration and repair tissue in the HSPP group was comparable to normal articular cartilage. Interestingly, in this study, the relaxation time was also significantly shorter than other experimental groups as shown in Figure 8(b) ($P < 0.05$).

*3.4.2. Gross Morphology Score of Neocartilage.* We scored the gross morphology of the formed neocartilage according to the Visual Histological Assessment Scale published by the ICRS. The scaffold treatment groups performed significantly better than the blank group, whether at 12 or 24 weeks as shown in Figure 9(a) ($P < 0.01$). These findings demonstrated that, when osteochondral damage occurs, corresponding interventions are required, which can effectively improve the degree of osteochondral repair. In this study, even the score of the blank scaffold group was significantly higher than the blank group as shown in Figure 9(b) ($P < 0.05$), indicating that the filling of the porous scaffold provided a favorable growth

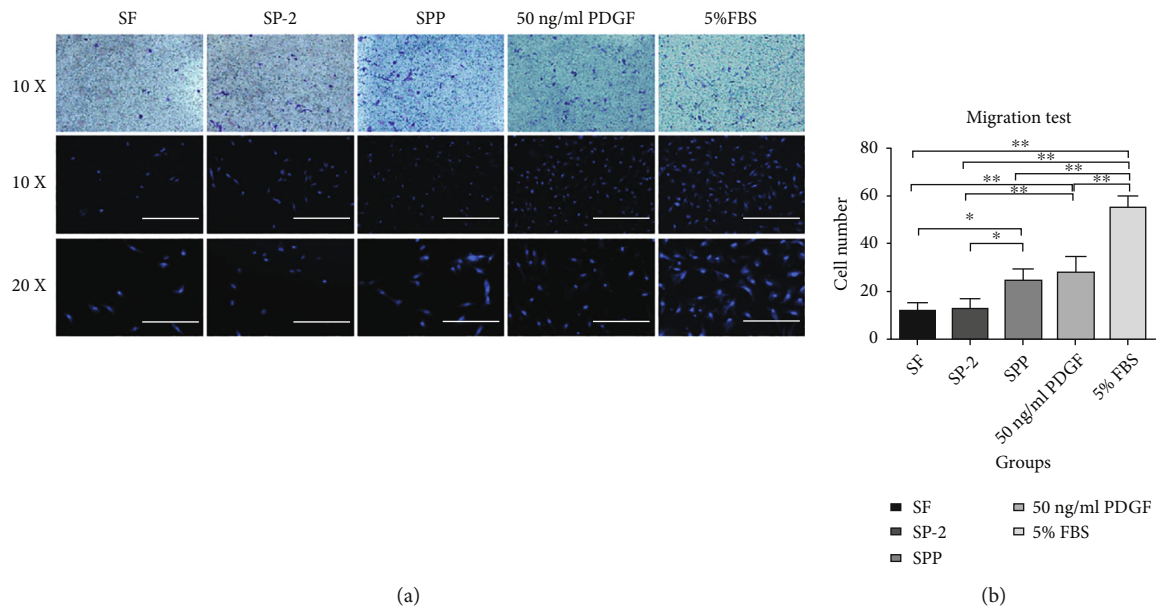


Figure 5: Transwell migration assay of the effects of PDGF released from the scaffolds on SMSCs migration. (a) Microscopic images of crystal violet and fluorescent staining of cells cultured in media that contained control or scaffold loaded with PDGF after 24 h of culture. (b) Quantitative comparison of migrated cells among the different groups, $^{*}P < 0.05$ and $^{**}P < 0.01$ compared with control.

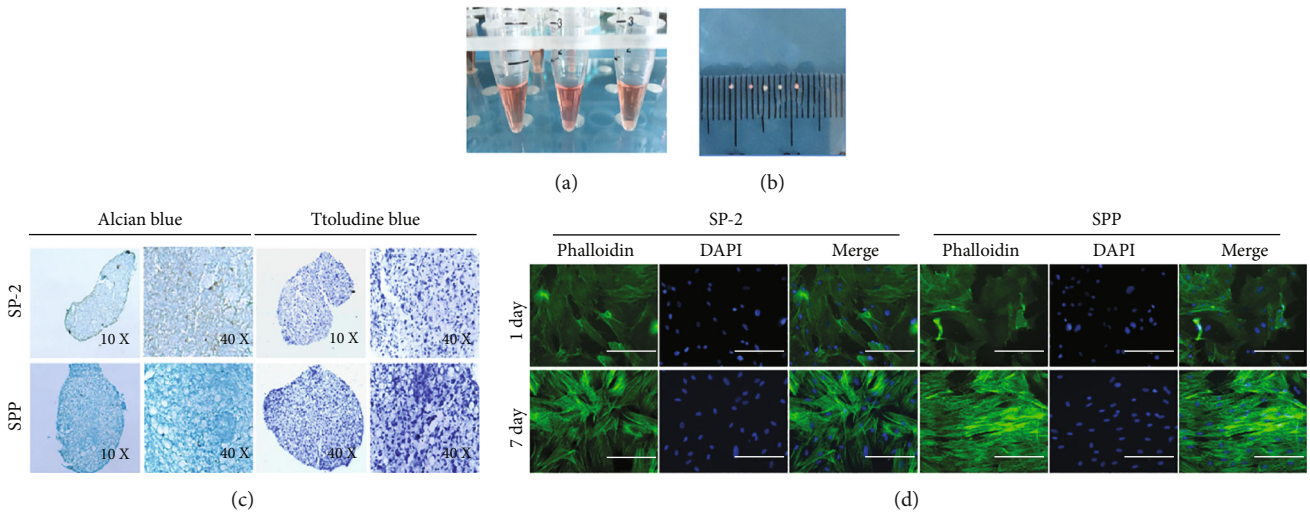


Figure 6: (a) Schematic diagram of pellet culture and (b) general view of pellet. (c) Alcian blue and toluidine blue staining showed the secretion of cartilage-specific extracellular matrix. (d) After 7 d coculture of SMSCs and scaffolds, the cytoskeleton was stained with phalloidin, and the nucleus was stained with DAPI to show the arrangement of skeletal proteins. Scale bar = 200 $\mu$m.

environment for cells. Furthermore, the HSPP group exhibited the best cartilage repair effect as more PDGF was released early to recruit surrounding SMSCs to the osteochondral bionic scaffold.

*3.4.3. Staining of Scaffold Samples.* Samples were harvested at 12 and 24 weeks. Following serial treatment, we performed H&E, Masson, and Safranin O/fast green staining in Figure 10, as well as immunohistochemical staining of Col-I, Col-II, and aggrecan in Figure 11. Using these different staining methods, we examined the regeneration of cartilage, secretion of ECM, and expression of cartilage-specific proteins.

We observed that large cavities and defects were still visible in the blank samples after staining. These cavities were filled by some fibrous cells, covering less than 50% of the area. We also found that the subchondral bone was partially filled with compact bone and fibrous tissue, resulting in loss of the basic structure of normal chondrocytes. However, we observed no cartilage lacuna around cells, and relatively little ECM was present. Our immunohistochemical analysis suggested the

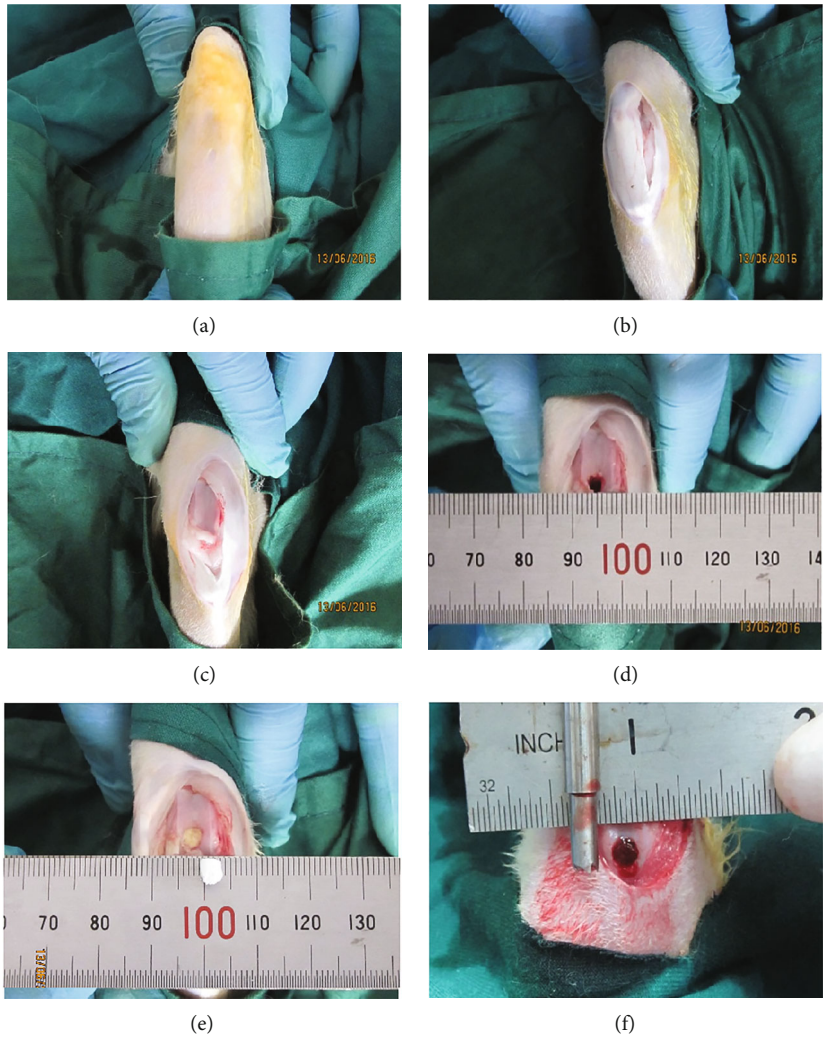


Figure 7: Modeling osteochondral defect and scaffold implantation. (a) Skin preparation after routine anesthesia. (b) Medial patellar incision. (c) Exposure of femoral trochlea. (d) Femoral trochlea osteochondral defect was successfully modeled. Three-phase scaffold (e) without and (f) with PDA treatment was implanted.

formation of significant Col-I in the repair tissue, whereas both cartilage-specific Col-II and aggrecan were absent ($P < 0.05$).

In the HSF group, our staining results indicated substantial filling defects in the samples. The defect area was filled with a significant amount of newly formed fibrous tissue ($P < 0.05$), which was slightly thicker than the surrounding normal cartilage. Only a few surface cracks were visible on the surface, and Safranin O staining was negative. In contrast, we observed little positive staining at the junction between the new tissue and the surrounding normal cartilage, suggesting a tendency for the formation of new cartilage at the junction. Our immunohistochemistry results indicated that the repaired tissues were mainly composed of Col-I, which exhibits relatively high strength, whereas lacking the expressions of cartilage-specific Col-II and aggrecan.

In both the HSP-1 and HSP-2 groups, repaired tissues accounted for over 50%, with over 50% of the scaffold material being degraded. We also observed a bilateral partial fusion in the repaired tissues around the normal cartilage, whereas the defect area was filled with hyaline cartilage-like repaired tissues. In addition, Safranin O staining was low positive near the cartilage area, and lacuna-like structures were evident in regenerated tissues. Although cells were scattered, there were still many fibroblasts present in the central region of the repaired tissue. According to our immunohistochemistry results, the repaired tissues exhibited expression of Col-I, Col-II, and aggrecan.

We further observed an excellent performance of cartilage repair in the HSPP group, exhibit a significant amount of specific ECM formation ($P < 0.05$). Afterwards, under the continuous action of PDGF, SMSCs differentiated into cartilage, secreting significant specific ECM ($P < 0.05$). At 12 weeks, we observed the perfect filling of new tissues, whereas the scaffold had been degraded by over 50%. Moreover, the new cartilage, which was a smooth hyaline cartilage-like tissue, was similar in thickness to the surrounding cartilage and it. As of 24 weeks, we detected the defect was almost filled with new cartilage, and the scaffold was almost completely

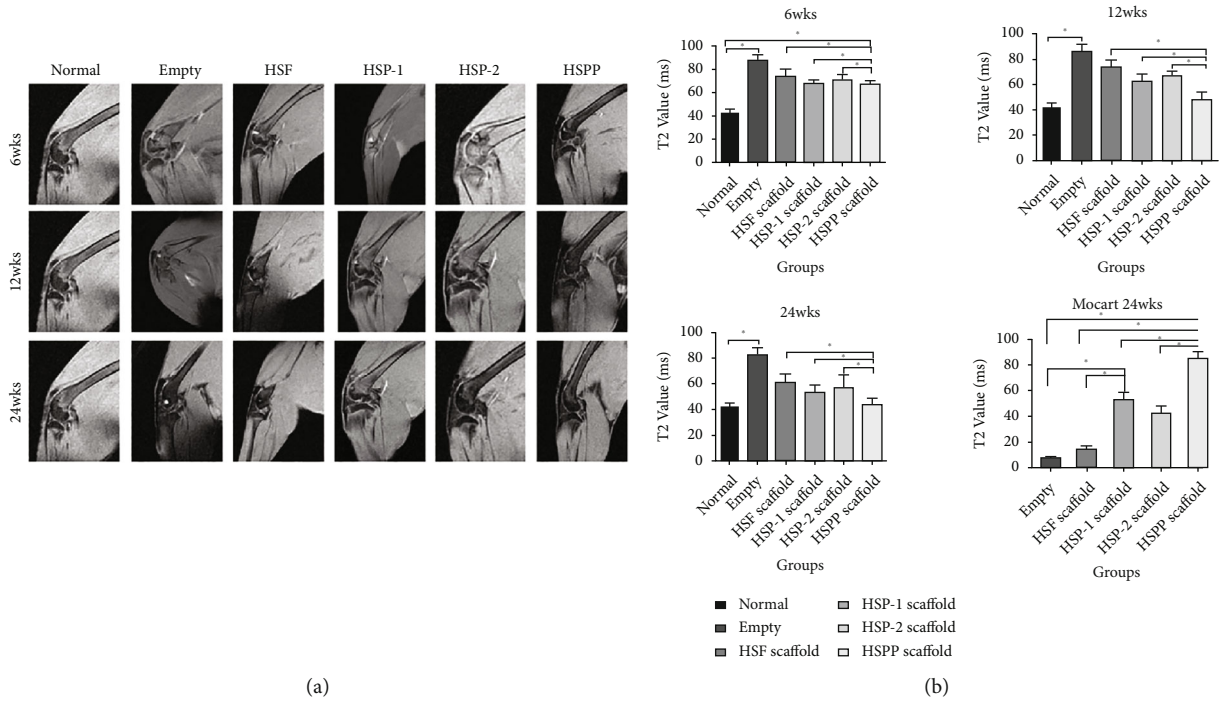


Figure 8: (a) MRI images of osteochondral defect regeneration in different groups at set time points and (b) their T2 value and MOCART scores of each group at 24 weeks.

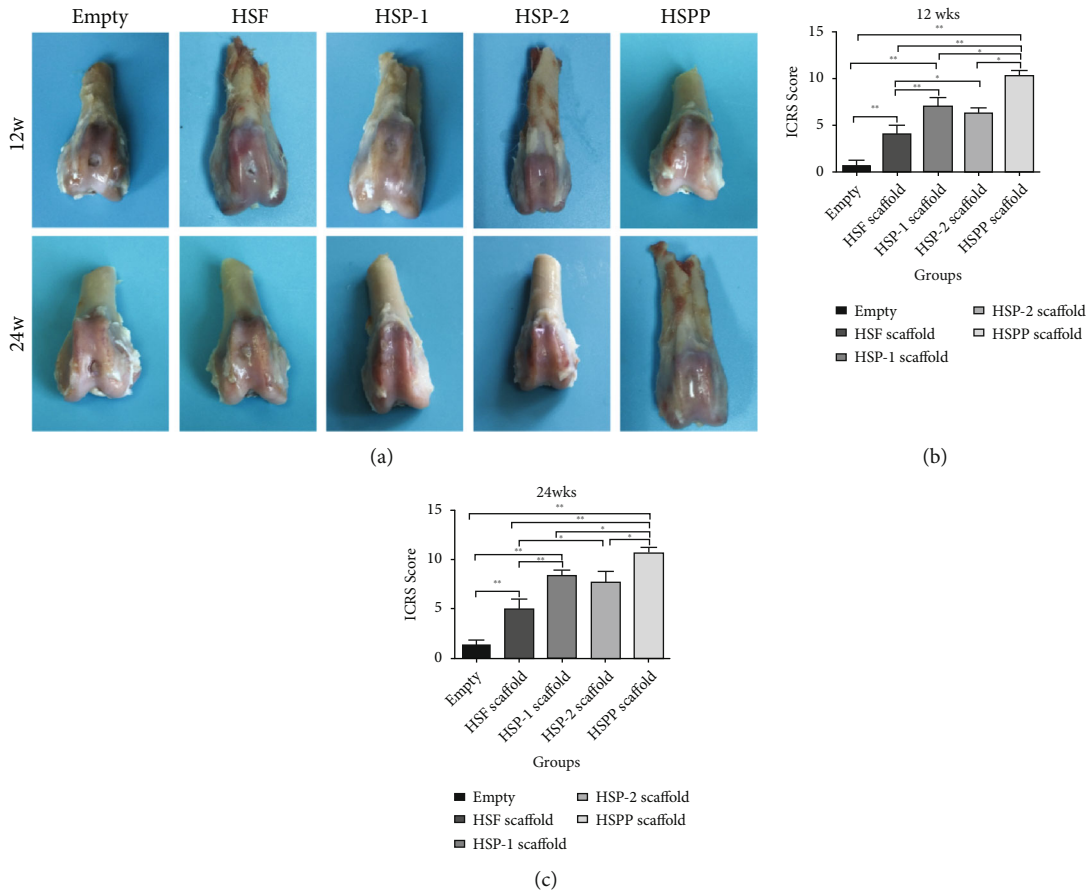


Figure 9: Appearance of gross specimens and ICRs scores at 12 and 24 weeks in each group.

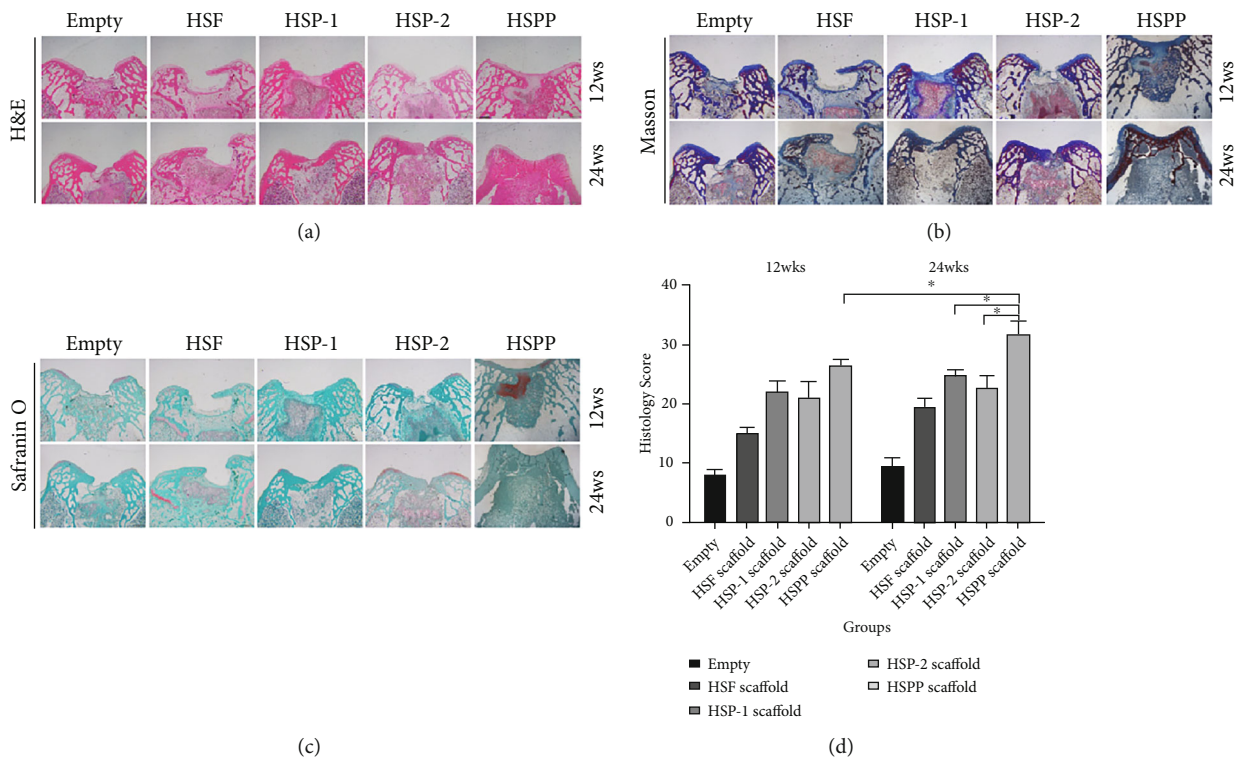


Figure 10: Histological evaluation of cartilage repair with different scaffolds in osteochondral defect models. (a) H&E staining. (b) Masson staining. (c) Safranine O fast green staining. (d) Histological scores at 12 and 24 weeks in each group.

degraded. The subchondral bone was normal cancellous bone, whereas the new cartilage was normal hyaline cartilage, which was well fused with surrounding normal cartilage. Safranin O staining was positive and immunohistochemistry suggested the high expression of Col-II and aggrecan in the repaired tissues. We detected expression of Col-I only in the interface layer. These findings indicated SMSCs differentiated well into cartilage, forming considerable cartilage-specific ECM.

## 4. Discussion

Due to its unique anatomical structure and the absence of nerves, blood vessels, and lymphatic system, articular hyaline cartilage receives most of its nutrition from the synovial fluid. Therefore, the articular cartilage has a limited capacity to repair itself once damaged [1, 3]. Because of the unique cartilage anatomy, researchers learned of the concept of osteochondral units and designed scaffolds with multilayer structures for cartilage repair [6–8]. According to Hunziker, growth factors are effective in promoting the migration of SMSCs to partially damaged cartilage for repair [16]. If full-thickness occurs osteochondral damage, the osteochondral units should be repaired. Xu et al. demonstrated the efficient repair of full-thickness osteochondral damage and evaluated gross and histological scores. They found that in the experimental group exhibiting good repair effects, both the subchondral bone and bone were well reconstructed, further confirming the definition of the osteochondral unit [3]. In this study, an SF/HAp three-layer osteochondral bionic scaffold was constructed successfully. The scaffold surface was modified with PDA and then loaded with PDGF. The surrounding endogenous pluripotent stem cells, SMSCs, were recruited to the damage site and induced to differentiate into cartilage, achieving a one-step tissue engineering repair of osteochondral damage.

The SF/HAp three-layer osteochondral bionic scaffold constructed in this study exhibited a sponge-like porous structure with a porosity above 40%. The pore size distributions of the three layers were generally uniform; however, the pore sizes were inconsistent among the three layers. The pore size of the cartilage phase was mainly in the 100–130 $\mu$m range. According to previous studies, this diameter is more favorable for the growth of chondrocytes, providing an ideal environment for cell adhesion. An appropriate pore size is also conducive to the differentiation of cells into cartilage [17, 18]. The pore size of the interface layer was mainly in the 75–100 $\mu$m range, which is relatively small and thus not conducive to the growth and passage of cells. To a certain extent, this layer could block the circulation of the medullary cavity and bone marrow cavity cells, as well as the transport of some nutrient molecules and metabolites [1]. Finally, the pore size of the bone phase was mainly in the 350–600 $\mu$m range. It has been previously reported that a pore size within this range is conducive to the adhesion and differentiation of osteoblasts, and the osteogenic ability of porous HAp scaffolds has also been widely confirmed in many studies [19, 20].

To achieve the loading and sustained release of PDGF, PDA was employed in this study to modify the scaffold surface. As dopamine contains a large amount of phenolic hydroxyl and amino groups, it serves as a good platform and can thus be used for grafting reactions [21, 22]. Wang et al. confirmed that, by immobilizing the nanocomposite on the

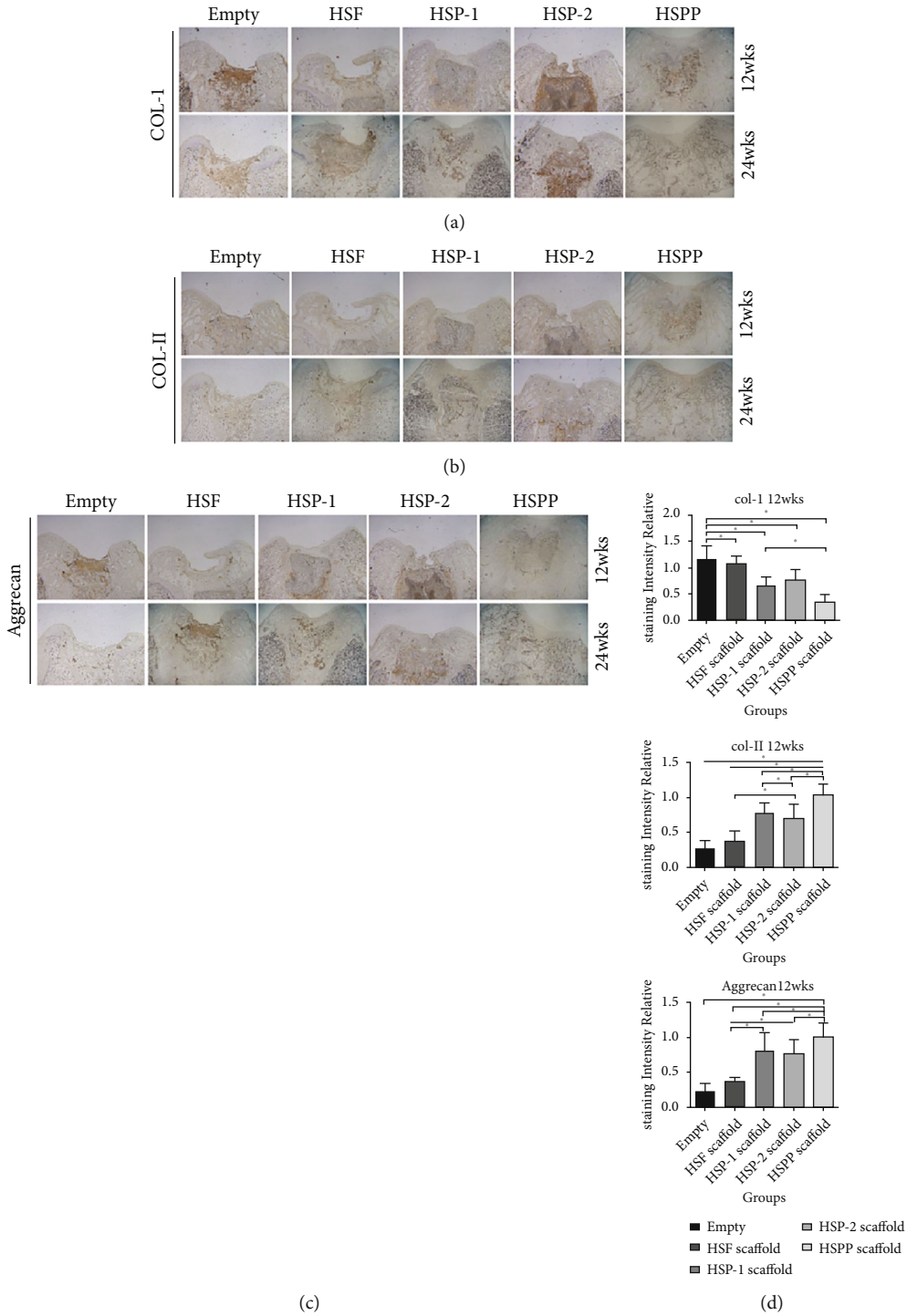


Figure 11: Continued.

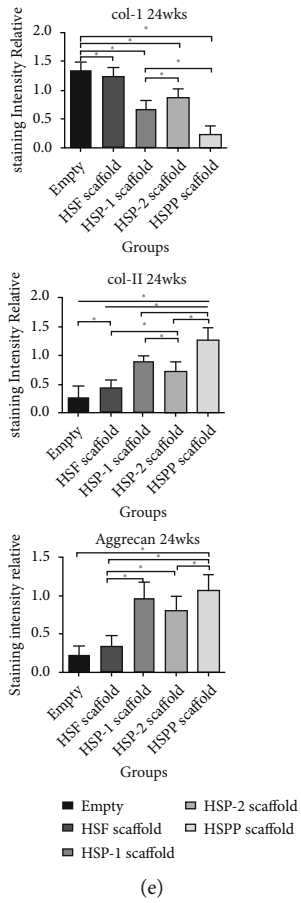


(e)

Figure 11: Immunohistochemical results of repaired tissues with different scaffolds. (a) CoL-I immunohistochemical staining. (b) Col-II immunohistochemical staining. (c) Aggrecan immunohistochemical staining. Relative expression of CoL-I, Col-II, and Aggrecan in different groups at (d) 12 weeks and (e) 24 weeks.

surface of the self-polymerizing coating of PDA, both the adhesion and spread of stem cells were effectively promoted, and the secretion of ECM was further enhanced [23]. *In vitro* release experiments performed in this study demonstrated that the PDA-modified osteochondral bionic scaffold prevented the burst release, allowing PDGF to be continuously released for 3 weeks, reaching a cumulative release of 71.74%. Thus, we demonstrated the effective loading and sustained release of growth factors in the scaffold, which promoted the differentiation of SMSCs toward cartilage and the synthesis of ECM.

Stem cell mobilization is widely regarded as a promising approach to treat orthopedic diseases, especially when using endogenous stem cells, which are more readily available [4, 24, 25]. The synovium is a loose connective tissue in the inner layer of the articular capsule. The embryonic origin of this tissue is like that of cartilage, as is its expression of surface antigens and differentiation potential [26]. If cartilage damage occurs, regeneration and repair signals are generated; these signals trigger the migration of SMSCs to the defect site to complete the repair process [13]. In addition, SMSCs have a rapid proliferation rate and a controlled differentiation ability, leading them to become one of the most popular seed cells in the research of tissue engineering for cartilage repair [27]. PDGF is a basic protein stored in platelet $\alpha$ particles. When osteochondral damage occurs, the local damage site develops many blood clots, which are rich in PDGF. Concurrently, macrophages that migrate in response to local damage synthesize a large amount of PDGF to promote the proliferation and differentiation of the remaining nearby chondrocytes, completing local cartilage regeneration and repair [12, 28, 29]. The $\alpha$ and $\beta$ receptors present on the surface of SMSCs allow PDGF-AB to exert a strong recruitment effect on them. Further, locally produced PDGF induces SMSCs in the peripheral synovium to migrate to the damaged area and proliferate [12]. Many studies have also demonstrated that under the action of PDGF, SMSCs differentiate into cartilage, secrete a large quantity of chondrocyte ECM arranged horizontally similar to the superficial layer of cartilage, maintain chondrocyte phenotypes, and complete osteochondral repair [13]. The arrangement of the generated ECM exhibits the advantages of locking moisture, improving tensile strength, distributing joint load, and facilitating joint movement. Thus, it affects the formation, growth, repair, and regeneration of cartilage [30].

The ultimate evaluation criterion is the *in vivo* cartilage repair effect. In this study, our MRI results showed that the blank group lacked collagen filling in the defect area, whereas the other groups showed varying degrees of repair. The HSPP group showed almost no high signals in the defect area at 12

weeks. At 24 weeks, its MRI image was almost identical to that of the normal knee joint, most notably in terms of cartilage defect filling, the fusion of the repaired tissue with the surrounding normal cartilage, the cartilage signal strength, and the internal structure of the repaired tissue. The HSPP group scored significantly higher than the other experimental groups ($P < 0.05$), indicating its promising cartilage repair effect. Trattnig et al. also used the T2 quantitative map to evaluate the articular cartilage repair effect, which can indicate the cartilage function and a more accurate assessment of the prognosis [31]. Observations of postoperative gross samples with blood scabs and inflammation during local damage revealed that macrophages could synthesize and secrete PDGF. However, because of the low concentration, early recruitment of surrounding SMSCs can be difficult. Instead, the nearby fibroblasts and bone marrow mesenchymal stem cells (BMSCs) in the medullary cavity will occupy the damaged site preemptively. Therefore, when osteochondral damage exceeds a critical defect, it is difficult for the damage to heal on its own, and much fibrous tissue is formed. A 3D porous scaffold with an oriented structure constructed by Liu et al. was effective at repairing osteochondral defects, further highlighting the significance of scaffold filling [32]. At 24 weeks, no significant difference was observed between the repaired and surrounding normal cartilage in the HSPP group ($P < 0.05$). Both tissues exhibited a red hyaline cartilage-like structure, exhibiting good luster and elasticity, showing no obvious separation boundaries, and demonstrating a good ability for repair and regeneration. Histological analysis showed that the relatively early release of high concentrations of PDGF led to the recruitment of many SMSCs to the damaged site, where they were differentiated into cartilage, secreting significant specific ECM under the continuous stimulation by PDGF ($P < 0.05$). Therefore, the HSPP group demonstrated perfect new tissue filling at 12 weeks, whereas at 24 weeks, the defect area was almost filled by the new cartilage, and the scaffold was nearly completely degraded. The formed subchondral bone was a normal cancellous bone, whereas the new cartilage, which was hyaline-like, fused well with the surrounding normal cartilage, exhibiting a positive Safranin O staining. Finally, immunohistochemical analysis indicated the high expression of Col-II and aggrecan in the repaired tissues and the formation of substantial cartilage-specific ECM.

## 5. Conclusions

The three-layer osteochondral bionic scaffold composed of SF and HAp met the requirements of osteochondral tissue engineering. Treatment of the scaffold with PDA allowed the loading and sustainable release of growth factors. In addition, the scaffold exhibited high biocompatibility and promoted the adhesion, proliferation, migration, and differentiation of SMSCs into cartilage. *In vivo* experiments showed that the three-layer SF/HAp osteochondral scaffold effectively filled osteochondral defects, provided a 3D environment for cell adhesion and proliferation, and may recruit surrounding SMSCs migrate to the damage site and differentiate into cartilage, thereby effectively improving the repair of osteochondral defects.

## Data Availability

The datasets used in the current study are available from the corresponding author on reasonable request by email.

## Conflicts of Interest

The authors declare there is no conflict of interest regarding the publication of this paper.

## Authors' Contributions

Yuan Luo and Xiaodong Cao contributed equally to this work.

## Acknowledgments

This work is supported by the Suzhou Science and Technology Development Project (grant number SYSD2018040).

## References

[1] D. J. Huey, J. C. Hu, and K. A. Athanasiou, "Unlike bone, cartilage regeneration remains elusive," *Science*, vol. 338, no. 6109, pp. 917–921, 2012.

[2] M. F. Rai, J. M. Cheverud, E. J. Schmidt, and L. J. Sandell, "Genetic correlations between cartilage regeneration and degeneration reveal an inverse relationship," *Osteoarthritis and Cartilage*, vol. 28, no. 8, pp. 1111–1120, 2020.

[3] X. Xu, D. Shi, Y. Shen et al., "Full-thickness cartilage defects are repaired via a microfracture technique and intraarticular injection of the small-molecule compound kartogenin," *Arthritis Research & Therapy*, vol. 17, 2015.

[4] Y. Tang, Z.-y. Pan, Y. Zou et al., "A comparative assessment of adipose-derived stem cells from subcutaneous and visceral fat as a potential cell source for knee osteoarthritis treatment," *Journal of Cellular and Molecular Medicine*, vol. 21, no. 9, pp. 2153–2162, 2017.

[5] A. J. Krych, D. B. F. Saris, M. J. Stuart, and B. Hacken, "Cartilage injury in the knee: assessment and treatment options," *The Journal of the American Academy of Orthopaedic Surgeons*, vol. 28, no. 22, pp. 914–922, 2020.

[6] W. Shi, M. Sun, X. Hu et al., "Structurally and functionally optimized silk-fibroin–gelatin scaffold using 3D printing to repair cartilage injury in vitro and in vivo," *Advanced Materials*, vol. 29, no. 29, 2017.

[7] E. A. Makris, A. H. Gomoll, K. N. Malizos, J. C. Hu, and K. A. Athanasiou, "Repair and tissue engineering techniques for articular cartilage," *Nature Reviews Rheumatology*, vol. 11, no. 1, pp. 21–34, 2015.

[8] V. P. Sivadas, S. Dhawan, J. Babu, V. Haridas, and P. D. Nair, "Glutamic acid-based dendritic peptides for scaffold-free cartilage tissue engineering," *Acta Biomaterialia*, vol. 99, pp. 196–210, 2019.

[9] B. Kundu, R. Rajkhowa, S. C. Kundu, and X. Wang, "Silk fibroin biomaterials for tissue regenerations," *Advanced Drug Delivery Reviews*, vol. 65, no. 4, pp. 457–470, 2013.

[10] P. J. Emans, F. Spaapen, D. A. M. Surtel et al., "A novel in vivo model to study endochondral bone formation; HIF-1alpha activation and BMP expression," *Bone*, vol. 40, no. 2, pp. 409–418, 2007.

[11] B. A. Jones and M. Pei, "Synovium-derived stem cells: a tissue-specific stem cell for cartilage engineering and regeneration," *Tissue Engineering. Part B, Reviews*, vol. 18, no. 4, pp. 301–311, 2012.

[12] M. Mizuno, H. Katano, K. Otabe et al., "Platelet-derived growth factor (PDGF)-AA/AB in human serum are potential indicators of the proliferative capacity of human synovial mesenchymal stem cells," *Stem Cell Research & Therapy*, vol. 6, p. 243, 2015.

[13] Y. Mishima and M. Lotz, "Chemotaxis of human articular chondrocytes and mesenchymal stem cells," *Journal of Orthopaedic Research*, vol. 26, no. 10, pp. 1407–1412, 2008.

[14] H. Liu, G. W. Xu, Y. F. Wang et al., "Composite scaffolds of nano-hydroxyapatite and silk fibroin enhance mesenchymal stem cell-based bone regeneration via the interleukin 1 alpha autocrine/paracrine signaling loop," *Biomaterials*, vol. 49, pp. 103–112, 2015.

[15] D. Du, N. Sugita, Z. Liu et al., "Repairing osteochondral defects of critical size using multiple costal grafts: an experimental study," *Cartilage*, vol. 6, no. 4, pp. 241–251, 2015.

[16] E. B. Hunziker, "Growth-factor-induced healing of partial-thickness defects in adult articular cartilage," *Osteoarthritis and Cartilage*, vol. 9, no. 1, pp. 22–32, 2001.

[17] A. C. Daly, F. E. Freeman, T. Gonzalez-Fernandez, S. E. Critchley, J. Nulty, and D. J. Kelly, "3D bioprinting for cartilage and osteochondral tissue engineering," *Advanced Healthcare Materials*, vol. 6, no. 22, 2017.

[18] G. H. Altman, F. Diaz, C. Jakuba et al., "Silk-based biomaterials," *Biomaterials*, vol. 24, no. 3, pp. 401–416, 2003.

[19] B. Zou, X. Chen, W. Zhi et al., "Promoted healing of femoral defects with in situ grown fibrous composites of hydroxyapatite and poly (DL-lactide)," *Journal of Biomedical Materials Research. Part A*, vol. 100, no. 6, pp. 1407–1418, 2012.

[20] J. J. Pearson, N. Gerken, C. Bae et al., "In vivo hydroxyapatite scaffold performance in infected bone defects," *Journal of Biomedical Materials Research. Part B, Applied Biomaterials*, vol. 108, no. 3, pp. 1157–1166, 2020.

[21] F. Wu, J. Li, K. Zhang et al., "Multifunctional coating based on hyaluronic acid and dopamine conjugate for potential application on surface modification of cardiovascular implanted devices," *ACS Applied Materials & Interfaces*, vol. 8, no. 1, pp. 109–121, 2016.

[22] R. Mrówczyński, J. Jurga-Stopa, R. Markiewicz, E. L. Coy, S. Jurga, and A. Woźniak, "Assessment of polydopamine coated magnetic nanoparticles in doxorubicin delivery," *RSC Advances*, vol. 6, no. 7, pp. 5936–5943, 2016.

[23] J.-l. Wang, B.-c. Li, Z.-j. Li et al., "Electropolymerization of dopamine for surface modification of complex-shaped cardiovascular stents," *Biomaterials*, vol. 35, no. 27, pp. 7679–7689, 2014.

[24] L. Huang, Y. Wang, Y. Jiang, Y. Wu, C. Hu, and H. Ouyang, "High levels of GSK-3$\beta$ signalling reduce osteogenic differentiation of stem cells in osteonecrosis of femoral head," *Journal of Biochemistry*, vol. 163, no. 3, pp. 243–251, 2018.

[25] Y. Wang, D. Yu, Z. Liu et al., "Exosomes from embryonic mesenchymal stem cells alleviate osteoarthritis through balancing synthesis and degradation of cartilage extracellular matrix," *Stem Cell Research & Therapy*, vol. 8, no. 1, p. 189, 2017.

[26] E. R. N. S. T. B. HUNZIKER and L. A. W. R. E. N. C. E. C. ROSENBERG, "Repair of partial-thickness defects in articular Cartilage," *Journal of Bone & Joint Surgery American Volume*, vol. 78, no. 5, pp. 721–733, 1996.

[27] D. Shi, X. Xu, Y. Ye et al., "Photo-cross-linked scaffold with kartogenin-encapsulated nanoparticles for cartilage regeneration," *ACS Nano*, vol. 10, no. 1, pp. 1292–1299, 2016.

[28] J. Fiedler, N. Etzel, and R. E. Brenner, "To go or not to go: migration of human mesenchymal progenitor cells stimulated by isoforms of PDGF," *Journal of Cellular Biochemistry*, vol. 93, no. 5, pp. 990–998, 2004.

[29] L. Fredriksson, H. Li, and U. Eriksson, "The PDGF family: four gene products form five dimeric isoforms," *Cytokine & Growth Factor Reviews*, vol. 15, no. 4, pp. 197–204, 2004.

[30] Q. Yang, J. Peng, Q. Guo et al., "A cartilage ECM-derived 3-D porous acellular matrix scaffold for in vivo cartilage tissue engineering with PKH26-labeled chondrogenic bone marrow-derived mesenchymal stem cells," *Biomaterials*, vol. 29, no. 15, pp. 2378–2387, 2008.

[31] S. Trattnig, S. A. Millington, P. Szomolanyi, and S. Marlovits, "MR imaging of osteochondral grafts and autologous chondrocyte implantation," *European Radiology*, vol. 17, no. 1, pp. 103–118, 2007.

[32] S. Liu, J. Wu, X. Liu et al., "Osteochondral regeneration using an oriented nanofiber yarn-collagen type I/hyaluronate hybrid/TCP biphasic scaffold," *Journal of Biomedical Materials Research. Part A*, vol. 103, no. 2, pp. 581–592, 2015.

Hindawi
Stem Cells International
Volume 2022, Article ID 5865011, 12 pages
https://doi.org/10.1155/2022/5865011

*Research Article*

# Aloin Regulates Matrix Metabolism and Apoptosis in Human Nucleus Pulposus Cells via the TAK1/NF-κB/NLRP3 Signaling Pathway

**Taiqiu Chen, Pengfei Li, Jincheng Qiu, Wenjun Hu, Shaoguang Li, Huihong Shi, Xianjian Qiu, Dongsheng Huang, Wenjie Gao, and Anjing Liang**

*Department of Orthopedics, Sun Yat-sen Memorial Hospital of Sun Yat-sen University, Guangzhou, Guangdong 510000, China*

Correspondence should be addressed to Wenjie Gao; gaowj7@mail.sysu.edu.cn and Anjing Liang; lianganj@mail.sysu.edu.cn

Received 1 November 2021; Accepted 7 December 2021; Published 6 January 2022

Academic Editor: Qiang Zhou



Intervertebral disc degeneration (IDD) is a degenerative disease that is characterized by decreased matrix synthesis and extra degradation, nucleus pulposus cells (NPCs) apoptosis, and infiltration of inflammatory factors. Aloin, a colored compound from aloe plants, has been shown to be effective against skeletal degenerative diseases, but it is unclear whether it is protective against IDD. Herein, we investigated the role of aloin in NPCs. In our study, the upregulation of proinflammatory factors, apoptosis, and unbalanced matrix metabolism were observed in degenerative NP tissues. We found that aloin had a curative effect on extracellular matrix metabolism and apoptosis in TNF-alpha- (TNF-α-) treated NPCs by inhibiting oxidative stress and the proinflammatory factor expression. Further investigation revealed that aloin treatment suppressed the TAK1/NF-κB pathway. Moreover, the expression level of the NLPR3 inflammasome was downregulated after aloin treatment in TNF-α-treated NPCs. In summary, our results demonstrated that aloin treatment can reverse TNF-α-induced unbalanced matrix metabolism and apoptosis of NPCs via the TAK1/NF-κB/NLRP3 axis. This study supports that aloin can be a promising therapeutic agent for IDD.

## 1. Introduction

Low back pain (LBP) is a universal symptom with a high incidence rate. Almost 80% of people have suffered from LBP in their lifetime, and the number continues to rise globally with the aging of the population [1, 2]. LBP is a serious problem for human health that reduces the quality of life, especially for young patients [3, 4]. It has been reported that the number of people with disabilities caused by LBP has increased in the past thirty years, especially in developing countries [5, 6].

Intervertebral disc degeneration (IDD) has been contemplated to be the primary cause of LBP. The intervertebral disc is made up of annulus fibrosus, nucleus pulposus, and endplates [7]. A variety of pathological changes are related to the etiology and progression of IDD, including unbalanced metabolism within the extracellular matrix (ECM), apoptosis of NPCs, and overexpression of inflammatory factors, including interleukin-1 beta and tumor necrosis factor-alpha [8, 9]. The ECM is secreted essentially by NPCs, and its destruction is characterized by inadequate anabolism and excessive catabolism, accompanied by the downregulation of collagen II and aggrecan and the upregulation of matrix metallopeptidases (MMPs) [10, 11]. Apoptosis of NPCs is also considered to be an important pathological change in IDD. Studies based on the nucleus pulposus tissue of IDD patients revealed an increased apoptosis rate and the overexpression of induced apoptosis factors in NPCs, including inflammatory factors and oxidative stress levels [12–14].

As an essential member of the TNF superfamily of ligands, TNF-α has been reported to be pivotally involved in the progression of IDD [15, 16]. It has been demonstrated that the concentration of TNF-α increases with the aggravation of IDD [17]. As the level of TNF-α increases, it can significantly enhance the expression of MMPs and ADAMTSs,

and reduce the expression levels of aggrecan and collagen II, resulting in degradation of the ECM [18, 19]. Moreover, TNF-$\alpha$ has been considered to play a critical role in NPC apoptosis and can enhance the expression levels of multiple proinflammatory cytokines, such as cytochrome C oxidase subunit 2 (COX-2), and inducible nitric oxide synthase (iNOS), which amplify the inflammatory response and aggravate the IDD [20–22]. Thus, TNF-$\alpha$ was used to induce the degeneration of NPCs in our study.

The nuclear factor kappa B (NF-$\kappa$B) pathway was found to be linked to the occurrence and development of IDD, especially with inflammatory microenvironment irritation [23, 24]. With TNF-$\alpha$ stimulation, proteins upstream of the pathway, such as Ikk-alpha/beta and transforming growth factor-$\beta$-activated kinase 1 (TAK1), are stimulated to phosphorylate I$\kappa$B$\alpha$. Phophorylated I$\kappa$B$\alpha$ then produces nuclear localization signals to activate and phosphorylate the p65 subunit of nuclear factor kappa B, which finally initiates the target gene transcription [25, 26]. Additionally, the NF-$\kappa$B pathway has been found to participate in the metabolism of the extracellular matrix, as well as apoptosis and autophagy of NPCs [27–29].

The NLR family pyrin domain containing 3 (NLRP3) inflammasome has been reported to be involved in the progression of various diseases [30]. As a target gene of phosphorylated p65, the NLRP3 inflammasome has been reported to be linked with IDD in previous studies [31–33]. In addition, the NLRP3 inflammasome might mediate the induction of inflammatory factors in NPCs, accelerating the progression of IDD.

Aloin, extracted from aloe plant species used in traditional medicinal medicine, has been shown to be effective both in vitro and in vivo against inflammation, skeletal degenerative disease, cancer, and cardiovascular diseases [34, 35]. Sun et al. found that aloin can diminish oxidative stress level and reduce the concentration of reactive oxygen in myocardial cells [36]. Another study found that aloin treatment can suppress the activation of the NF-$\kappa$B/NLRP3 signaling pathway [37]. Moreover, it has been reported that aloin ameliorates the development of osteoarthritis and shows a protective effect on anabolism and catabolism of ECM in chondrocytes through the PI3K/AKT/NF-$\kappa$B pathway [38]. However, the effect and underlying mechanism of aloin on NPCs remain unknown. Thus, based on the anti-inflammatory and bone-protective effects, we hypothesized that aloin may regulate both matrix metabolism and apoptosis in NPCs via the TAK1/NF-$\kappa$B/NLRP3 axis. Our study aims to provide additional evidence for aloin in therapy of IDD.

## 2. Material and Methods

*2.1. Antibodies and Reagents.* Antibodies against GAPDH, COL2A1, ACAN, ADAMTS4, ADAMTS5, MMP9, MMP13, TNF-$\alpha$, NOX1, NOX2, iNOS, COX2, and NLRP3 were purchased from Abcam Inc. Catalase, SOD1, BAX, BCL2, Caspase3, Cleaved-caspase3, TAK1/NF-$\kappa$B signaling proteins (TAK1, phosphor-TAK1, P65, phosphor-P65, I$\kappa$B$\alpha$, and phosphor-I$\kappa$B$\alpha$), and IgG secondary antibodies were purchased from Cell Signaling Technology Inc. Antibody against GAPDH was from Proteintech Group Inc. Aloin reagent was from MedChemExpress, and human TNF-$\alpha$ was from R&D Systems. Abbreviations and descriptions were shown in Supplement Table 1.

*2.2. Tissue Samples of Controls and Patients.* Degenerative nucleus pulposus (NP) tissues were gained from patients who underwent discectomy surgery due to disc herniation, while the normal NP tissues were obtained from those who received a surgery due to trauma without disc degeneration. Tissues were fixed, decalcified, embedded and cut into sections for immunohistochemistry (IHC) analysis. Meanwhile, extra tissues were stored in -80°C for RNA and protein extraction by using high-throughput tissue grinder.

*2.3. Human Nucleus Pulposus Cell Acquisition and Culture.* In this study, the human nucleus pulposus cells (NPCs) were obtained from ScienCell. With the confluence of about 70%-90%, they were trypsinized and plated again. The NPCs were cultured in 6-well plate at a density of approximately $1.0 \times 10^6$ cells/ml with about 8 ml human NPC medium (ScienCell) in 3-6 passages, and they were given the indicated treatment at 12 h after plating for subsequent experiments.

*2.4. Immunohistochemistry.* Paraformaldehyde was used to fix the tissues, and then, they were decalcified, dehydrated, and embedded. After being treated with 0.1% Triton X-100 solution for 15 minutes, the tissue sections were incubated with 3% peroxidase for 20 minutes and washed 3 times with PBS. As the blocking reagent, bovine serum albumin (5%, Sigma-Aldrich) was available at 37°C for 30 minutes. As follows, the Histostain Plus kit was used for IHC analysis. Finally, an Olympus BX63 microscope (Olympus, Tokyo, Japan) was used for photographing at magnifications of 200 and 400.

*2.5. Real-Time qPCR.* The total RNA was extracted from tissues and cells by using RNA-iso Plus reagent. After converting to cDNA, qPCR was performed, and the expression levels of mRNAs in different groups were calculated and analyzed referring to the expression level of *GAPDH* gene. All primers' sequences used for our research were included in Supplement Table 2.

*2.6. Western Blot.* Firstly, we extracted the total proteins from cells and tissues. Subsequently, samples were subjected in SDS-PAGE with equal amounts and transferred to NC transfer membranes. Next, the membranes were blocked and incubated with the designated antibodies at 4°C overnight. After being washed 3 times with PBS, they were incubated with the secondary antibodies for 1 h and then were visualized. The bands were determined and quantified using the ImageJ software.

*2.7. Cell Viability Assay.* NPCs were digested, centrifugated, and plated in 96-well plates at the density of $1.0 \times 10^4$ cells/ml. After being cultured for 12 h, aloin at different concentrations was added for 24 and 48 h, respectively. NPCs were washed with PBS at the indicated time, and 10%

CCK-8 reagent was added in each well. Finally, we measured the absorbance by using the microplate reader at 450 nm.

*2.8. Immunofluorescence.* NPCs were seeded on cover glasses in 24-well plates for 24 h and then were under different treatment for 48 h. Then, NPCs were washed, fixed, permeabilized, and blocked. Next, the cover glasses were incubated with antibody at 4°C overnight. After that, secondary antibodies (1 : 100) were used for incubation, and then, they were labelled with DAPI for 5 min. At last, an Olympus BX63 microscope was used for photographing.

*2.9. Tunel Cell Apoptosis Detection.* NPCs were seeded on cover glasses in 24-well plates for 24 h and then were under different treatments for 48 h. At the target confluence, NPCs were washed and fixed. Secondly, they were washed and treated with 0.1% Triton X-100 solution. Tunel working solution (Beyotime, China) was added, and images were photographed using an Olympus BX63 microscope.

*2.10. Flow Cytometer.* NPCs were cultured in the 6-well plates and collected after different treatments. Annexin V/PI apoptosis detection kit (Elabscience, China) was used to detect apoptotic rate. And then, binding buffer was added, and flow cytometry system was used for analyzing immediately.

*2.11. Statistical Analysis.* $t$-test for two comparisons or one-way ANOVA for multiple comparisons was used. All quantitative data were presented as the mean ± standard deviation. All analyses were conducted by using the GraphPad Software 8.0 (San Diego, CA, USA). Statistically significance was considered when $P < 0.05$.

*2.12. Ethics Statement.* Our research was approved by the Institutional Research Ethical Committee of Sun Yat-sen University (Guangzhou, China), and the written informed consent was obtained from all subjects participating in the study.

## 3. Results

*3.1. Dysregulated ECM Metabolism, Increased Apoptosis, and Inflammatory Infiltration in Degenerated NP Tissue.* To determine the pathogenesis of IDD, immunohistochemistry was used to evaluate the expressions of ECM metabolism markers and inflammatory factors in different human NP tissues. We found that the expression of ACAN was significantly reduced, and the expressions of ADAMTS4 and TNF-$\alpha$ were upregulated in the patient group (Figure 1(a)). Protein and mRNA were then extracted from normal and degenerated human NP tissues and assessed. As shown in Figures 1(b)–1(d), the expression of *COL2A1* was suppressed, and the matrix-degrading enzyme *ADAMTS4* was increased in the patient group. Furthermore, the expression levels of *TNF-α*, the apoptotic gene *BAX*, and the proinflammatory factors *iNOS* and *COX2* were upregulated in degenerative tissues compared to normal tissues (Figures 1(b)–1(d)).

*3.2. Aloin Treatment Enhances the Anabolism and Suppresses the Catabolism in TNF-α-Treated NPCs.* The chemical structure of aloin is shown in Figure 2(a) (quoted from http://www.medchemexpress.cn/.). First, various concentrations of aloin were added to the medium (0, 50, 100, 200, 400, and 800 $\mu$M), and we used the CCK-8 test to assess whether the cytotoxic effect of aloin on NPCs was exerted. As shown in Figure 2(b), we found that aloin had no significant cytotoxicity on the NPCs at concentrations up to 200 $\mu$M; however, aloin reduced cell viability at concentrations of 400 $\mu$M ($P < 0.05$) within 48 h. Next, we evaluated the expression levels of COL2A1, MMPs, and ADAMTSs by using qPCR and western blot, and the results showed that aloin treatment promoted ECM synthesis and significantly inhibited ECM degradation in TNF-$\alpha$-treated NPCs (Figures 2(c) and 2(d)). As expected, the immunofluorescence analysis also showed that aloin treatment reversed the changes in ADAMTS4 and COL2A1 induced by TNF-$\alpha$ (Figure 2(e)).

*3.3. Aloin Treatment Reduced the Apoptosis Rate in TNF-α-Treated NPCs.* Subsequently, apoptosis was detected in NPCs. The qPCR results showed that aloin treatment (200 $\mu$M) in TNF-$\alpha$-treated NPCs upregulated *BCL2* and downregulated *BAX* (Figure 3(a)). The western blot results also showed that the apoptotic markers BAX and Cleaved-caspase3 were downregulated, and the antiapoptotic marker BCL2 was upregulated with aloin treatment (Figure 3(b)). Next, to assess the apoptosis rate, TUNEL immunofluorescence staining and flow cytometry were used. As shown in Figures 3(c) and 3(d), we found a significantly higher apoptosis rate in TNF-$\alpha$-treated NPCs, whereas it was inhibited with aloin treatment at a concentration of 200 $\mu$M (Figures 3(c) and 3(d)). Our results indicated that aloin treatment can reduce the apoptosis rate in TNF-$\alpha$-induced NPCs.

*3.4. Aloin Treatment Ameliorates the Levels of Oxidative Stress and Proinflammatory Factors.* Then, we detected the effects of aloin treatment on proinflammatory factors and oxidative stress levels. The results indicated that markers of oxidation indices (*NOX1* and *NOX2*) were downregulated, and antioxidant enzymes (*SOD1* and *Catalase*) were upregulated with aloin treatment (200 $\mu$M) (Figures 4(a) and 4(b)). In addition, the inhibition of proinflammatory factors (*iNOS*, *COX2*, *IL-1β*, and *IL-6*) was observed with aloin treatment by using qPCR (Figure 4(c)). The protein levels of iNOS and COX2 were downregulated in the aloin-treated group, as shown by using western blot analysis (Figure 4(d)). These data suggested that aloin can inhibit the levels of oxidative stress and the production of proinflammatory factors in TNF-$\alpha$-induced NPCs.

*3.5. Aloin Suppresses the Activation of the TAK1/NF-κB Pathway.* Subsequently to explore the underlying mechanism, we evaluated the activation of the TAK1/NF-$\kappa$B axis under TNF-$\alpha$ treatment. As shown in Figures 5(a)–5(c), higher ratios of p-TAK1/TAK1, p-I$\kappa$B$\alpha$/I$\kappa$B$\alpha$, and p-P65/P65 were observed in TNF-$\alpha$-treated NPCs, but aloin

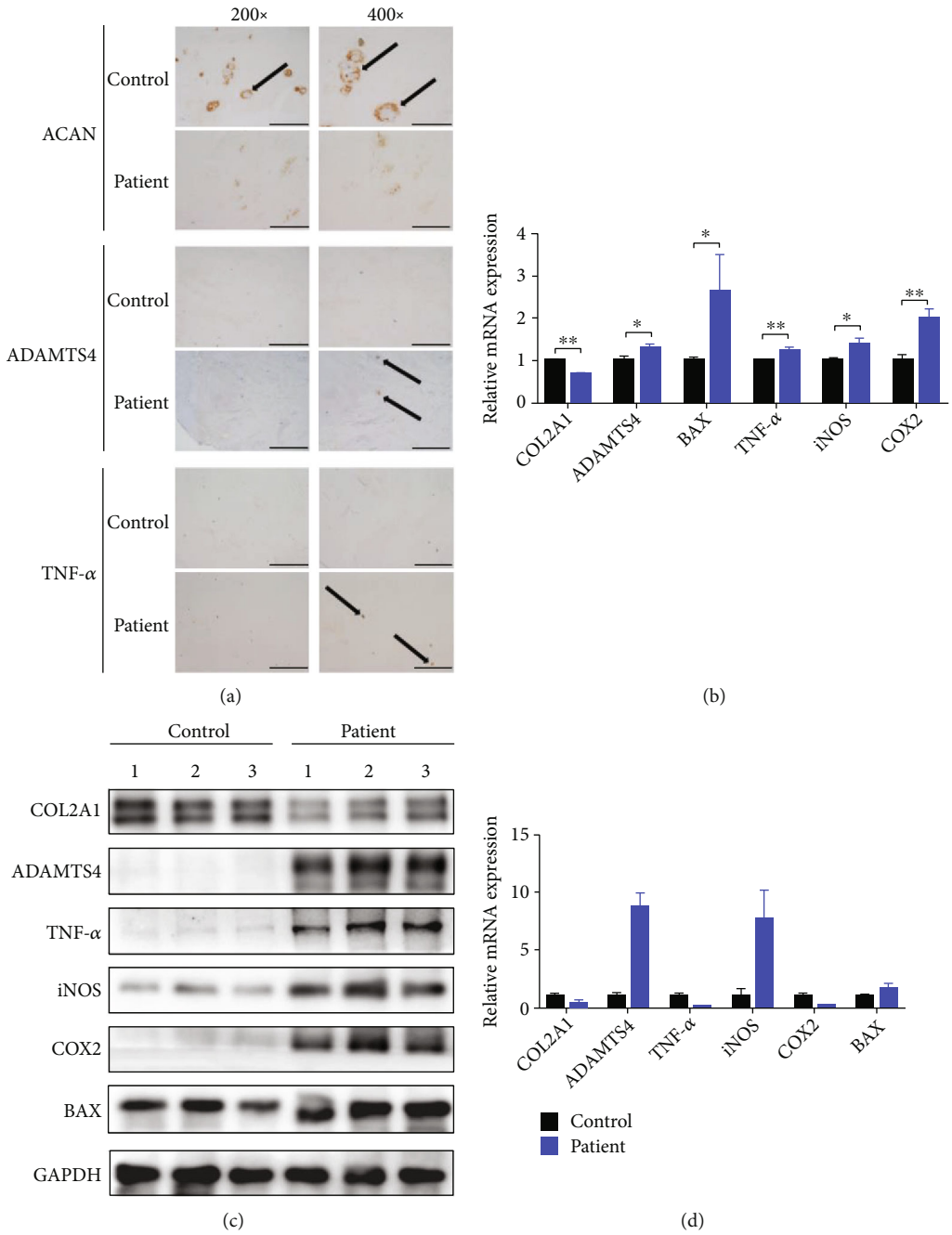


Figure 1: Dysregulated ECM metabolism, increased apoptosis, and inflammatory infiltration in degenerated NP tissue. (a) Immunohistochemical staining assay of ACAN, ADAMTS4, and TNF-α in normal and degenerated human NP tissues. (b) The mRNA expression levels of *COL2A1*, *ADAMTS4*, *BAX*, *TNF-α*, *iNOS*, and *COX2* were detected by qPCR in normal and degenerated human NP tissues. (c, d) Protein expression levels of COL2A1, ADAMTS4, BAX, TNF-α, iNOS, and COX2 were detected by western blotting in normal and degenerated human NP tissues. The densities of the protein bands were assessed and quantified using the ImageJ software. The left images (magnification: ×200, scale bar: 100 μm) and the right images (magnification: ×400, scale bar: 50 μm) are shown. $^{*}P < 0.05$, $^{**}P < 0.01$.

(200 μM) treatment significantly reversed these changes in the ratios of p-TAK1/TAK1, p-IκBα/IκBα, and p-P65/P65 (Figures 5(a)–5(c)). We further assessed the localization of P65 via immunofluorescence and found that the proportion of P65 translocated from the cytoplasm into the nucleus was upregulated under TNF-α treatment, whereas aloin treatment attenuated the translocation of P65 (Figure 5(d)). These results suggested that aloin treatment can suppress the activation of the TAK1/NF-κB pathway.

*3.6. Aloin Treatment Inhibits the Expression of the NLRP3 Inflammasome.* As reported previously, the NLRP3 inflammasome is involved in inflammation-related NPCs and the progression of IDD [32]. To further investigate whether

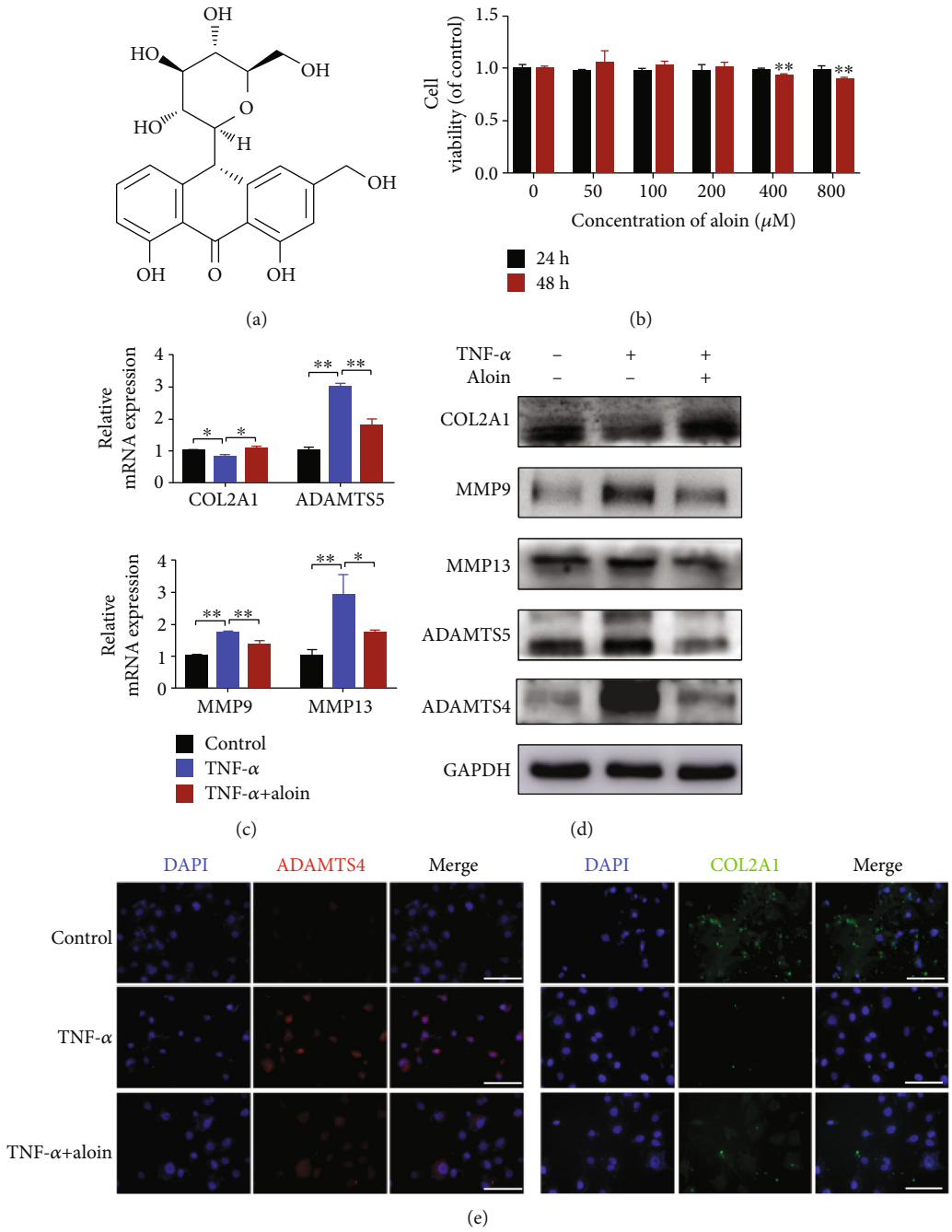


Figure 2: Aloin treatment enhances the anabolism and suppresses the catabolism in TNF-$\alpha$-treated NPCs. (a) The chemical structure of aloin is shown (quoted from http://www.medchemexpress.cn/.) (b) Detection of aloin's cytotoxic effect on NPCs at various concentrations at 24 and 48 h posttreatment using a CCK-8 assay (0, 50, 100, 200, 400, and 800 $\mu$M). (c) The mRNA expression levels of *COL2A1*, *ADAMTS5*, *MMP9*, and *MMP13* in the different groups were detected by qPCR. (d) Protein expression of COL2A1, ADAMTS5, MMP9, and MMP13 was detected by western blotting in the different groups. (e) Both ADAMTS4 and COL2A1 were detected by immunofluorescence staining. DAPI was used to stain for the nuclei. Images (magnification: ×400, scale bar: 50 $\mu$m). In this (c–e), aloin was used at the concentration of 200 $\mu$M, while TNF-$\alpha$ was at the concentration of 10 ng/ml. $^{*}P < 0.05$, $^{**}P < 0.01$.

aloin regulated NLRP3 inflammasome activity in NPCs in an inflammatory microenvironment, we assessed the level of the NLRP3 inflammasome and found that it was higher in degenerated disc tissue than in normal tissues at both the mRNA and protein levels (Figures 6(a) and 6(b)). We then observed the expression of the NLRP3 inflammasome was inhibited upon aloin treatment by qPCR and western blot in TNF-$\alpha$-treated NPCs (Figures 6(c) and 6(d)). In addition, immunofluorescence also showed that aloin treatment downregulated the expression of *NLRP3* in TNF-$\alpha$-treated NPCs. These results suggested that aloin treatment reduced the expression of *NLRP3*.

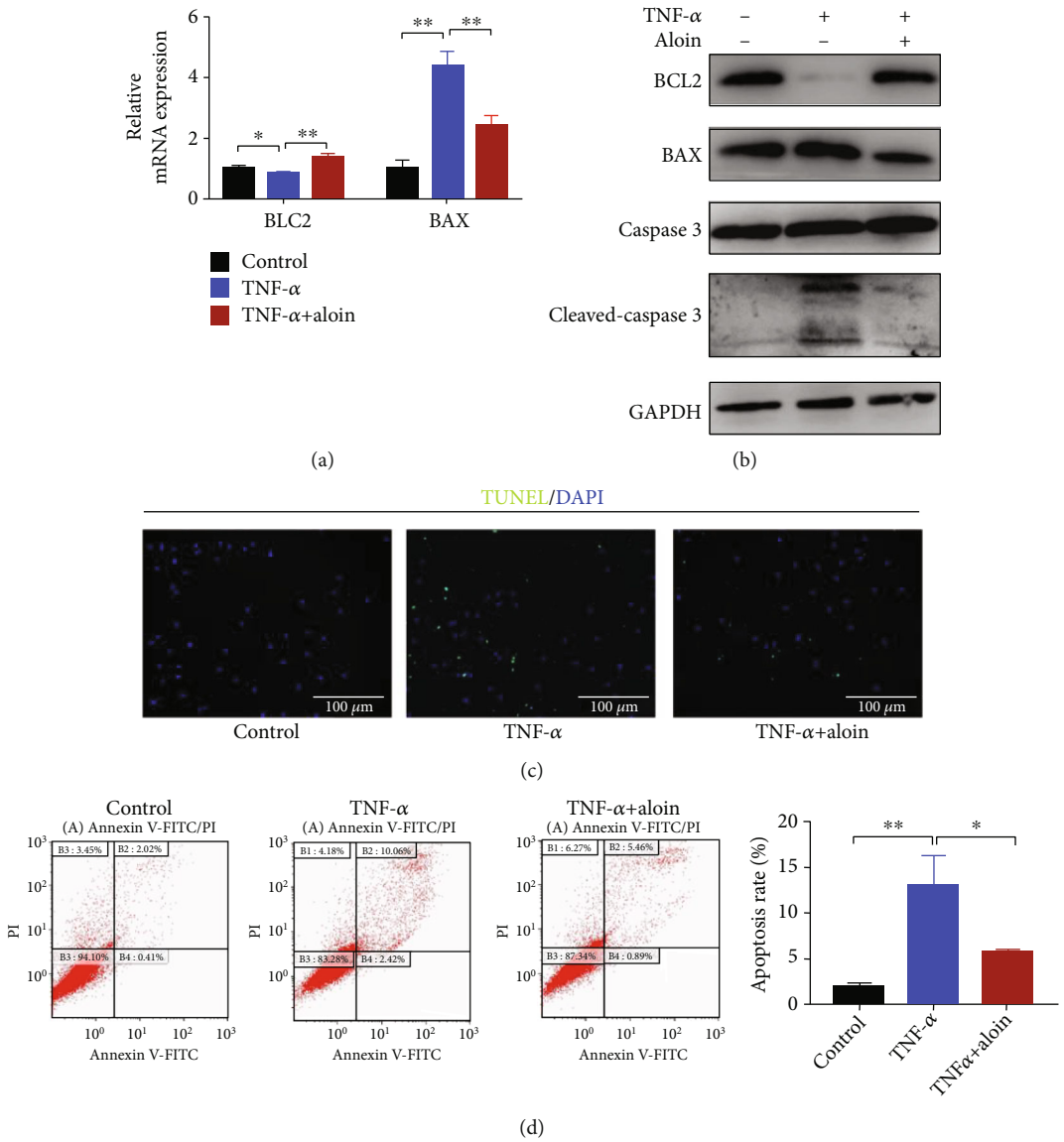


Figure 3: Aloin treatment reduced the apoptosis rate in TNF-$\alpha$-treated NPCs. (a) The mRNA expression levels of *BCL2* and *BAX* were detected by qPCR in the different groups. (b) Protein expression levels of BCL2, BAX, Caspase3, and Cleaved-caspase3 were detected by western blotting in the different groups. (c) TUNEL immunofluorescence staining in the different groups. (d) Flow cytometry and apoptosis rate analysis in the different groups ($n = 3$). Images (magnification: ×200, scale bar: 100 $\mu$m). In this figure, aloin was used at the concentration of 200 $\mu$M, while TNF-$\alpha$ was at the concentration of 10 ng/ml. $^{*}P < 0.05$, $^{**}P < 0.01$.

## 4. Discussion

IDD, a common degenerative disease, is also considered to be the main cause of the high incidence of LBP, which causes pain and even disability [3, 4, 39]. However, searching for effective treatment drugs for IDD is still a huge challenge. Aloin, extracted from aloe plants, has been shown to have anti-inflammatory, antioxidant, and bone protective activities, but its effects on IDD have not been confirmed [37, 38, 40]. In our study, we demonstrated that aloin treatment can reverse TNF-$\alpha$-induced extracellular matrix metabolism disorder, apoptosis, oxidative stress, and the production of proinflammatory factors in NPCs through the TAK1/NF-$\kappa$B/NLRP3 pathway. These results indicated that aloin may be a promising therapeutic method for IDD.

Aloin has been shown to have important protective effects on the skeletal system, including ameliorating the progression of osteoarthritis, promoting the expression levels of osteoblast differentiation genes (*BMP2* and *RUNX2*) in a dose-dependent manner, and suppressing osteoclastogenesis and bone resorption in previous studies [38, 41–43]. To assess the potential protective effect on NPCs, we first determined nontoxic concentrations of aloin in NPCs. We further demonstrated that aloin can reverse extracellular matrix metabolism disorders, apoptosis, oxidative stress, and the production of proinflammatory factors in

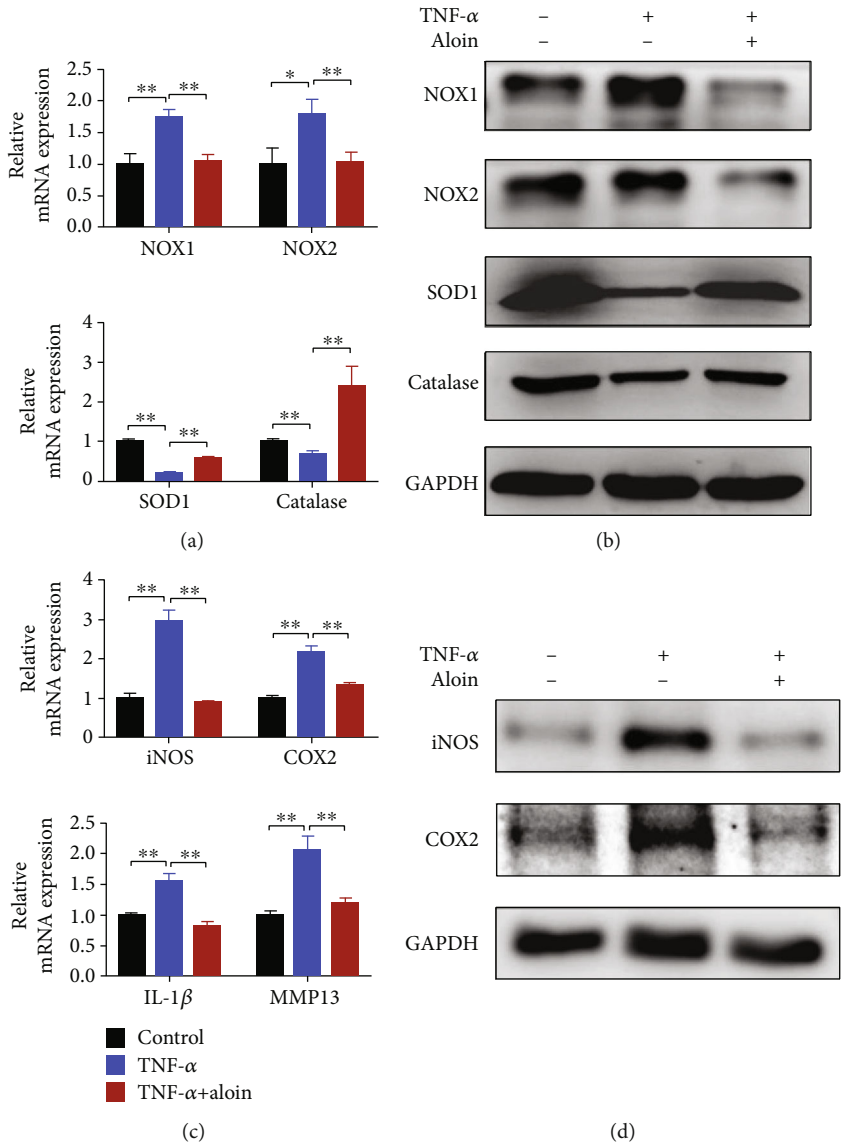


Figure 4: Aloin treatment ameliorates the levels of oxidative stress and proinflammatory factors. (a) The mRNA expression levels of *NOX1*, *NOX2*, *SOD1*, and *Catalase* were detected by qPCR. (b) Protein expression levels of NOX1, NOX2, SOD1, and Catalase were detected by western blotting. (c) The mRNA expression levels of *iNOS*, *COX2*, *IL-β*, and *IL-6* were detected by qPCR. (d) Protein expression levels of iNOS and COX2 were detected by western blotting. In this figure, aloin was used at the concentration of 200 $\mu$M, while TNF-$\alpha$ was at the concentration of 10 ng/ml. $^{*}P < 0.05$, $^{**}P < 0.01$.

TNF-$\alpha$-treated NPCs in vitro. Similarly, a previous study showed that aloin treatment significantly inhibited both inadequate anabolism and excessive catabolism of the extracellular matrix in chondrocytes [38], while another study found that aloin effectively increased the activity of antioxidant enzymes and inhibited the levels of reactive oxygen species [44].

Previous studies have shown that TNF-$\alpha$ plays a conclusive role in the occurrence and development of IDD; thus, inhibiting inflammation effectively can ameliorate the progression of IDD [15–17, 45–47]. It has been demonstrated that aloin is effective in reducing the production of inflammatory and proinflammatory factors [37, 38]. A previous study reported that aloin treatment significantly decreased the expression of iNOS and TNF-$\alpha$ [48], while other studies found that aloin exerted anti-inflammatory activity and reduced the release of inflammatory cytokines [49, 50]. Correspondingly, we demonstrated the protective effects of aloin on TNF-$\alpha$-treated NPCs.

In our study, we demonstrated that aloin treatment suppressed the activation of the TAK1/NF-$\kappa$B pathway and inhibited the level of NLRP3 inflammasome. As previous studies had reported, the TAK1/NF-$\kappa$B/NLRP3 pathway played an important role in TNF-$\alpha$-induced inflammation in NPCs [51, 52]. Our study confirmed that the importance of this inflammation-related signaling pathway in the progression of IDD. Similarly, it had been reported that aloin treatment inhibited the activation of NF-$\kappa$B signaling in lipopolysaccharide-induced acute lung injury, IL-1 beta-stimulated chondrocytes, and D-galactose-induced cognitive

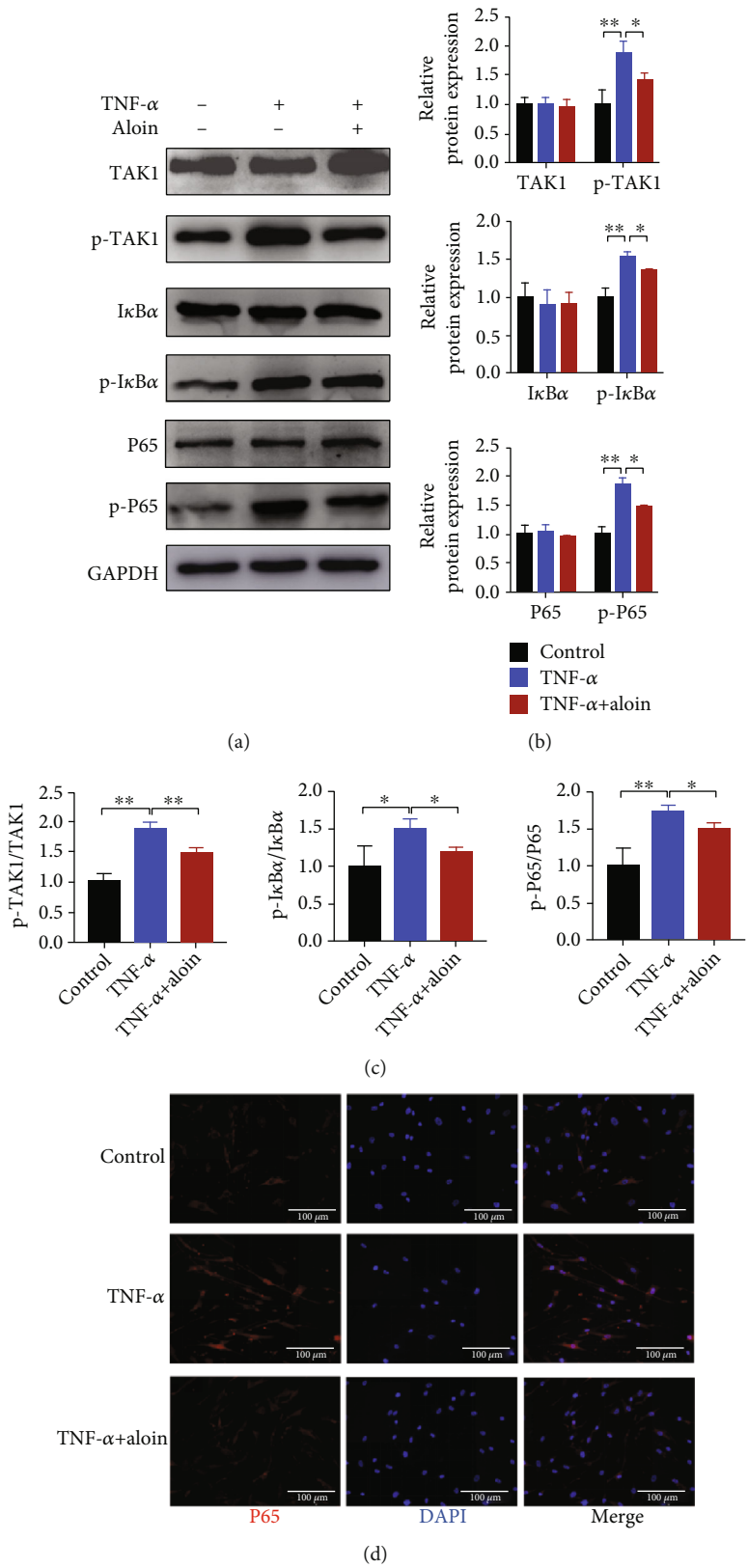


Figure 5: Aloin suppresses the activation of the TAK1/NF-κB pathway. (a) Protein expression levels of the TAK1/NF-κB signaling pathway (TAK1, p-TAK1, IκBα, p-IκBα, P65, p-P65) were detected by western blotting in different groups. (b) The protein bands were quantified using the ImageJ software. (c) The expression ratios of p-TAK1/TAK1, p-IκBα/IκBα, and p-P65/P65 in the different groups. (d) Localization of P65 was assessed via immunofluorescence. Images (magnification: ×200, scale bar: 100 μm). In this figure, aloin was used at the concentration of 200 μM, while TNF-α was at the concentration of 10 ng/ml. $^{*}P < 0.05$, $^{**}P < 0.01$.

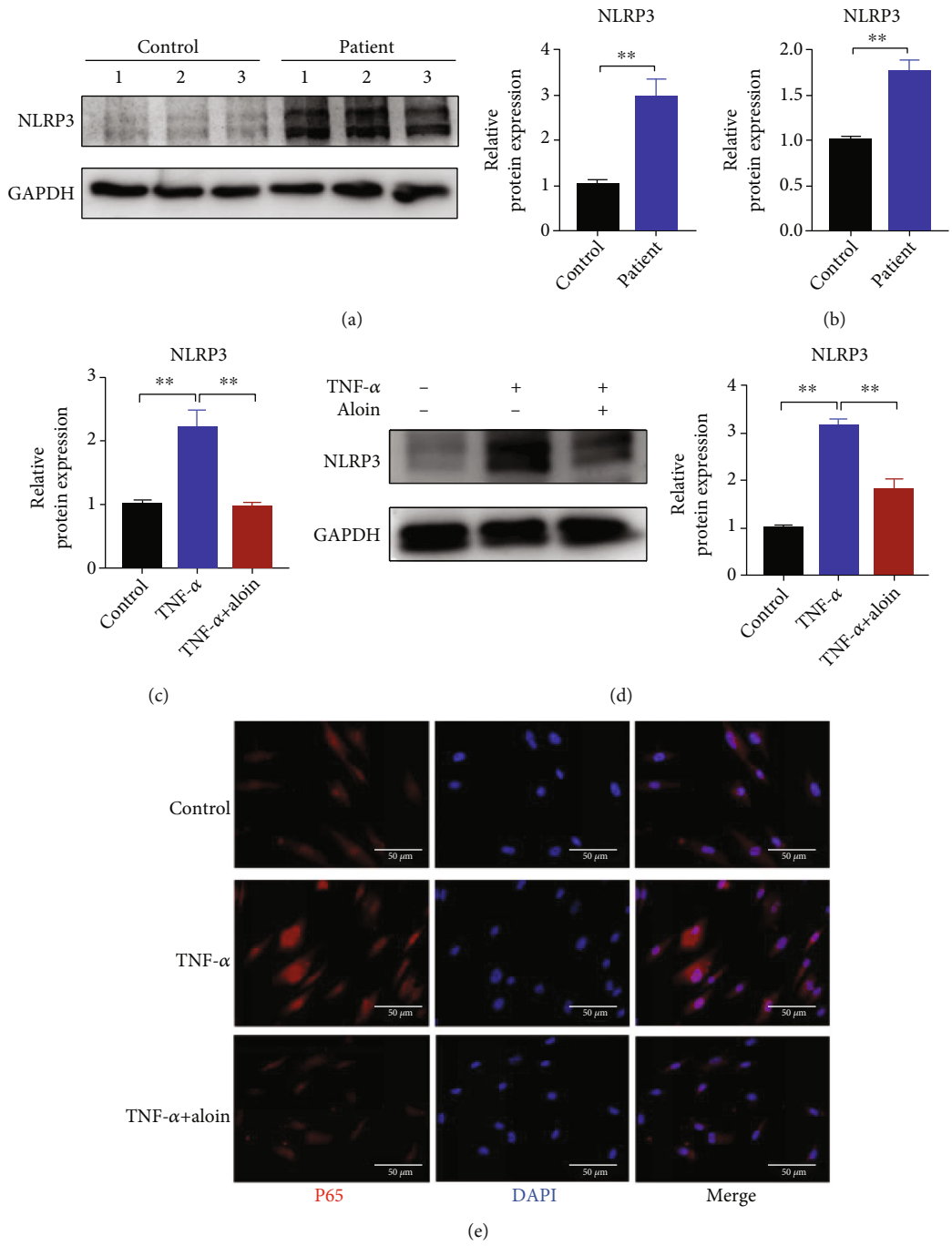


Figure 6: Aloin treatment inhibits the expression of the NLRP3 inflammasome. (a) The expression level of NLRP3 was detected by western blot in normal and degenerated human NP tissues. The protein bands were quantified using the ImageJ software. (b) The mRNA level of *NLRP3* was detected by qPCR in normal and degenerated human NP tissues. (c) The mRNA expression of *NLRP3* was detected by qPCR in the different groups. (d) The expression of NLRP3 was detected at the protein level by western blotting (left panel). The protein bands were quantified by the ImageJ software (right panel). (e) NLRP3 detection by using immunofluorescence. Images (magnification: ×400, scale bar: 50 $\mu$m). In this figure, aloin was used at the concentration of 200 $\mu$M, while TNF-$\alpha$ was at the concentration of 10 ng/ml. $^{*}P < 0.05$, $^{**}P < 0.01$.

impairment and inflammation [37, 38, 44]. Our results provided more evidences on the powerful anti-inflammatory activity of aloin on NPCs.

LBP, which is associated with IDD, is widespread and has a high incidence. However, existing treatments do not counteract the IDD process. In our study, a new potential treatment was proposed. Aloin, with obvious effects including regulating ECM metabolism, inhibiting apoptosis, and anti-inflammatory and antioxidant activity in NPCs, may be a therapeutic agent for IDD. However, further study is essential to elucidate the effect of aloin on IDD in vivo.

## 5. Conclusion

We assessed the protective effects of aloin on NPCs and demonstrated the underlying mechanism. In our study, we discovered that aloin promoted extracellular matrix homeostasis, inhibited apoptosis, and reduced the production of proinflammatory factors and the levels of oxidative stress in TNF-$\alpha$-induced NPCs. In mechanistically, we found that aloin treatment suppressed the activation of the TAK1/NF-$\kappa$B/NLRP3 pathway. Our research indicates that aloin may be a therapeutic agent for IDD in the future.

## Data Availability

The data used to support the findings of this study are available from the corresponding author upon request.

## Conflicts of Interest

We declare that there is no conflict of interest regarding the publication of this paper.

## Authors' Contributions

WJG and AJL designed the experiments. TQC, PFL, JCQ, WJH, SGL, HHS, XJQ, and DSH conducted the experiments. TQC, PFL, and JCQ acquired the data. TQC, PFL, JCQ, WJG, and AJL analyzed the data. TQC, WJG, and AJL wrote the manuscript. All authors read and approved the final manuscript. Taiqiu Chen, Pengfei Li, and Jincheng Qiu contributed equally to this work and should be considered as co-first authors.

## Acknowledgments

This work was supported by the grants from the National Natural Science Foundation of China (No. 81572134), the Guangdong Basic and Applied Basic Research Foundation (No. 2019A1515110122 and No. 2021A1515012619), the Fundamental Research Funds for the Central Universities (No. 20ykpy94), the Sun Yat-sen Scholarship for Young Scientist for Wenjie Gao, and the Science and Technology Program of Guangzhou, China (No. 202102010159). We thank LetPub (http://www.letpub.com/) for its linguistic assistance during the preparation of this manuscript.

## Supplementary Materials

Supplement Table 1: abbreviations and descriptions. Supplement Table 2: primers' sequences for RT-qPCR. *(Supplementary Materials)*

## References

[1] A. Delitto, S. Z. George, L. van Dillen et al., "Low back pain," *The Journal of Orthopaedic and Sports Physical Therapy*, vol. 42, no. 4, pp. A1–57, 2012.

[2] J. W. S. Vlaeyen, C. G. Maher, K. Wiech et al., "Low back pain," *Nature Reviews. Disease Primers*, vol. 4, no. 1, p. 52, 2018.

[3] G. B. Andersson, "Epidemiological features of chronic low-back pain," *Lancet*, vol. 354, no. 9178, pp. 581–585, 1999.

[4] S. Clark and R. Horton, "Low back pain: a major global challenge," *Lancet*, vol. 391, no. 10137, p. 2302, 2018.

[5] J. Hartvigsen, M. J. Hancock, A. Kongsted et al., "What low back pain is and why we need to pay attention," *Lancet*, vol. 391, no. 10137, pp. 2356–2367, 2018.

[6] A. L. Golob and J. E. Wipf, "Low back pain," *The Medical Clinics of North America*, vol. 98, no. 3, pp. 405–428, 2014.

[7] P. P. Raj, "Intervertebral disc: anatomy-physiology-pathophysiology-treatment," *Pain Practice*, vol. 8, no. 1, pp. 18–44, 2008.

[8] S. Roberts, H. Evans, J. Trivedi, and J. Menage, "Histology and pathology of the human intervertebral disc," *The Journal of Bone and Joint Surgery. American Volume*, vol. 88, suppl_2, pp. 10–14, 2006.

[9] F. Wang, F. Cai, R. Shi, X. H. Wang, and X. T. Wu, "Aging and age related stresses: a senescence mechanism of intervertebral disc degeneration," *Osteoarthritis and Cartilage*, vol. 24, no. 3, pp. 398–408, 2016.

[10] M. V. Risbud and I. M. Shapiro, "Role of cytokines in intervertebral disc degeneration: pain and disc content," *Nature Reviews Rheumatology*, vol. 10, no. 1, pp. 44–56, 2014.

[11] J. Wang, C. Huang, Z. Lin et al., "Polydatin suppresses nucleus pulposus cell senescence, promotes matrix homeostasis and attenuates intervertebral disc degeneration in rats," *Journal of Cellular and Molecular Medicine*, vol. 22, no. 11, pp. 5720–5731, 2018.

[12] S. Z. Wang, Y. F. Rui, J. Lu, and C. Wang, "Cell and molecular biology of intervertebral disc degeneration: current understanding and implications for potential therapeutic strategies," *Cell Proliferation*, vol. 47, no. 5, pp. 381–390, 2014.

[13] P. Cazzanelli and K. Wuertz-Kozak, "MicroRNAs in intervertebral disc degeneration, apoptosis, inflammation, and mechanobiology," *International Journal of Molecular Sciences*, vol. 21, no. 10, p. 3601, 2020.

[14] F. Zhang, X. Zhao, H. Shen, and C. Zhang, "Molecular mechanisms of cell death in intervertebral disc degeneration (review)," *International Journal of Molecular Medicine*, vol. 37, no. 6, pp. 1439–1448, 2016.

[15] C. A. Séguin, R. M. Pilliar, P. J. Roughley, and R. A. Kandel, "Tumor necrosis Factor$\alpha$ modulates matrix production and catabolism in nucleus pulposus tissue," *Spine (Phila Pa 1976)*, vol. 30, no. 17, pp. 1940–1948, 2005.

[16] C. Wang, X. Yu, Y. Yan et al., "Tumor necrosis factor-$\alpha$: a key contributor to intervertebral disc degeneration," *Acta Biochim Biophys Sin (Shanghai)*, vol. 49, no. 1, pp. 1–13, 2017.

[17] C. L. Le Maitre, J. A. Hoyland, and A. J. Freemont, "Catabolic cytokine expression in degenerate and herniated human intervertebral discs: IL-1$\beta$ and TNF$\alpha$ expression profile," *Arthritis Research & Therapy*, vol. 9, no. 4, p. R77, 2007.

[18] S. Ye, J. Wang, S. Yang et al., "Specific inhibitory protein Dkk-1 blocking Wnt/$\beta$-catenin signaling pathway improve protectives effect on the extracellular matrix," *Journal of Huazhong University of Science and Technology. Medical Sciences*, vol. 31, no. 5, pp. 657–662, 2011.

[19] S. J. Millward-Sadler, P. W. Costello, A. J. Freemont, and J. A. Hoyland, "Regulation of catabolic gene expression in normal and degenerate human intervertebral disc cells: implications for the pathogenesis of intervertebral disc degeneration," *Arthritis Research & Therapy*, vol. 11, no. 3, p. R65, 2009.

[20] C. K. Kepler, D. Z. Markova, A. S. Hilibrand et al., "Substance P stimulates production of inflammatory cytokines in human disc cells," *Spine (Phila Pa 1976)*, vol. 38, no. 21, pp. E1291–E1299, 2013.

[21] M. A. Gabr, L. Jing, A. R. Helbling et al., "Interleukin-17 synergizes with IFN$\gamma$ or TNF$\alpha$ to promote inflammatory mediator release and intercellular adhesion molecule-1 (ICAM-1) expression in human intervertebral disc cells," *Journal of Orthopaedic Research*, vol. 29, no. 1, pp. 1–7, 2011.

[22] C. C. Zhang, G. P. Cui, J. G. Hu et al., "Effects of adenoviral vector expressing hIGF-1 on apoptosis in nucleus pulposus cells in vitro," *International Journal of Molecular Medicine*, vol. 33, no. 2, pp. 401–405, 2014.

[23] J. Li, W. Yuan, S. Jiang et al., "Prolyl-4-hydroxylase Domain Protein 2 Controls NF-$\kappa$B/p65 Transactivation and Enhances the Catabolic Effects of Inflammatory Cytokines on Cells of the Nucleus Pulposus," *The Journal of Biological Chemistry*, vol. 290, no. 11, pp. 7195–7207, 2015.

[24] J. Hong, S. Li, D. Z. Markova et al., "Bromodomain-containing protein 4 inhibition alleviates matrix degradation by enhancing autophagy and suppressing NLRP3 inflammasome activity in NP cells," *Journal of Cellular Physiology*, vol. 235, no. 7-8, pp. 5736–5749, 2020.

[25] X. Dolcet, D. Llobet, J. Pallares, and X. Matias-Guiu, "NF-kB in development and progression of human cancer," *Virchows Archiv*, vol. 446, no. 5, pp. 475–482, 2005.

[26] T. Lawrence, "The nuclear factor NF-kappaB pathway in inflammation," *Cold Spring Harbor Perspectives in Biology*, vol. 1, no. 6, article a001651, 2009.

[27] G. Z. Zhang, M. Q. Liu, H. W. Chen et al., "NF-$\kappa$B signalling pathways in nucleus pulposus cell function and intervertebral disc degeneration," *Cell Proliferation*, vol. 54, no. 7, article e13057, 2021.

[28] Z. Yao, L. Nie, Y. Zhao et al., "Salubrinal suppresses IL-17-induced upregulation of MMP-13 and extracellular matrix degradation through the NF-kB pathway in human nucleus pulposus cells," *Inflammation*, vol. 39, no. 6, pp. 1997–2007, 2016.

[29] G. Gao, F. Chang, T. Zhang et al., "Naringin protects against interleukin 1$\beta$ (IL-1$\beta$)-induced human nucleus pulposus cells degeneration via downregulation nuclear factor kappa B (NF-$\kappa$B) pathway and p53 expression," *Medical Science Monitor*, vol. 25, no. 25, pp. 9963–9972, 2019.

[30] B. Z. Shao, Z. Q. Xu, B. Z. Han, D. F. Su, and C. Liu, "NLRP3 inflammasome and its inhibitors: a review," *Frontiers in Pharmacology*, vol. 5, no. 6, p. 262, 2015.

[31] Y. Tian, Z. Bao, Y. Ji, X. Mei, and H. Yang, "Epigallocatechin-3-Gallate protects $H^2O^2$-Induced nucleus pulposus cell apoptosis and inflammation by inhibiting cGAS/sting/NLRP3 Activation," *Drug Design, Development and Therapy*, vol. - Volume 14, no. 14, pp. 2113–2122, 2020.

[32] Y. Huang, Y. Peng, J. Sun et al., "Nicotinamide phosphoribosyl transferase controls NLRP3 inflammasome activity through MAPK and NF-$\kappa$B signaling in nucleus pulposus cells, as suppressed by melatonin," *Inflammation*, vol. 43, no. 3, pp. 796–809, 2020.

[33] Y. Zhou, Z. Chen, X. Yang et al., "Morin attenuates pyroptosis of nucleus pulposus cells and ameliorates intervertebral disc degeneration via inhibition of the TXNIP/NLRP3/Caspase-1/IL-1$\beta$ signaling pathway," *Biochemical and Biophysical Research Communications*, vol. 559, no. 559, pp. 106–112, 2021.

[34] M. Sánchez, E. González-Burgos, I. Iglesias, and M. P. Gómez-Serranillos, "Pharmacological update properties of aloe vera and its major active constituents," *Molecules*, vol. 25, no. 6, p. 1324, 2020.

[35] B. Salehi, S. Albayrak, H. Antolak et al., "Aloe genus plants: from farm to food applications and phytopharmacotherapy," *International Journal of Molecular Sciences*, vol. 19, no. 9, p. 2843, 2018.

[36] W. Sun, Z. Wang, M. Sun, W. Huang, Y. Wang, and Y. Wang, "Aloin antagonizes stimulated ischemia/reperfusion-induced damage and inflammatory response in cardiomyocytes by activating the Nrf2/HO-1 defense pathway," *Cell and Tissue Research*, vol. 384, no. 3, pp. 735–744, 2021.

[37] J. Lei, Y. Shen, G. Xv, Z. di, Y. Li, and G. Li, "Aloin suppresses lipopolysaccharide-induced acute lung injury by inhibiting NLRP3/NF-$\kappa$B via activation of SIRT1 in mice," *Immunopharmacology and Immunotoxicology*, vol. 42, no. 4, pp. 306–313, 2020.

[38] C. Zhang, Z. Shao, X. Hu et al., "Inhibition of PI3K/Akt/NF-$\kappa$B signaling by aloin for ameliorating the progression of osteoarthritis: in vitro and in vivo studies," *International Immunopharmacology*, vol. 89, no. Part B, article 107079, 2020.

[39] R. A. Deyo and J. N. Weinstein, "Low back pain," *The New England Journal of Medicine*, vol. 344, no. 5, pp. 363–370, 2001.

[40] Q. Xu, Y. Fan, J. J. Loor et al., "Aloin protects mice from diet-induced non-alcoholic steatohepatitisviaactivation of Nrf2/HO-1 signaling," *Food & Function*, vol. 12, no. 2, pp. 696–705, 2021.

[41] P. Li, J. Kong, Z. Chen et al., "Aloin promotes osteogenesis of bone-marrow-derived mesenchymal stem cells via the ERK1/2-dependent Runx2 signaling pathway," *Journal of Natural Medicines*, vol. 73, no. 1, pp. 104–113, 2019.

[42] Y. Pengjam, H. Madhyastha, R. Madhyastha, Y. Yamaguchi, Y. Nakajima, and M. Maruyama, "NF-$\kappa$B pathway inhibition by anthrocyclic glycoside aloin is key event in preventing osteoclastogenesis in RAW264.7 cells," *Phytomedicine*, vol. 23, no. 4, pp. 417–428, 2016.

[43] Y. Pengjam, H. Madhyastha, R. Madhyastha, Y. Yamaguchi, Y. Nakajima, and M. Maruyama, "Anthraquinone glycoside aloin induces osteogenic initiation of MC3T3-E1 cells: involvement of MAPK mediated Wnt and Bmp signaling," *Biomolecules & Therapeutics*, vol. 24, no. 2, pp. 123–131, 2016.

[44] J. Zhong, F. Wang, Z. Wang et al., "Aloin attenuates cognitive impairment and inflammation induced by d-galactose via down-regulating ERK, p38 and NF-$\kappa$B signaling pathway," *International Immunopharmacology*, vol. 72, pp. 48–54, 2019.

[45] F. Ding and X. Li, "Apigenin mitigates intervertebral disc degeneration through the amelioration of tumor necrosis factor $\alpha$ (TNF-$\alpha$) signaling pathway," *Medical Science Monitor*, vol. 26, no. 26, article e924587, 2020.

[46] Y. Liu, J. Lin, X. Wu et al., "Aspirin-mediated attenuation of intervertebral disc degeneration by ameliorating reactive oxygen species in vivo and in vitro," *Oxidative Medicine and Cellular Longevity*, vol. 2019, Article ID 7189854, 20 pages, 2019.

[47] S. Wang, J. Wei, Y. Fan et al., "Progranulin is positively associated with intervertebral disc degeneration by interaction with IL-10 and IL-17 through TNF pathways," *Inflammation*, vol. 41, no. 5, pp. 1852–1863, 2018.

[48] W. Lee, S. Yang, C. Lee et al., "Aloin reduces inflammatory gene iNOS via inhibition activity and p-STAT-1 and NF-$\kappa$B," *Food and Chemical Toxicology*, vol. 126, pp. 67–71, 2019.

[49] L. A. Birari, U. B. Mahajan, K. R. Patil et al., "Aloin protects against arsenic trioxide-induced myocardial membrane damage and release of inflammatory cytokines," *Naunyn-Schmiedeberg's Archives of Pharmacology*, vol. 393, no. 8, pp. 1365–1372, 2020.

[50] M. Y. Park, H. J. Kwon, and M. K. Sung, "Dietary aloin, aloesin, or aloe-gel exerts anti-inflammatory activity in a rat colitis model," *Life Sciences*, vol. 88, no. 11-12, pp. 486–492, 2011.

[51] Y. Zhao, C. Qiu, W. Wang et al., "Cortistatin protects against intervertebral disc degeneration through targeting mitochondrial ROS-dependent NLRP3 inflammasome activation," *Theranostics*, vol. 10, no. 15, pp. 7015–7033, 2020.

[52] J. Zhang, X. Wang, H. Liu et al., "TNF-$\alpha$ enhances apoptosis by promoting chop expression in nucleus pulposus cells: role of the MAPK and NF-$\kappa$B pathways," *Journal of Orthopaedic Research*, vol. 37, no. 3, pp. 697–705, 2019.